Award Number: W81XWH-12-1-0100

TITLE: The Role of Trop2 Cleavage Products in Prostate Tumorigenesis

PRINCIPAL INVESTIGATOR: Tanya Stoyanova

CONTRACTING ORGANIZATION: University of California at Los Angeles
Los Angeles, CA 90095-2000

REPORT DATE: October 2014

TYPE OF REPORT: Final Summary

PREPARED FOR: U.S. Army Medical Research and Materiel Command
Fort Detrick, Maryland 21702-5012

REPORT DOCUMENTATION PAGE

Form Approved
OMB No. 0704-0188

1. REPORT DATE	2. REPORT TYPE	3. DATES COVERED
October 2014	Final Summary	1 July 2012 - 30 June 2014

4. TITLE AND SUBTITLE

The Role of Trop2 Cleavage Products in Prostate Tumorigenesis

5a. CONTRACT NUMBER

5b. GRANT NUMBER
W81XWH-12-1-0100

5c. PROGRAM ELEMENT NUMBER

6. AUTHOR(S)

Tanya Stoyanova

E-Mail: tstoyanova@mednet.ucla.edu

5d. PROJECT NUMBER

5e. TASK NUMBER

5f. WORK UNIT NUMBER

7. PERFORMING ORGANIZATION NAME(S) AND ADDRESS(ES)

University of California at Los Angeles

Los Angeles, CA 90095-2000

8. PERFORMING ORGANIZATION REPORT NUMBER

9. SPONSORING / MONITORING AGENCY NAME(S) AND ADDRESS(ES)
U.S. Army Medical Research and Materiel Command
Fort Detrick, Maryland 21702-5012

10. SPONSOR/MONITOR'S ACRONYM(S)

11. SPONSOR/MONITOR'S REPORT NUMBER(S)

12. DISTRIBUTION / AVAILABILITY STATEMENT
Approved for Public Release; Distribution Unlimited

13. SUPPLEMENTARY NOTES

14. ABSTRACT
We have now shown that Trop2 is a new regulator of stem/progenitor activity and tumorigenesis in the prostate. Trop2 is necessary for prostate cancer initiation. Trop2 controls self-renewal, proliferation and tissue hyperplasia through two cleavage products (ICD and ECD) generated by RIP. The intracellular domain of Trop2 is released from the membrane and accumulates in the nucleus. Nuclear ICD is found in human prostate cancer but not in the cancer-adjacent benign tissue, suggesting a role for Trop2 cleavage in tumorigenesis. Heightened expression of Trop2 intracellular or extracellular domains are sufficient to initiate precursor lesions to prostate cancer *in vivo*. Importantly, we demonstrate that Trop2 loss of function cleavage mutants are deficient in inducing self-renewal and tumorigenesis in the prostate. These findings suggest that heightened expression of Trop2 is selected for in epithelial cancers to enhance the stem- like properties of self-renewal and proliferation. Identifying the factors that regulate self-renewal and cancer initiation will enhance our understanding of the tumorigenic process and lead to the design of novel cancer therapies.

15. SUBJECT TERMS
Prostate cancer, stem cells, regulated intramembrane proteolysis (RIP)

16. SECURITY CLASSIFICATION OF:			17. LIMITATION OF ABSTRACT	18. NUMBER OF PAGES	19a. NAME OF RESPONSIBLE PERSON
a. REPORT	b. ABSTRACT	c. THIS PAGE			USAMRMC
U	U	U	UU	61	19b. TELEPHONE NUMBER *(include area code)*

Table of Contents

Page

INTRODUCTION

Trop2 is a type-I trans-membrane glycoprotein over-expressed in numerous carcinomas including prostate cancer[1-12]. In addition to its elevated levels in epithelial cancers, Trop2 is a marker of stem/progenitor cells in the prostate[13]. The overall goal of the proposed project is to uncover the biology behind Trop2 signaling in prostate cancer.

Our previous data demonstrated that Trop2 is highly expressed in human prostate cancer and mouse models of prostate cancer driven by epithelial AKT or stromal FGF10. Trop2 has oncogenic potential in vivo measured by prostate tissue regeneration assay. To explore the connection between Trop2, transformation and stem/progenitor cells in the prostate, we investigated the role of Trop2 in self-renewal. Using in vitro sphere assay and in vivo prostate regeneration assays, we established that Trop2 regulates adult prostate stem/progenitor self-renewal and prostate tubule formation.

We have also determined that Trop2 is activated by regulated intramembrane proteolysis (RIP), and the resulting cleavage products drive self-renewal and proliferation. RIP is a two step process--an initial proteolytic cut, taking place at a site outside of the membrane, shedding the extracellular domain (ECD) of Trop2 followed by a second cut within the cellular membrane generating free intracellular domain (ICD). We have established that TNF-α converting enzyme (TACE) mediates the initial proteolysis since inhibition of the enzyme by small molecules (TAPI-2) leads to a dramatic increase of full length Trop2. gamma-secretase complex containing PS-1 and PS-2 enzymes mediates a second cleavage, assessed by the appearance of an intermediate cleavage product (ICP) upon chemical inhibition of gamma-secretase by DAPT (Fig. 3A). The 15 kDa ICP can be detected only if the first proteolytic cut by TACE takes place, while the second step of processing is being blocked (Fig. 3A). Trop2 ICD and ECD alone were sufficient to increase self-renewal activity measured by sphere number and proliferation assessed by sphere size in primary prostate cells in vitro.

In this proposal, we aim to delineate the functional role of Trop2 in prostate carcinogenesis and self-renewal and the molecular mechanism though which Trop2 regulates these processes. Understanding the mechanism of Trop2 function may provide insights into novel and more effective therapies. Identification of the molecular mechanism and pathways regulated by Trop2 may point the way to novel strategies for inhibiting the action of other target proteins. The knowledge gained by completion of the proposed research could be applied in the future to create novel drugs that could potentially inhibit Trop2 or Trop2 regulated signaling.

BODY

Proposed Tasks:

Task 1: Define the functional role of Trop2 in prostate tumorigenesis and stem/progenitor cell self-Renewal (Accomplished).

Task 2: Identify the molecular mechanism through which Trop2 regulates prostate stem/progenitor self- renewal activity and transformation (Accomplished).

Task 3: Determine if Trop2 proteolytic activation is sufficient to transform naïve epithelium (Accomplished).

Progress:

Task 1: Define the functional role of Trop2 in prostate tumorigenesis and stem/progenitor cell self-renewal (Accomplished).

To establish the functional role of Trop2 in prostate tumorigenesis we addressed whether Trop2 is necessary for the transformation process by down-regulating its expression in the prostate epithelia in combination with PI3K pathway using activated AKT (myrAKT) in the *in vivo* regeneration assay. Trop2 expression was down-regulated in the dissociated prostate cells via transduction with lentivirus carrying either scrambled and

GFP or Trop2 specific miRNA and GFP combined with lentivirus carrying myrAKT and RFP. Transduced epithelial cells were combined with UGSM. The grafts composed of prostate cells and UGSM were engrafted under the kidney capsule of SCID mice, allowing regeneration of prostate gland-like structures. Eight weeks post-implantation, grafts will be harvested and evaluated by histological analysis. Histology and presence of scrambled and GFP, Trop2 specific miRNA and GFP, myrAKT and RFP are presented (Fig. 1).

To investigate the functional role of Trop2 in human prostate cancer, we first generated a model of aggressive human prostate cancer. Fresh human prostate tissues were obtained from patients and benign tissue is mechanically separated from cancer. Naïve human prostate epithelium was transduced with the oncogenes commonly altered in human prostate tumors such as Myc and myristoylated/activated AKT (Myc/myrAKT) via lentivirus. Infected cells generate large tumors expressing characterized with castration resistance and high level of Trop2 (Fig. 2). This model will give us the opportunity to test whether Trop2 is necessary for prostate tumorigenesis in human model of advanced prostate cancer.

Task 2: Identify the molecular mechanism through which Trop2 regulates prostate stem/progenitor self- renewal activity and transformation (Accomplished).

Trop2 is cleaved at two distinct sites. Based on Notch cleavage sites[14,15], we predicted the likely TACE cleavage site within the ECD (between alanine 187 and valine 188) and gamma-secretase cleavage site within the transmembrane domain (between glycine 285 and valine 286) (Fig. 3A). Each valine was substituted to a lysine through site directed mutagenesis (V188K and V286K). We tested if mutation at the gamma-secretase cleavage site would result in the appearance of ICP. Similar to previously shown treatment with DAPT accumulation of ICP was observed in the V286K mutant but not in the wild type Trop2 (Fig. 3B). We further tested if the V188K mutant is cleaved. Precipitated media from prostate cells expressing TACE cleavage mutant (V188K), wild-type Trop2-Myc-tag (mTrop2) or RFP (Control) lentivirus was subjected to western blot analysis with antibodies against Myc-tag (ICD) and ECD. Cleaved and shed ECD was detected in the media from cells expressing wild-type Trop2 (mTrop2) but not from the cells expressing the V188K cleavage mutant (Fig. 3C).

Similar results were obtained utilizing TACE and gamma-secretase inhibitors. DAPT and TAPI-2 resulted in significant decrease of ICD localized in the nucleus (Fig. 3D). Knock-down of PS-1 and PS-2 subunits of gamma-secretase resulted in increase of uncleaved membranous Trop2 (Fig. 3E). These results address the proposed Task 2.

Cleavage of Trop2 is required for its self-renewal and proliferative activity. Prior to functionally test the Trop2 cleavage mutants we established their proper sub-cellular localization (Fig. 4A). PEB cells were transduced with the gamma-secretase cleavage mutant (V286K), TACE cleavage mutant (V188K), wild-type Trop2-Myc-tag (mTrop2) or RFP (Control) lentivirus. V286K and V188K localize on the cell surface similarly to the wild type Trop2 as measured by FACS (Fig. 4A). Next, we tested if wild type or mutant Trop2 over-expression increases the percent of cycling cells in benign epithelial cells. Both cleavage mutants V286K and V188K failed to increase proliferation and demonstrated cell cycle profiles similar to the control, while heightened Trop2 led to an increase in cycling cells (Fig 4B). We further tested the effect of Trop2 cleavage mutants on prostate stem/progenitor self-renewal. Prostate stem/progenitor cells ($LSCT^{hi}$) cells were infected with lentivirus expressing RFP (Control), mTrop2, V286K or V188K cleavage mutants and plated in the in vitro sphere assay (Fig. 4C). While heightened levels of wild-type Trop2 promoted sphere formation, the cleavage mutants V286K and V188K failed to enhance self-renewal (Fig. 4C). Moreover, V286K negatively affected sphere formation (Fig. 4C). These results demonstrate that V286K may have a dominant negative effect on endogenous Trop2 while V188K acts as a loss of function mutant**.** Pharmacological inhibition of Trop2 cleavage was also tested in the sphere assay. DAPT and TAPI-2 negatively impacted sphere formation in $LSCT^{hi}$ cells by

reducing sphere number and size (Fig. 5). These results address the proposed Task 2.

Task 3: Determine if Trop2 proteolytic activation is sufficient to transform naïve epithelium (Accomplished).

Heightened expression of ICD and ECD initiates prostatic intraepithelial neoplasia in vivo. We hypothesized that the expression of ICD alone will mimic active Trop2, while a cleavage mutant will represent a loss of function in vivo. ICD to mimic active Trop2, gamma-secretase cleavage mutant V286K and RFP alone were introduced into primary mouse prostate cells via lentiviral infection and subjected to in vivo regeneration assay. Infection efficiency was assessed by the presence of RFP color marker carried by each lentiviral vector. Enhanced expression of V286 and mICD was confirmed by immunofluorescence or immunohistochemistry analysis in three independent grafts. Over-expression of ICD giving rise to lesions that morphologically resemble PIN, a precursor to carcinoma (Fig. 6). V286K regenerated grafts resembled RFP control and showed normal tubule regeneration, demonstrating that cleavage and activation of Trop2 is required for its transformation activity (Fig. 6). ECD alone was also sufficient to induce neoplastic lesions in the prostate in vivo regeneration assay (Fig. 7). These results address the proposed Task 3.

Generationanti-Trop2 ICD antibody. Anti-ICD rabbit polyclonal antibody was generated following the Open Biosystems Custom Polyclonal Antibody Production protocol. Briefly, KLH conjugated mouse and human ICD peptides were used as antigens to immunize two rabbits (mouse peptide: TKRRKSGKYKKVELKELGEMRSEPSL human peptide: TNRRKSGKYKKVEIKELGELRKEPSL). Both rabbits were subjected to a primary injection with 0.25 mg antigen performed by Open Biosystems. 14 days later rabbits were boosted with 0.10 mg antigen followed by serum collection at Day 28. Second booster was performed at day 42, followed by serum collection at day 56. Last booster was performed at day 56 followed by serum collection at day 70 and 72. Each bleed from each rabbit was tested on ELISA, IP, IF and IHC for reactivity with mouse and human ICD. Immunoglobulin fraction was purified from the rabbit serum through protein A/G purification. Purified immunoglobulins were tested by ELISA, IP, IF and IHC for reactivity with mouse and human ICD. IF test is shown in Fig. 8.

Trop2 is cleaved in human prostate cancer. We next asked if cleavage of Trop2 is observed in human prostate cancer. Frozen serial sections (4 micron thickness) of tissues from 11 prostate cancer patients containing both benign and cancer regions were subjected to co-immunofluorescence with antibodies against the ICD and ECD of human Trop2 or H&E staining (Fig. 9). Stained tissues were analyzed for ICD and ECD cellular localization by confocal microscopy. Nuclear ICD was detected only in the cancer specimens, but not in the benign counterparts in 6 out of the 11 patient samples analyzed (6/11) (Fig. 9 and Fig.10). ECD was detected only in the cytoplasm and on the membrane in all patient samples in both cancer and benign regions (Fig. 9 and Fig. 10). We also analyzed the localization of Trop2 ICD in advanced metastatic prostate cancer specimens (Fig. 11). These results indicate that cleavage and activation of Trop2 are associated with human prostate cancer. These results address the proposed Task 3.

KEY RESEARCH ACCOMPLISHMENTS AND MILESTONES:

- We established that Trop2 is necessary for prostate tumorigenesis
- We generated a human model of prostate adenocarcinoma expressing high level of Trop2 for future preclinical testing of Trop2 inhibition and down-regulation.
- We have identified the TACE and gamma secretase cleavage sites within Trop2.
- Cleavage of Trop2 is necessary for its self-renewal and proliferative function.
- ICD and ECD alone drive hyperplasia in vivo.
- ICD localizes in the nucleus in advanced human prostate cancer, but not in the benign prostate.
- The findings outlined here gave us insights into new strategies to inhibit Trop2 signaling in cancer such as

inhibition of cleavage and activation of the molecule.

REPORTABLE OUTCOMES:

Mauscripts:

1. Stoyanova T, Goldstein AS, Cai H, Drake JM, Huang J and Witte ON. (2012). Regulated proteolysis of Trop2 drives epithelial hyperplasia and stem cell self-renewal via beta-catenin signaling. *Genes Dev.*, 26(20):2271-85. PMCID: PMC3475800

2. Stoyanova T, Cooper AR, Drake JM, Liu X, Armstrong AJ, Zhang H, Kohn DB, Huang J, Witte ON and Goldstein AS (2013). Prostate cancer originating in basal cells progresses to adenocarcinoma propagated by luminal-like cells. ***Proc Natl Acad Sci U S A.***, 110(50):20111-6. PMCID: PMC3864278

CONCLUSION:

We have now shown that Trop2 is a new regulator of stem/progenitor activity and tumorigenesis in the prostate. Trop2 controls self-renewal, proliferation and tissue hyperplasia through two cleavage products (ICD and ECD) generated by RIP. The intracellular domain of Trop2 is released from the membrane and accumulates in the nucleus. Nuclear ICD is found in human prostate cancer but not in the cancer-adjacent benign tissue, suggesting a role for Trop2 cleavage in tumorigenesis. Heightened expression of Trop2 intracellular or extracellular domains are sufficient to initiate precursor lesions to prostate cancer *in vivo*. Importantly, we demonstrate that Trop2 loss of function cleavage mutants are deficient in inducing self-renewal and tumorigenesis in the prostate. These findings suggest that heightened expression of Trop2 is selected for in epithelial cancers to enhance the stem-like properties of self-renewal and proliferation. Identifying the factors that regulate self-renewal will enhance our understanding of the tumorigenic process and lead to the design of novel cancer therapies.

REFERENCES:

1. Fang, Y.J., *et al.* Elevated expressions of MMP7, TROP2, and survivin are associated with survival, disease recurrence, and liver metastasis of colon cancer. *Int J Colorectal Dis* 24, 875-884 (2009).
2. Kobel, M., *et al.* Ovarian carcinoma subtypes are different diseases: implications for biomarker studies. *PLoS Med* 5, e232 (2008).
3. Muhlmann, G., *et al.* TROP2 expression as prognostic marker for gastric carcinoma. *J Clin Pathol* 62, 152-158 (2009).
4. Fong, D., *et al.* High expression of TROP2 correlates with poor prognosis in pancreatic cancer. *Br J Cancer* 99, 1290-1295 (2008).
5. Ohmachi, T., *et al.* Clinical significance of TROP2 expression in colorectal cancer. *Clin Cancer Res* 12, 3057-3063 (2006).
6. Nakashima, K., *et al.* Serological identification of TROP2 by recombinant cDNA expression cloning using sera of patients with esophageal squamous cell carcinoma. *Int J Cancer* 112, 1029-1035 (2004).
7. Fong, D., *et al.* TROP2: a novel prognostic marker in squamous cell carcinoma of the oral cavity. *Mod Pathol* 21, 186-191 (2008).
11. Trerotola, M., *et al.* Upregulation of Trop-2 quantitatively stimulates human cancer growth. *Oncogene* (2012).
12. Wang, J., Day, R., Dong, Y., Weintraub, S.J. & Michel, L. Identification of Trop-2 as an oncogene and an attractive therapeutic target in colon cancers. *Mol Cancer Ther* 7, 280-285 (2008).
13. Goldstein, A.S., *et al.* Trop2 identifies a subpopulation of murine and human prostate basal cells with stem cell characteristics. *Proc Natl Acad Sci U S A* 105, 20882-20887 (2008).
14. Schroeter, E.H., Kisslinger, J.A. & Kopan, R. Notch-1 signalling requires ligand-induced proteolytic release of intracellular domain. *Nature* 393, 382-386 (1998).

15. Mumm, J.S., *et al.* A ligand-induced extracellular cleavage regulates gamma-secretase-like proteolytic activation of Notch1. *Mol Cell* 5, 197-206 (2000).

APPENDICES:
Supporting Data:

Figure 1. Trop2 is necessary for prostate transformation driven by myrAKT.

Figure 2. Generation of a human model of prostate adenocarcinoma expressing high levels of Trop2

Figure 3. Trop2 is cleaved at two distinct sites by TACE and gamma secretase.

Figure 4. Cleavage of Trop2 is necessary for its self-renewal and proliferative function.

Figure 5. Cleavage of Trop2 is necessary for its self-renewal function.

Figure 6. ICD alone drive hyperplasia in vivo.

Figure 7. ECD alone drive hyperplasia in vivo.

Figure 8. Immunofluorescence using anti-Trop2 ICD antibody.

Figure 9. Nuclear localization of ICD is found in human prostate cancer.

Figure 10. ICD localizes in the nucleus in human prostate cancer, but not in the benign prostate.

Figure 11. ICD localizes in the nucleus in advanced metastatic human prostate cancer, but not in the benign prostate.

Figure 1

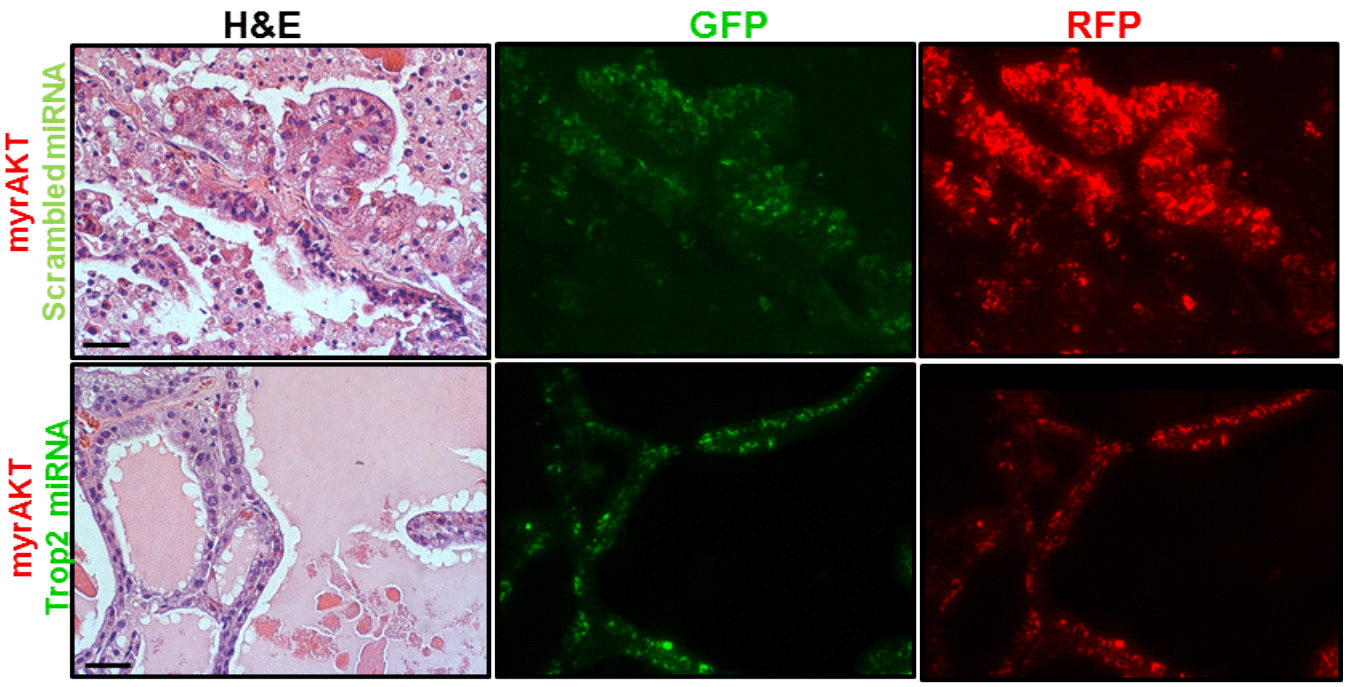

Figure 1. Trop2 is necessary for prostate transformation driven by myrAKT. Trop2 expression was down-regulated in dissociated primary prostate cells via transduction with lentivirus carrying GFP and Trop2 specific miRNA or as a control scrambled miRNA followed by the *in vivo* regeneration assay. Histology of the recovered grafts is presented in the left panels. Scale bars represent 50 microns. RFP and GFP represents infection efficiency with myrAKT expressing lentivirus or miRNA expressing lentivirus (right panels).

Figure 2.

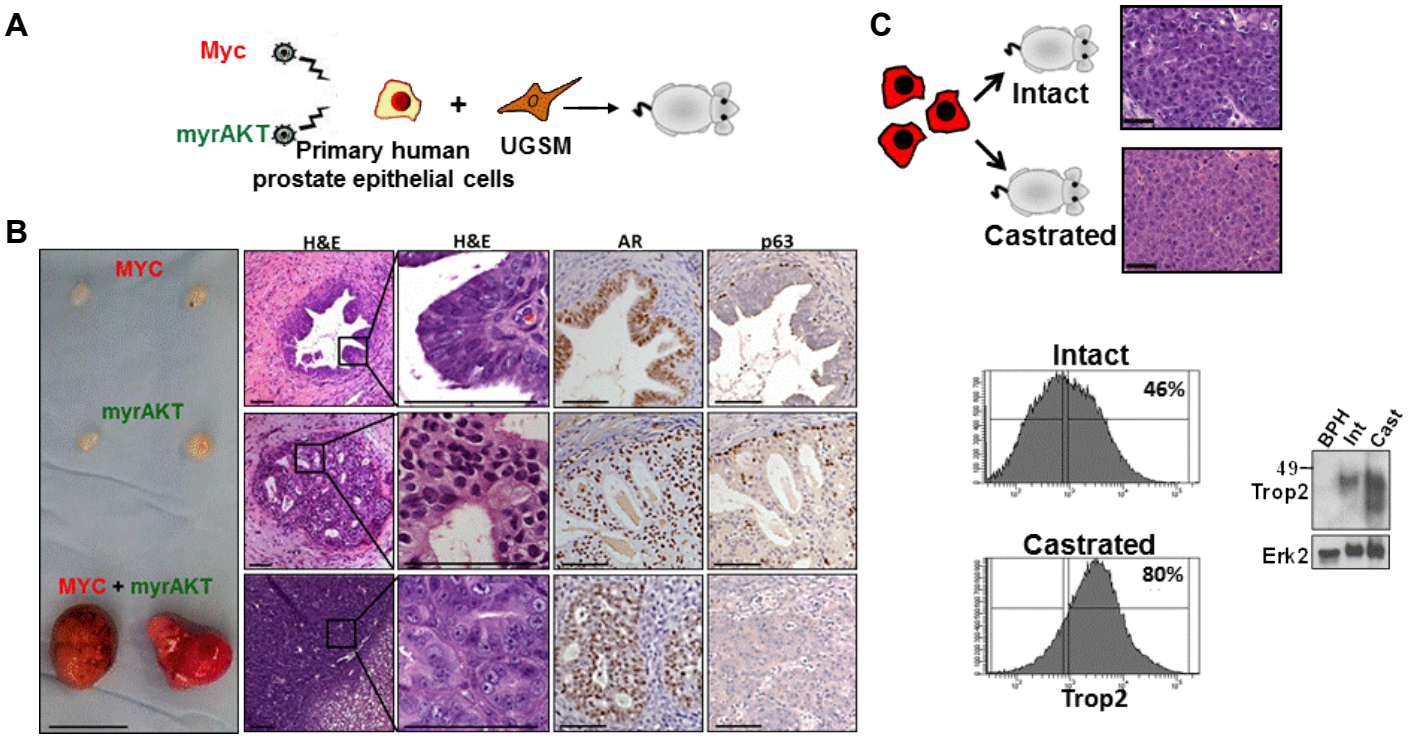

Figure 2. Generation of a human model of prostate adenocarcinoma expressing high levels of Trop2. (A) Schematic representation of generation of human model of advanced prostate adenocarcinoma initiated from primary human epithelial cells. **(B)** $1x10^5$ primary human epithelial cells were transduced with Myc/myrAKT. Infected human epithelial cells were combined transplanted into immunodeficient mice. Recovered tumors for each condition are presented. **(C)** FACS staining showing cell surface expression of Trop2 in the Myc/myrAKT model prior and post adndogen ablation (castration). Western blot for Trop2 of benign human prostatic hyperplasia (BPH) and secondary Myc/myrAKT tumor recovered from intact (Int) or castrated recipients (Cast).

Figure 3

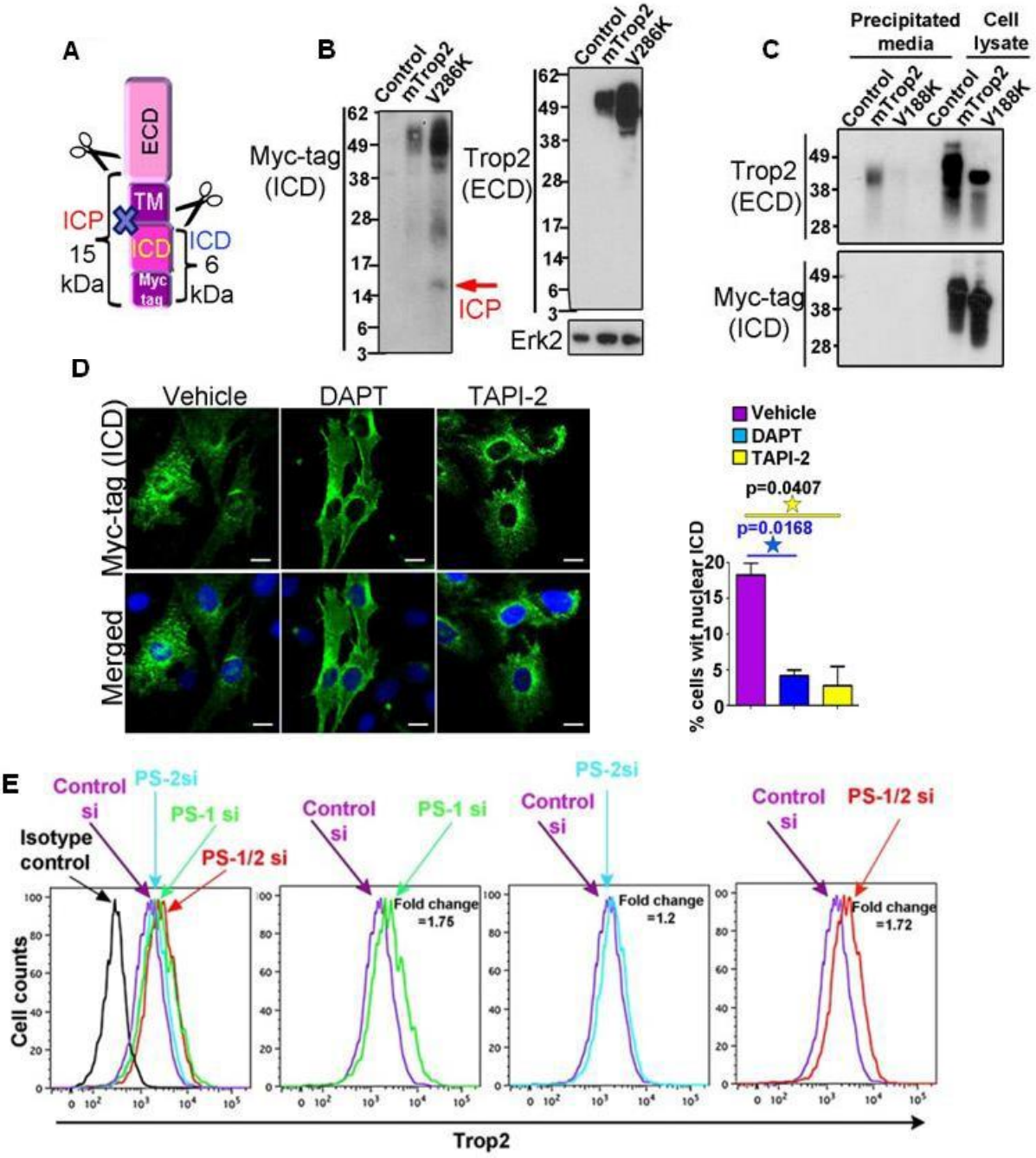

Figure 3. Trop2 is cleaved at two distinct sites by TACE and gamma secretase. (A) Schematic representation of generation of intermediate cleavage product (ICP) upon inhibition of gamma secretase. **(B)** PEB cells were infected with lentivirus expressing RFP (Control), mTrop2-Myc-tag and RFP (mTrop2) or V286K-Myc-tag (V286) mutant. Cells were subjected to western blot with antibodies against Myc-tag or the ECD of Trop2. Red arrow shows ICP appearance in V286K demonstrating not fully processed Trop2 and the blue arrow indicates full length Trop2 (FLTrop2). **(C)** Serum free media from TRAMP-C2 cells transduced with RFP lentivirus (Control), mTrop2-Myc-tag (mTrop2) or V188K-Myc-tag (V188K) was precipitated followed by western blot. Only the ECD of Trop2 was detected in the precipitated media from cells expressing wild-type Trop2, but not from cells expressing V188K. **(D)** TRAMP-C2 expressing mTrop2 with a C-teminal Myc-tag to follow the ICD were treated with DMSO (Vehicle), DAPT or TAPI-2. 24hours post treatment cells were fixed and stained with anti-Myc-tag or anti-ECD antibody and DAPI and subjected to confocal microscopy. Scale bar represents 10 microns. **(E)** PEB cells expressing mTrop2-RFP were transfected with control, PS-1, PS-2 or both PS-1 and PS-2 siRNA and stained with anti-Trop2 ECD antibody followed by FACS analysis. Fold change of mean fluorescent intensity compared to control siRNA is shown.

Figure 4

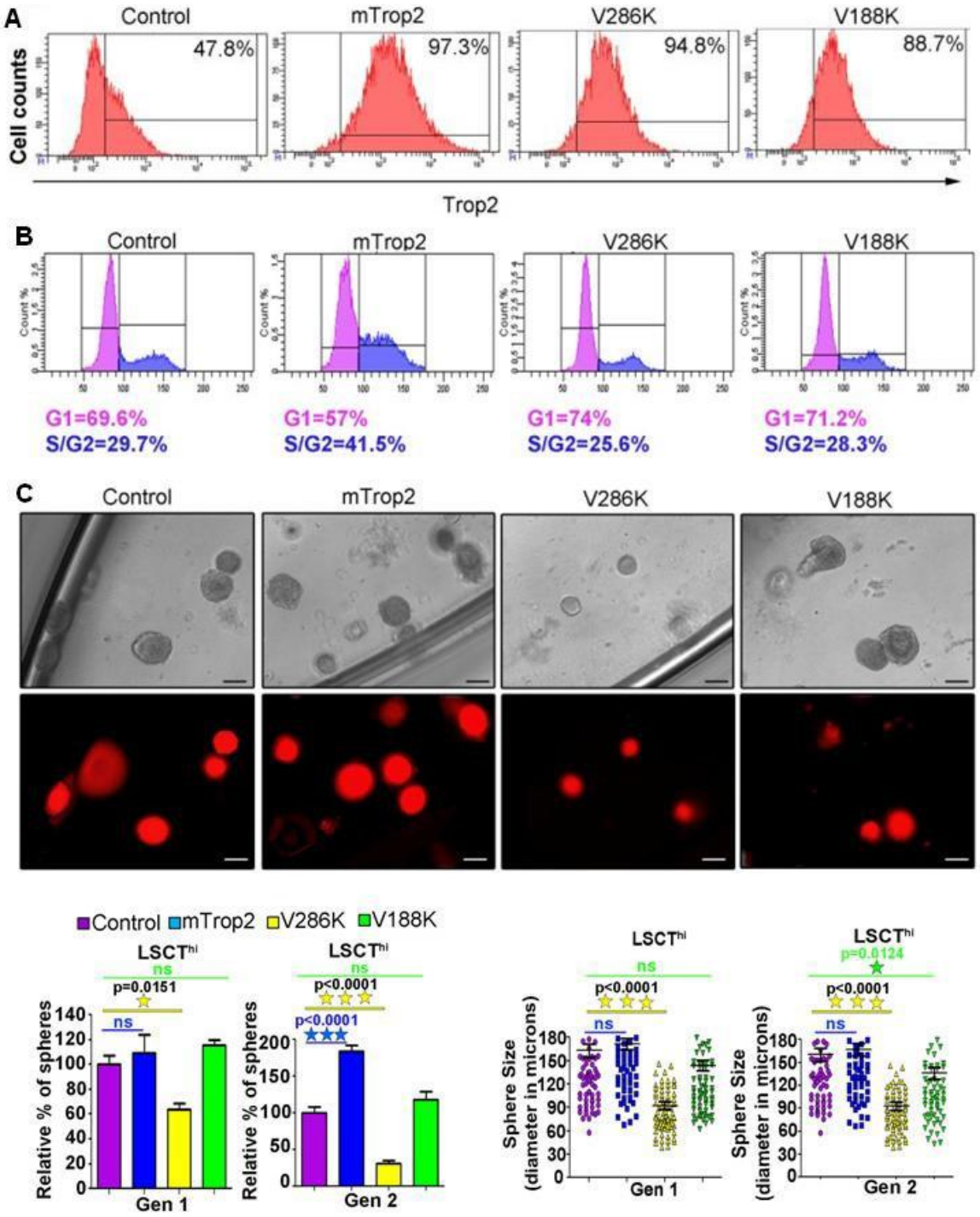

Figure 4. Cleavage of Trop2 is necessary for its self-renewal and proliferative function. (A) FACS analysis of PEB cells transduced with lentivirus carrying RFP (Control), mTrop2, V188K or V286K and stained with anti-Trop2 ECD antibody for analysis by FACS. **(B)** Cell cycle analysis of PEB cells transduced with lentivirus carrying RFP (Control), mTrop2, V188K or V286K and stained with PI. **(C)** LSCT^{hi} cells were isolated by FACS. Equal number of cells were infected with RFP (Control), mTrop2, V286K or V188K mutants expressing lentivirus and plated in sphere assay in triplicates. Representative pictures of spheres expressing mTrop2, V286K or V188K mutants are shown. Scale bars represent 100 microns. Sphere number and diameter in microns were quantified after generations 1 (Gen 1) and 2 (Gen 2). Sphere number in each sample is presented as percentage normalized to the RFP infected spheres (Control) (left graphs). Data are represented as mean +/- SEM.

Figure 5

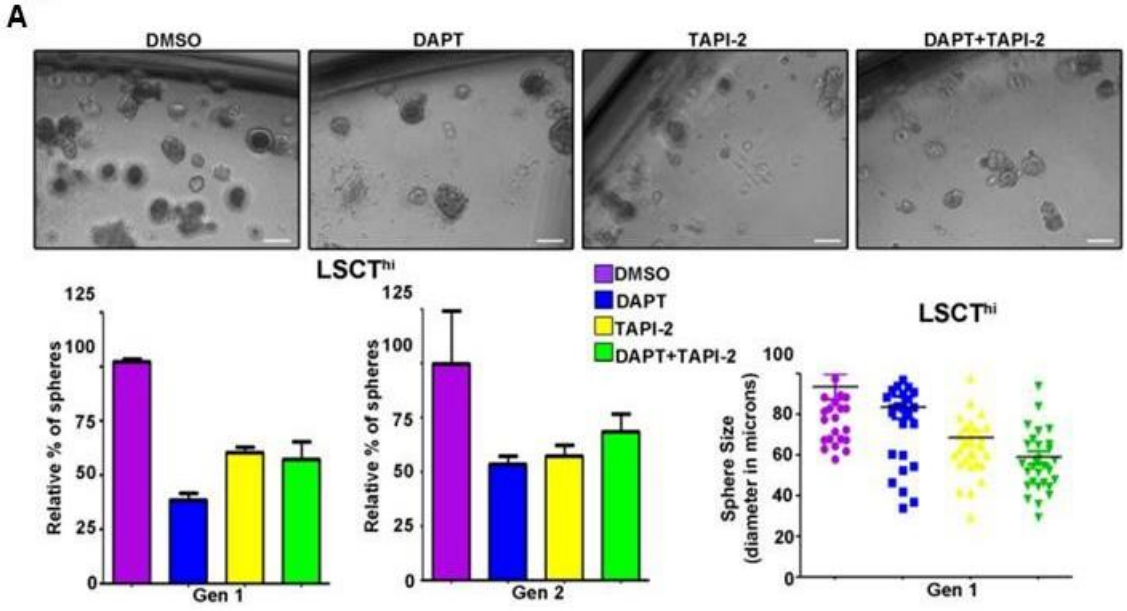

Figure 5. Cleavage of Trop2 is necessary for its self-renewal function. Equal numbers of progenitor cells ($LSCT^{hi}$) were plated in triplicate and treated with DMSO, DAPT, TAPI-2 or the combination of DAPT and TAPI-2 every 48h hours. Upper panels show images of spheres grown in the indicated conditions. Scale bars represent 100 microns. Sphere number and sphere size was reduced upon treatment with DAPT and TAPI-2 (bottom graphs). Sphere size was measured at Gen 1.

Figure 6

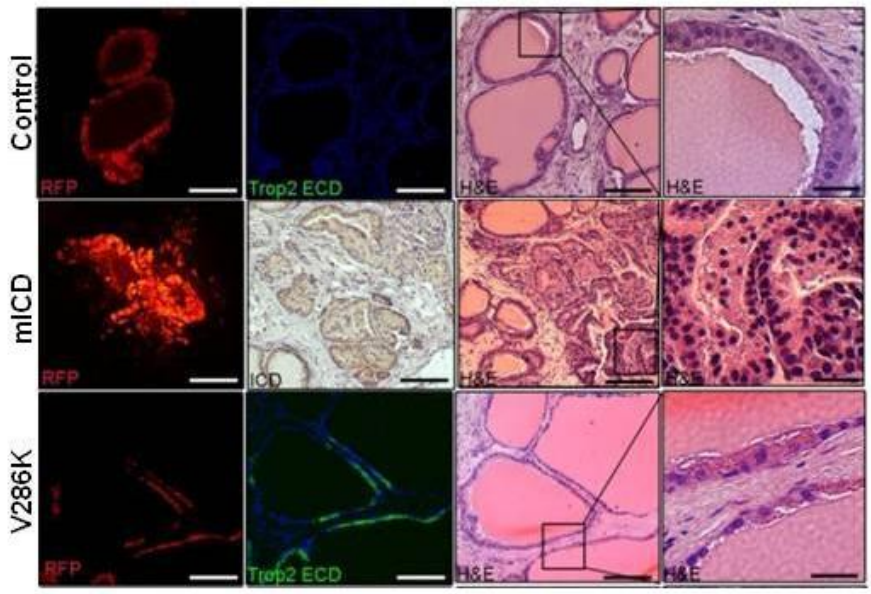

Figure 6. ICD alone drive hyperplasia in vivo. Dissociated primary prostate cells were transduced with RFP (Control), mICD or V286K expressing lentivirus. Infected prostate cells were combined with UGSM and subjected to the in vivo regeneration assay. Eight weeks later grafts were recovered, fixed in formalin and sectioned for histological analysis. Left panels represents immunofluorescence (IF) showing infected tubules, middle panel shows immunofluorescence with anti-Trop2 ECD or immunohistochemistry (IHC) with anti-ICD or anti-AKT respectively. Right two panels show the histology of the recovered grafts. One out of three independent experiments is shown. Scale bars represent 200 or 50 (right panels) microns.

Figure 7

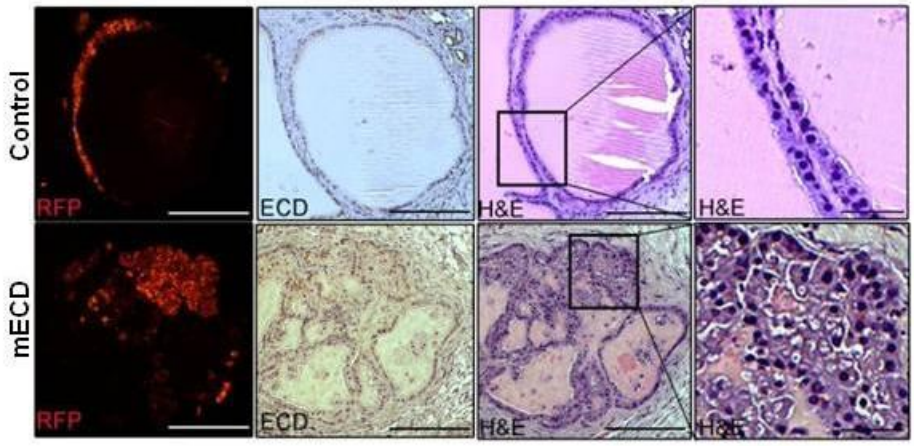

Figure 7. ECD alone drive hyperplasia in vivo. Dissociated primary prostate cells were transduced with lentivirus carrying RFP (Control) or ECD-Fc. Infected prostate cells were combined with UGSM and subjected to the *in vivo* regeneration assay. Eight weeks later, tissues were removed and gland histology was examined. Left panels represent immunofluorescence (IF) showing infected tubules, middle panels show immunofluorescence with anti-Trop2 ECD. Right two panels show the histology of the recovered grafts. One out of two independent experiments is shown. Scale bars represent 100 or 50 (right panels) microns.

Figure 8

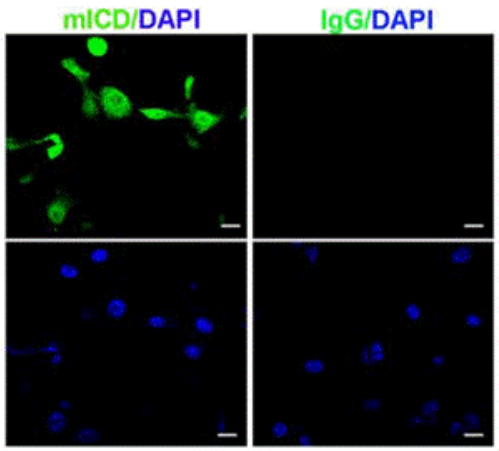

Figure 8. Immunofluorescence using anti-Trop2 ICD antibody. TRAMP-C2 cells were infected with lentivirus expressing mouse Trop2 ICD (mICD). Cells were fixed and subjected to immunofluorescence using anti-ICD or a control (IgG) antibody. Confocal microscopy images are presented. Scale bars represent 10 microns.

Figure 9

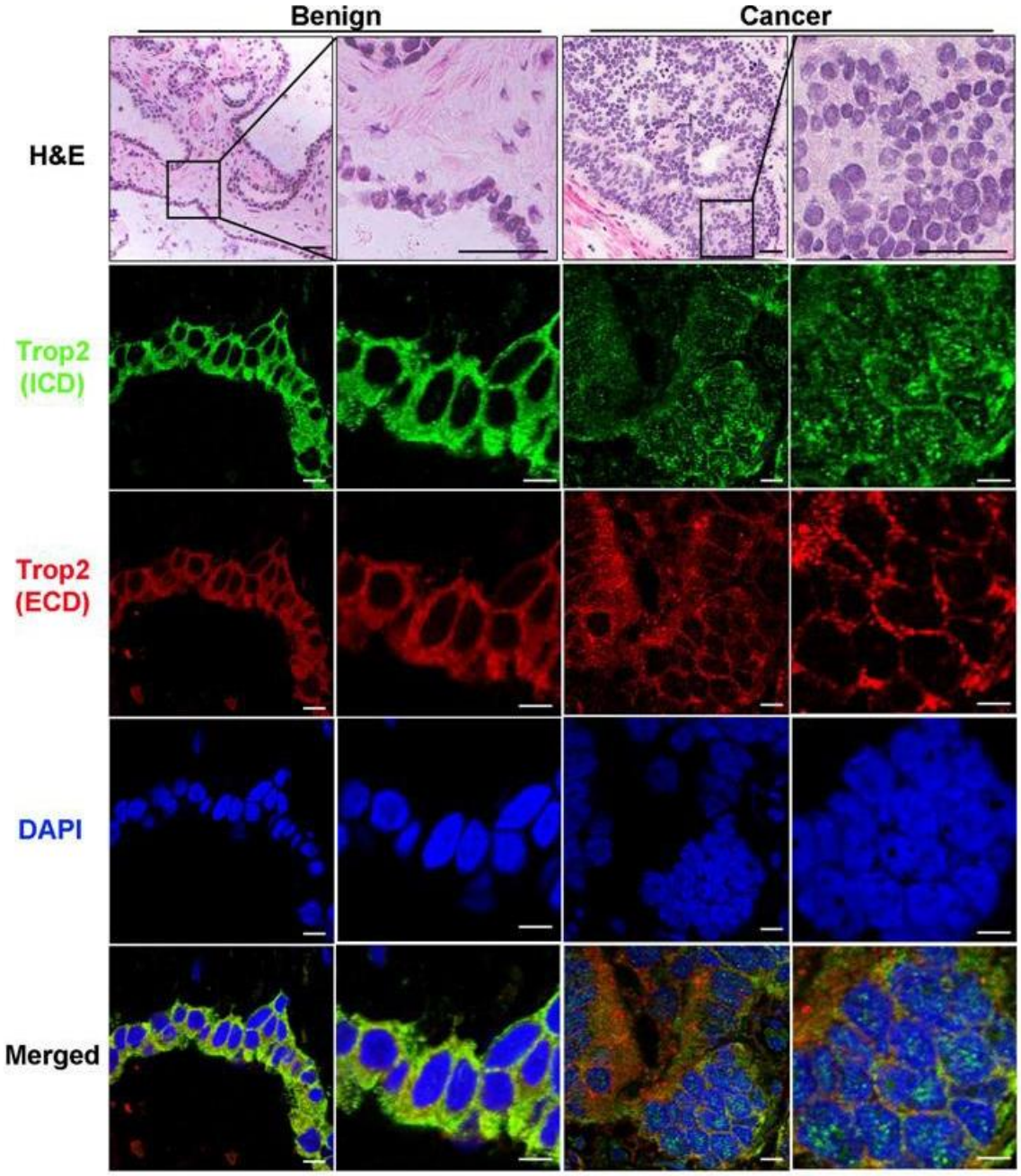

Figure 9. Nuclear localization of ICD is found in human prostate cancer. Immunofluorescence with anti-ECD, anti-ICD antibodies and DAPI of tissues from human prostate cancer patients. One out of eleven patient samples is shown. A benign region is presented in the left two columns and a cancer region is shown in the right two columns. Histology is shown in the upper two panels by H&E staining. Scale bars represent 100 microns. ICD nuclear localization can be detected only in cancer, but not in the benign prostate (green). ECD is found in the cytoplasm and on the membrane in the benign and cancer regions (Red). DAPI demonstrates nuclear staining (blue). Merged images are presented in the bottom panels. Scale bars in the immunofluorescence images represent 10 microns to visualize ICD and ECD localization.

Figure 10

Prostatic Adenocarcinoma			Nuclear ICD	
Gleason grade	Pathologic stage	Age	Benign	Cancer
9	pT3a pN0 Mx	60	No	Yes
9	pT3a pN0 Mx	60	No	Yes
8	pT3a N1 Mx	71	No	Yes
7	pT2c Nx Mx	52	No	No
7	pT2c Nx Mx	56	No	Yes
7	pT2c Nx Mx	67	No	Yes
7	pT2a N0 Mx	71	No	No
7	pT3a Nx Mx	56	No	Yes
7	pT3b N0 Mx	60	No	No
7	pT3b N0 Mx	68	No	No
6	pT2b N0 Mx	49	No	No

Figure 10. ICD localizes in the nucleus in human prostate cancer, but not in the benign prostate. Table shows patient samples analyzed in Figure 4. Pathologic stage is based on the 7th Edition AJCC Cancer Staging Manual. The presence of nuclear ICD is shown in the last two columns.

Figure 11

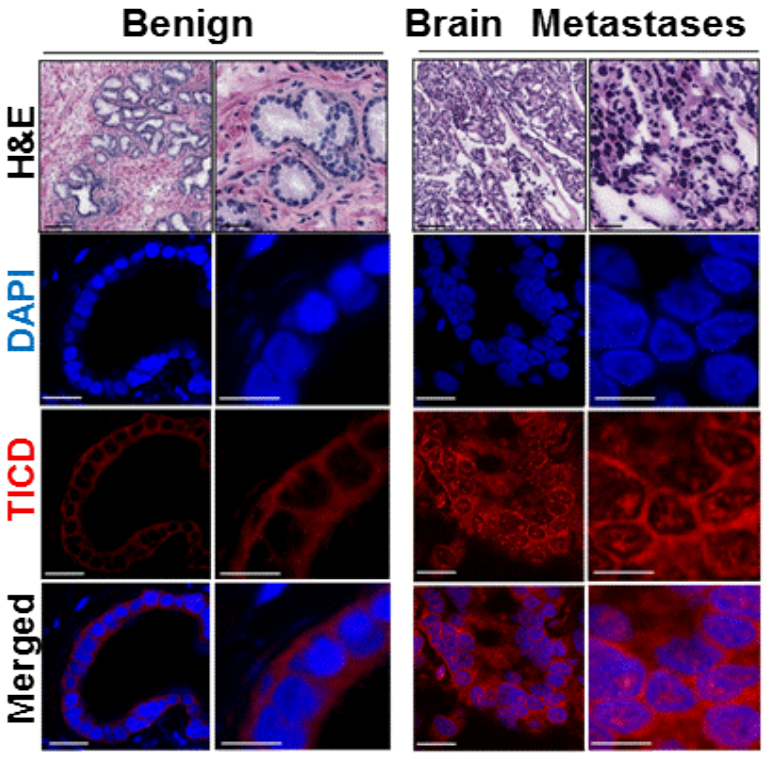

Figure 11. Nuclear localization of ICD is found in advanced metastatic human prostate cancer. Serial frozen sections of benign prostate and brain metastatic CRPC (Dura Met) were either stained with hematoxylin and eosin (H&E) (upper panels) or co-stained with anti-Trop2 ICD intracellular domain (in red) and DAPI (blue). Histology is presented in the upper panels. Scale bars show 100 and 30 microns. Single color or merged images of Trop2 ICD and DAPI co-staining were shown as indicated. Scale bars represent 20 and 10 microns.

Regulated proteolysis of Trop2 drives epithelial hyperplasia and stem cell self-renewal via β-catenin signaling

Tanya Stoyanova, Andrew S. Goldstein, Houjian Cai, et al.

Genes Dev. 2012 26: 2271-2285
Access the most recent version at doi:10.1101/gad.196451.112

Regulated proteolysis of Trop2 drives epithelial hyperplasia and stem cell self-renewal via β-catenin signaling

Tanya Stoyanova,[1] Andrew S. Goldstein,[2,3,4] Houjian Cai,[1,7] Justin M. Drake,[1] Jiaoti Huang,[5] and Owen N. Witte[1,2,3,4,6,8]

[1]Department of Microbiology, Immunology, and Molecular Genetics, University of California at Los Angeles, Los Angeles, California 90095, USA; [2]Department of Molecular and Medical Pharmacology, University of California at Los Angeles, Los Angeles, California 90095, USA; [3]Jonsson Comprehensive Cancer Center, University of California at Los Angeles, Los Angeles, California 90095, USA; [4]Eli and Edythe Broad Center of Regenerative Medicine and Stem Cell Research, University of California at Los Angeles, Los Angeles, California 90095, USA; [5]Department of Pathology and Laboratory Medicine, University of California at Los Angeles, Los Angeles, California 90095, USA; [6]Howard Hughes Medical Institute, University of California at Los Angeles, Los Angeles, California 90095, USA

The cell surface protein Trop2 is expressed on immature stem/progenitor-like cells and is overexpressed in many epithelial cancers. However the biological function of Trop2 in tissue maintenance and tumorigenesis remains unclear. In this study, we demonstrate that Trop2 is a regulator of self-renewal, proliferation, and transformation. Trop2 controls these processes through a mechanism of regulated intramembrane proteolysis that leads to cleavage of Trop2, creating two products: the extracellular domain and the intracellular domain. The intracellular domain of Trop2 is released from the membrane and accumulates in the nucleus. Heightened expression of the Trop2 intracellular domain promotes stem/progenitor self-renewal through signaling via β-catenin and is sufficient to initiate precursor lesions to prostate cancer in vivo. Importantly, we demonstrate that loss of β-catenin or Trop2 loss-of-function cleavage mutants abrogates Trop2-driven self-renewal and hyperplasia in the prostate. These findings suggest that heightened expression of Trop2 is selected for in epithelial cancers to enhance the stem-like properties of self-renewal and proliferation. Defining the mechanism of Trop2 function in self-renewal and transformation is essential to identify new therapeutic strategies to block Trop2 activation in cancer.

[*Keywords*: Trop2; self-renewal; transformation; regulated intramembrane proteolysis; β-catenin]

Supplemental material is available for this article.

Received May 15, 2012; revised version accepted September 6, 2012.

Trop2 is a type I transmembrane glycoprotein highly expressed in various epithelial cancers, such as advanced squamous cell carcinoma of the oral cavity and colorectal, pancreatic, gastric, and ovarian cancer, and its high levels correlate with poor prognosis and survival (Nakashima et al. 2004; Ohmachi et al. 2006; Fong et al. 2008a,b; Kobel et al. 2008; Fang et al. 2009; Muhlmann et al. 2009). Monoclonal antibodies targeting Trop2 exhibit potent anti-cancer activity through cytotoxicity in multiple xenograft models of cancer, including prostate, pancreatic, breast, colon, endometrial, and lung cancer (Young et al. 2008; Govindan et al. 2009; Alberti 2012). Knockdown of Trop2 abrogates the growth of colon cancer cell lines and inhibits tumor initiation and progression in mice (Wang et al. 2008; Trerotola et al. 2012a). Recently, Trop2 was demonstrated to play dual functions in tumorigenesis—as a tumor suppressor and an oncogene (Wang et al. 2008, 2011).

Cancer cells share multiple characteristics with adult tissue stem cells, such as self-renewal and proliferative capacity. Many factors that regulate stem/progenitor function and development have been found altered in prostate cancer. Activation of the PI3K pathway promotes self-renewal and has a prominent role in prostate malignancy (Yoshimoto et al. 2006; Mulholland et al. 2009). The Polycomb protein Bmi-1 regulates both self-renewal and tumorigenesis in the murine prostate, and its increased expression correlates with unfavorable outcome (van Leenders et al. 2007; Lukacs et al. 2010). Other pathways, such as Wnt and Notch, control the balance between stem/progenitor self-renewal and differentiation

[7]Present address: Hollings Cancer Center, Department of Medicine, Medical University of South Carolina, Charleston, SC 29425, USA.
[8]Corresponding author
E-mail owenwitte@mednet.ucla.edu
Article is online at http://www.genesdev.org/cgi/doi/10.1101/gad.196451.112. Freely available online through the *Genes & Development* Open Access option.

and are also frequently dysregulated in prostate cancer (Shou et al. 2001; Chen et al. 2004; Wang et al. 2006).

Several groups have demonstrated that Trop2 is a marker of stem/progenitor cells in adult tissues. Trop2 is not expressed in the normal liver but appears on the undifferentiated oval cells shortly after their activation due to liver injury (Okabe et al. 2009). Trop2 also enriches for endometrial-regenerating cells in a dissociated cell tissue recombination assay (Memarzadeh et al. 2010). In the human and mouse prostate, the Trop2-expressing subpopulation of basal cells ($Trop2^{hi}$) possesses stem cell capacities such as self-renewal, tissue regeneration, and multilineage differentiation (Goldstein et al. 2008, 2010).

Despite its broad expression in cancer, little is known about Trop2-mediated signaling. A recent study demonstrated that Trop2 inhibits cell adhesion by promoting the interaction between β-1 integrin and RACK1 in prostate cancer cell lines (Trerotola et al. 2012b). Trop2 has been reported to control the interaction with the extracellular matrix during kidney development (Tsukahara et al. 2011). Finally, Trop2 is demonstrated to regulate Ca^{2+} signaling, and its cytoplasmic tail is phosphorylated by protein kinase C (PKC) in vitro (Basu et al. 1995; Ripani et al. 1998). The downstream signals transmitted upon phosphorylation of Trop2 remain to be defined.

Regulated intramembrane proteolysis (RIP) is a mechanism of processing and activation of transmembrane proteins, including adhesion molecules such as N-cadherin and E-cadherin (Brown et al. 2000; Maretzky et al. 2005; Lal and Caplan 2011; Solanas et al. 2011). Members of the Notch family of receptors, involved in cell fate decisions, are also regulated by RIP (De Strooper et al. 1999). RIP has been recently associated with cancer. Activating mutations of Notch 1 resulting in its cleavage are found in 56% of patients suffering from T-ALL (T-cell acute lymphoblastic leukemia) and are also associated with various solid tumors (Weng et al. 2004; Lobry et al. 2011; Ranganathan et al. 2011). A recent study revealed that EpCAM, an adhesion protein that shares 50% homology with Trop2, functions in cellular transformation via RIP cleavage mechanisms (Maetzel et al. 2009). High levels of activated EpCAM are detected in breast, prostate, head and neck, and esophageal cancers and has been associated with poor prognosis in thyroid cancer (Ralhan et al. 2010a,b).

Although Trop2 expression is elevated in various carcinomas and serves as a marker of stem/progenitor cells, the functional role of Trop2 in self-renewal, its relation to transformation, and the molecular mechanisms by which Trop2 transmits signals to regulate these processes remain unclear. In the present study, we demonstrate that Trop2 controls stem/progenitor self-renewal and tissue regeneration in the prostate. Trop2 is activated by RIP, and its cleavage is carried out by the TNF-α-converting enzyme (TACE) followed by γ-secretase cleavage within the transmembrane domain, resulting in shedding of the extracellular domain (ECD) and accumulation of the intracellular domain (ICD) to the nucleus. Nuclear ICD is found in human prostate cancer but not in the cancer-adjacent benign tissue, suggesting a role for Trop2 cleavage in tumorigenesis. The ICD alone promotes self-renewal, initiates prostatic intraepithelial neoplasia (PIN), and is involved in a signaling cascade dependent on β-catenin. Nuclear β-catenin colocalizes with nuclear ICD in human prostate cancer. Moreover, loss of β-catenin abolishes Trop2-driven self-renewal and transformation activity. Blocking cleavage of Trop2 by mutating its cleavage sites abrogates its self-renewal and transformation capacity, demonstrating that RIP is required for Trop2 activity. Defining the functional role of Trop2 in self-renewal and transformation and delineating the molecular mechanism of Trop2 action may promote development of new therapeutic strategies to inhibit Trop2 signaling in a wide range of epithelial tumors.

Results

Trop2 regulates self-renewal of stem/progenitor cells and tissue regeneration in the adult prostate

Stem/progenitor cells can be expanded in an in vitro sphere assay in which sphere number over multiple passages measures self-renewal activity, and sphere size is a reflection of progenitor proliferation capacity (Reynolds and Weiss 1996; Dontu et al. 2003a,b, 2004; Xin et al. 2007; Lukacs et al. 2010). By using cell surface markers CD49f, Sca-1, and Trop2, we previously demonstrated the ability to enrich for luminal ($CD49f^{lo}$, Sca-1^{-}) and basal (LSC or $CD49f^{hi}$, $Sca1^{+}$) cells and to further subdivide the basal cells into $Trop2^{lo}$ ($LSCT^{lo}$) and stem/progenitor enriched $Trop2^{hi}$ fractions ($LSCT^{hi}$) (Supplemental Fig. S1A; Lawson et al. 2007; Goldstein et al. 2008). To investigate the functional role of Trop2 in stem/progenitor cell self-renewal, we constructed lentiviral vectors expressing a potent Trop2 microRNA (miRNA) mimic (miRNA Trop2) to diminish the levels of Trop2 or a nontargeting scrambled miRNA (miRNA scrambled) carrying the green fluorescent protein (GFP) for visualization of transduced cells (Supplemental Fig. S1B). The progenitor-enriched population $LSCT^{hi}$ was transduced with miRNA Trop2 or miRNA scrambled, plated in the sphere assay, and further passaged to second-generation spheres to measure self-renewal (Gen 2) (Fig. 1A). Trop2 knockdown resulted in a fourfold reduction in self-renewal activity, as measured by sphere number upon passaging (Gen 2) (Fig. 1A). The progenitor proliferation capacity assessed by the sphere size was also significantly reduced upon knockdown of Trop2, as demonstrated by the twofold reduction in sphere diameter (Fig. 1A).

Dissociated prostate cells are able to regenerate prostatic tubules when combined with urogenital sinus mesenchyme (UGSM) and implanted under the kidney capsule of severe combined immunodeficiency (SCID) mice (Cunha and Lung 1978; Xin et al. 2003). Previous interrogation of different epithelial subpopulations revealed that only $LSCT^{hi}$ basal stem/progenitor cells possess regenerative activity and can give rise to a prostate-like structure in the in vivo regeneration assay (Goldstein et al. 2008). To assess the role of Trop2 in prostate tubule formation and

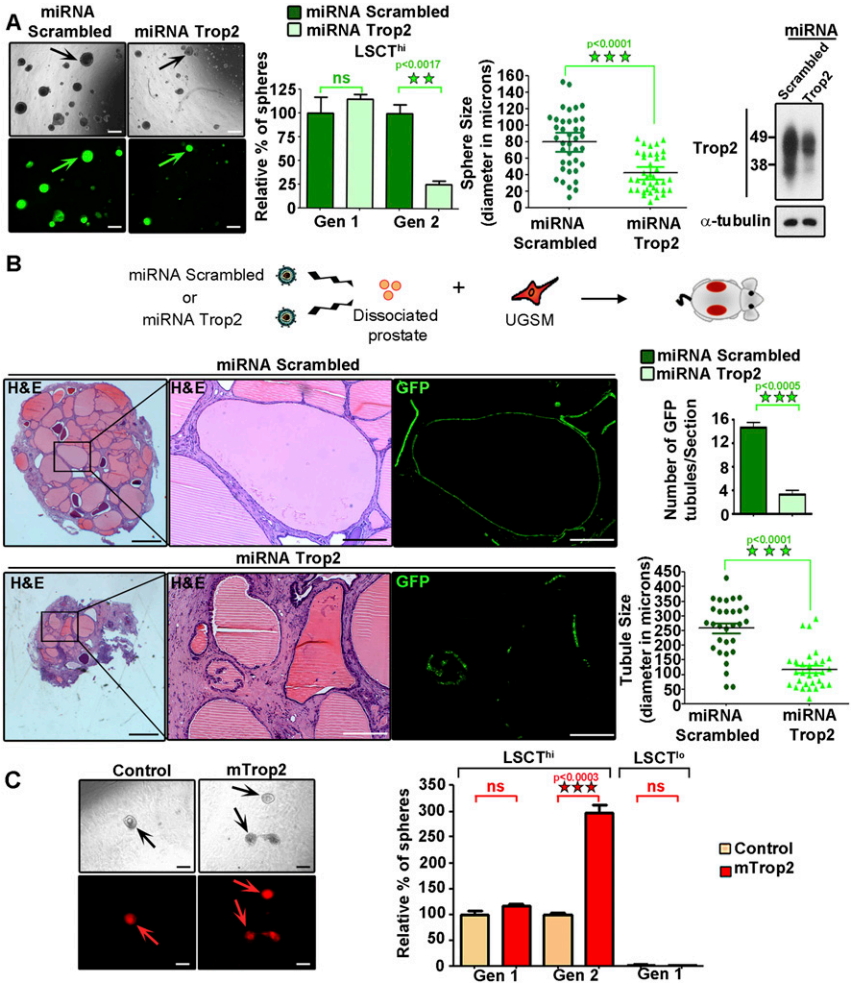

Figure 1. Trop2 regulates self-renewal in the prostate. (*A*) Prostate progenitor cells ($LSCT^{hi}$) were isolated by fluorescence-activated cell sorting (FACS). An equal number of $LSCT^{hi}$ cells was infected with a lentivirus expressing scrambled miRNA and GFP (miRNA Scrambled) or a lentivirus expressing Trop2 miRNA and GFP (miRNA Trop2), followed by the in vitro sphere assay. Each sample in the experiment was plated in triplicate. Three independent experiments were performed. The *left* panels show representative sphere pictures and nearly 100% infection efficiency, assessed by GFP-positive spheres. Bar, 100 μm. Sphere number and diameter, referred to as sphere size in microns, were counted at generation 1 (Gen 1). Spheres were dissociated into single cells, and an equal number of cells was plated for passaging to generation 2 (Gen 2). Sphere number is presented as percentage normalized to miRNA Scrambled. Data are represented as mean of the triplicates ± SEM. Statistical analysis is shown. (ns) Nonsignificant. The level of Trop2 knockdown is shown by Western blot in spheres at Gen 1 prior to replating for Gen 2. Trop2 is highly glycosylated and appears as an irregular band between 35 and 50 kD (Supplemental Fig. S1C). (*B*) Trop2 expression was downregulated in dissociated primary prostate cells via transduction with miRNA Scrambled or miRNA Trop2 lentivirus expressing GFP followed by the in vivo regeneration assay. One out of three representative recovered grafts for each condition is shown. Bars: *left* panels, 800 μm; *right* panels, 100 μm. The number of GFP tubules per section for each graft was counted in miRNA Scrambled or miRNA Trop2 grafts and plotted as mean ± SEM. Diameter of 30 GFP-positive tubules was measured in microns. (*C*) An equal number of $LSCT^{hi}$ or $LSCT^{lo}$ cells was transduced with a RFP-expressing (control) or mouse Trop2- and RFP-expressing (mTrop2) lentivirus and plated in triplicate for each sample in an in vitro sphere assay. Three independent experiments were performed. The *left* panels represent spheres from $LSCT^{hi}$ transduced with either RFP (control) or mTrop2 and RFP (mTrop2). Bars, 100 μm. $LSCT^{hi}$ sphere number was counted at Gen 1 and Gen 2, while $LSCT^{lo}$ sphere number was counted only at Gen 1, since no growth was observed. Sphere number is presented as percentage normalized to RFP transduced spheres and presented as mean of the triplicates ± SEM.

regeneration in vivo, dissociated primary prostate cells (2.5×10^5) were transduced with miRNA Trop2 or miRNA scrambled lentivirus at an equivalent multiplicity of infection (MOI = 50) (Fig. 1B). Transduced prostate cells were combined with UGSM cells (2.5×10^5) and subjected to an in vivo regeneration assay (Fig. 1B). Upon histological analysis of the recovered grafts, we observed that Trop2 knockdown grafts contained fourfold fewer infected tubules when compared with the control (Fig. 1B). Tubules derived from Trop2 knockdown epithelium were also smaller, with an average diameter of 100 μm, in contrast to the control grafts, with an average diameter of 260 μm (Fig. 1B). Trop2 loss attenuates prostate regeneration in vivo and sphere formation in vitro, demonstrating that Trop2 not only is a marker for stem/progenitor cells, but also functionally regulates adult tissue self-renewal and prostate regeneration.

The functional role of Trop2 in self-renewal was also assessed by measuring sphere formation upon Trop2 overexpression. $LSCT^{lo}$ and $LSCT^{hi}$ basal cells were infected with either mouse Trop2- and RFP-expressing (mTrop2) or RFP-expressing (Control) lentivirus (Fig. 1C; Supplemental Fig. S1D). Heightened Trop2 promoted a threefold expansion of Gen 2 cells (Fig. 1C). Consistent with our previous report, $LSCT^{lo}$ cells lack sphere-forming activity (Goldstein et al. 2008). Ectopic expression of Trop2 was not sufficient to induce sphere growth in $LSCT^{lo}$ cells (Fig. 1C), suggesting that $Trop2^{lo}$ cells may lack signaling components important for Trop2 activity. Previous studies demonstrating that β-catenin promotes the expansion of prostate spheres (Lukacs et al. 2010; Shahi et al. 2011) led us to test the status of β-catenin in $LSCT^{lo}$ versus $LSCT^{hi}$ basal cells. Confocal microscopy revealed significantly lower levels

of β-catenin in LSCT^{lo} in comparison with LSCT^{hi} (Supplemental Fig. S2).

Trop2 is processed by proteolytic cleavage, generating the ICD and ECD

We noted Trop2 localization in the nucleus in a small fraction of cells. To quantitatively measure Trop2 localization, a mouse prostate epithelial basal (PEB) cell line (Salm et al. 2000) that expresses endogenous Trop2 was used. PEB cells were infected with lentivirus expressing RFP or RFP and Trop2 modified with a C-terminal Myc tag to follow Trop2 ICD. Confocal microscopy revealed that the ICD is found on the membrane in 100% of the cells and within the nucleus in 15% of the cells, while Trop2 ECD can be detected only on the plasma membrane and in the cytoplasm (Fig. 2A). We performed further analysis to determine whether Trop2 ECD is shed from the cellular membrane in PEB and another prostate epithelial cell line, TRAMP-C2, cells (Foster et al. 1997). Trop2 ECD, but not ICD, was detected in precipitated medium from cells expressing Trop2 (Fig. 2B). Taken together, these data support a model where Trop2 is cleaved, resulting in shedding of the ECD and accumulation of the ICD in the nucleus (Fig. 2A,B).

Trop2 cleavage products independently stimulate self-renewal and proliferation

Given that Trop2 is cleaved, releasing two fragments (ECD and ICD), we asked whether these different domains serve alternative functional roles in the prostate. Lentivirus carrying either the ICD or the secreted ECD fused to the Fc region of human IgG1 to ensure proper secretion and stability (Trop2-ECD-Fc fusion) was generated (Supplemental Fig. S1D). ICD expression is demonstrated by immunofluorescence (Supplemental Fig. S3A). Dissociated primary mouse prostate cells were infected with either control lentivirus expressing RFP (control) or lentivirus expressing mouse Trop2 ICD and RFP (mICD) and were plated in the sphere assay. The ICD was sufficient to increase sphere formation and stem/progenitor proliferation, measured by sphere number and size, even prior to replating in Gen 1, suggesting that the ICD is the functionally dominant portion of the molecule (Fig. 2C). Further passaging showed continued enhancement of self-renewal activity, as measured by sphere number in Gen 2 (Fig. 2C).

Next, we tested the role of the ECD in self-renewal and proliferation. 293T cell lines were transduced with either a control lentivirus expressing RFP or a lentivirus expressing both ECD-Fc and RFP to generate secreted ECD that we confirmed by Western blot (Fig. 2D). LSCT^{hi} cells were plated in the sphere assay and treated with either conditioned medium from the control 293T (CM) or conditioned medium containing ECD-Fc (CM+ECD) (Fig. 2D). Secreted ECD caused an increase in sphere size but not in sphere number, suggesting that the ECD increases the proliferation of prostate stem/progenitor cells (Fig. 2D). The activation of RIP is induced by ligand binding to its receptor (Schroeter et al. 1998; Mumm et al. 2000). Trop2 is an orphan receptor without a known ligand. We investigated the effects of the ECD on Trop2 processing. Upon treatment of prostate cells with secreted ECD by 293T cells, we observed the appearance of small-molecular-weight fragments at a size of 6 kD, suggesting that Trop2 is cleaved (Supplemental Fig. S3B). Further studies will be necessary to rule out whether the ECD induces Trop2 cleavage by direct homophilic interaction or through distinct binding partners.

Trop2 is cleaved by RIP

Detection of the ECD and ICD at different cellular compartments and their independent function in self-renewal and proliferation led us to investigate the mechanisms through which Trop2 is being cleaved. TACE is a member of the ADAM family of proteases that mediates the initial proteolysis and ectodomain shedding of several transmembrane proteins during RIP, followed by intramembrane proteolysis carried out by the γ-secretase complex. To test whether TACE and γ-secretase play a role in Trop2 processing, PEB cells expressing Trop2-Myc tag were treated with the TACE inhibitor (TAPI-2) or γ-secretase inhibitor (DAPT). Treatment with TAPI-2 resulted in a significant increase in the levels of uncleaved full-length Trop2 (Fig. 3A; Supplemental Fig. S4A). Treatment of PEB cells with DAPT caused a significant increase in the full-length Trop2 as well as the appearance of an intermediate cleavage product (ICP) (Fig. 3A, Supplemental Fig. S4A). The ICP of ~15 kD in size can be generated if Trop2 is not fully processed, but the first TACE cut still takes place (Fig. 3A). Treatment with DAPT and TAPI-2 also resulted in significant decrease of ICD localized in the nucleus (Fig. 3B). While RIP has been implicated in the activation of several transmembrane proteins, for the first time, we demonstrate that Trop2 is cleaved and its processing involves RIP.

Presenilin 1 (PS-1) and PS-2 are catalytic subunits of the γ-secretase complex. Full-length Trop2 increases upon silencing of PS-1 and to a lesser extent upon silencing of PS-2 by siRNA (Fig. 3C; Supplemental Fig. S4B,C). Upon knockdown of either PS-1 or PS-2, we observed accumulation of Trop2 ICP similar to DAPT treatment (Fig. 3C). Knockdown of both PS-1 and PS-2 has an additive effect on Trop2 processing, as we observed a greater accumulation of ICP (Fig. 3C). An increase in Trop2 on the cell surface was detected upon PS-1 knockdown and to a lesser extent upon PS-2 knockdown, as measured by fluorescence-activated cell sorting (FACS) analysis (Supplemental Fig. S4C). These observations suggest that PS-1 is the major protease involved in Trop2 processing.

Trop2 and EpCAM have distinct expression patterns in the adult mouse prostate

Related proteins can often carry out different functions in distinct cell populations. Since we found that Trop2 is processed through RIP, we investigated the expression patterns of Trop2 and EpCAM, a related molecule previously demonstrated to be regulated by RIP (Maetzel

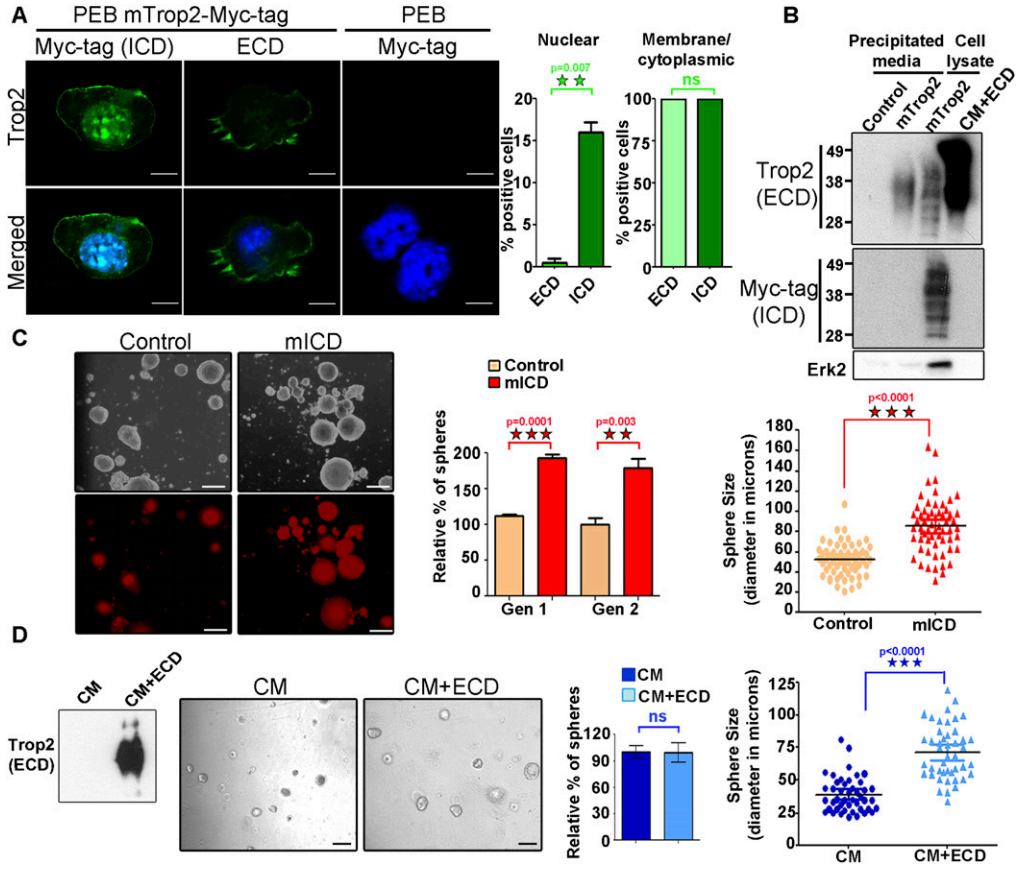

Figure 2. Trop2 ECD and ICD localize at distinct sites within the cell. Trop2 regulates stem/progenitor self-renewal through ICD and ECD cleavage products. (*A*) Confocal microscopy of PEB cells stained with anti-Myc tag or anti-ECD antibody and DAPI. The *right* two panels represent PEB cells infected with lentivirus expressing RFP (PEB) as a negative control to determine whether anti-Myc tag antibody recognizes any endogenous myc. Staining of PEB cells expressing mTrop2 with a C-terminal Myc tag to follow the ICD with the indicated antibodies is presented in the *left* four panels. Bar, 10 μm. One out of three independent experiments is shown. Graphs represent the percentage of cells with nuclear ICD or ECD (*left* graph) and cytoplasmic and membrane ICD or ECD (*right* graph). (*B*) Serum-free medium from TRAMP-C2 cells transduced with RFP lentivirus (control) or mTrop2-Myc tag (mTrop2) was precipitated (precipitated media), followed by Western blot using commercial anti-ECD antibody or anti-Myc tag recognizing the ICD or Erk2 as a marker for cell lysate. Cell lysates from TRAMP-C2 cells expressing mTrop2-Myc tag (mTrop2) and CM produced by 293T expressing secreted Trop2-ECD-Fc (CM+ECD) were used as positive controls. Only the ECD of Trop2 was detected in the precipitated media. Highly glycosylated Trop2 is shown between 35 and 50 kD. Four independent experiments were performed. (*C*) An equal number progenitor cells ($LSCT^{hi}$) was transduced with a control RFP-expressing (control) or Trop2 ICD-expressing (mICD) lentivirus and plated in triplicates in the sphere assay. Representative pictures are presented in the *left* panels. Bars, 100 μm. Seven days later, we observed an increase in sphere size and number as early as Gen 1 (graphs presented on the *right*). Orange panels represent RFP-infected spheres (control), and red panels show mICD-infected spheres. The ICD alone enhance self-renewal, as measured by sphere number in Gen 2. Sphere number in each sample is presented as the percentage normalized to the RFP-infected spheres (control). Data are represented as mean ± SEM. (*Right* graph) Sphere size is presented in diameter in microns. Three independent experiments were performed. (*D*) Generation of 293T cells line expressing secreted ECD. (*Left*) Conditioned medium produced by 293T expressing RFP (CM) or Trop2-ECD-Fc and RFP (CM+ECD) was subjected to Western blot analysis with anti-ECD antibody. Equal numbers of progenitor cells ($LSCT^{hi}$) were plated in triplicate and treated with conditioned medium from control 293T cells infected with RFP (CM) or 293T cells stably expressing and secreting Trop2-ECD-Fc and RFP (CM+ECD). Images show spheres grown in the presence of CM or CM+ECD. Bars, 100 μm. No difference in sphere number was observed (*left* graph), while there was a significant increase in sphere size upon treatment with CM+ECD at Gen 1 (*right* graph). Dark-blue bars represent spheres treated with CM, and light-blue bars represents spheres treated with CM+ECD. Three independent experiments were performed.

et al. 2009). The spatial patterns of Trop2 and EpCAM in the mouse prostate revealed dramatic differences in their cellular localization. While Trop2 expression was restricted to the progenitor-enriched region most proximal to the urethra, as previously reported (Goldstein et al. 2008), EpCAM was expressed evenly in all epithelial cells (Supplemental Fig. S5A). FACS analysis demonstrated that Trop2 is expressed primarily in a subpopulation of $Sca\text{-}1^{+}CD49f^{hi}$ basal cells and is rarely expressed on luminal cells, while EpCAM was expressed in all $CD49f^{lo}$ luminal and $CD49f^{hi}$ basal epithelial cells (Supplemental Fig. S5B). We hypothesize that EpCAM and Trop2 regulate

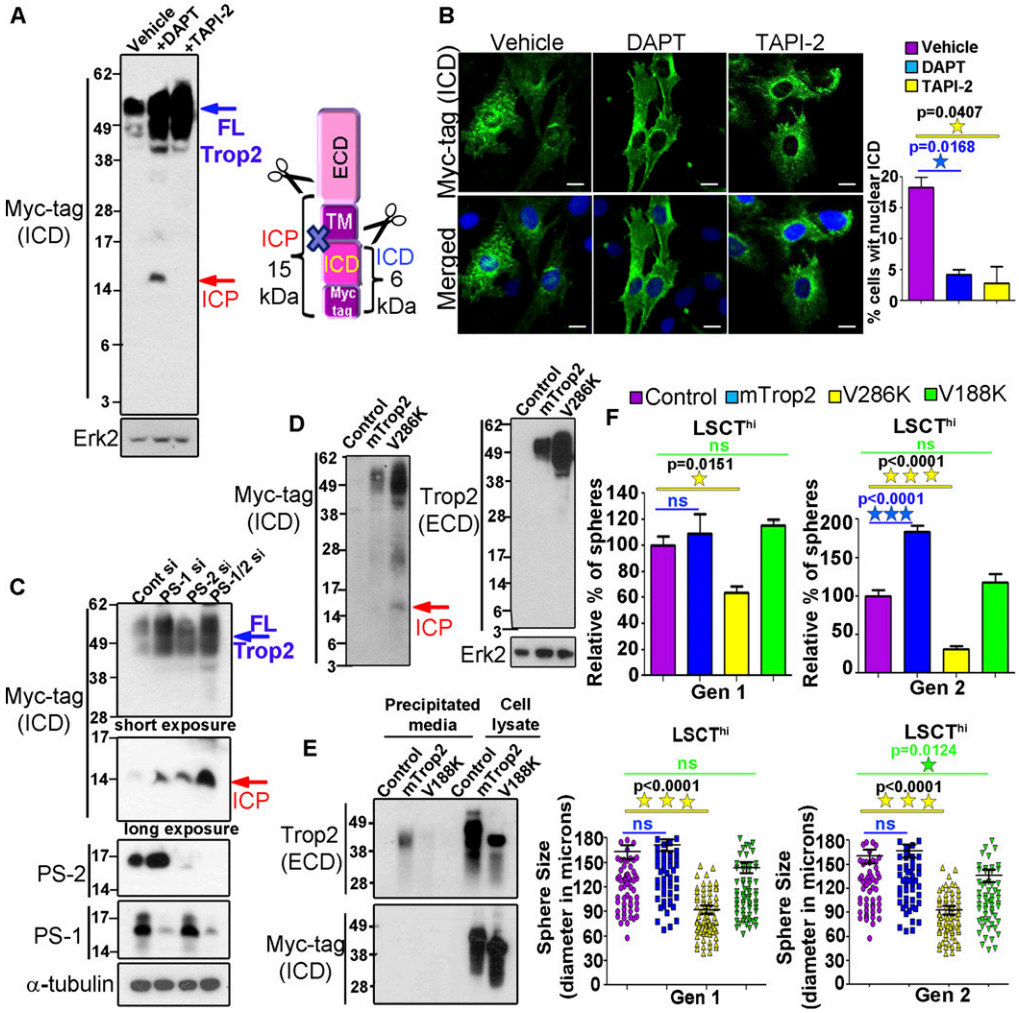

Figure 3. Trop2 is cleaved by RIP. Trop2 cleavage mutants are deficient in inducing self-renewal in vitro. (*A*) PEB-Trop2-Myc tag cells were treated with either DMSO (vehicle), DAPT, or TAPI-2, followed by Western blot. The red arrow indicates accumulated ICP. The ICD cannot be detected without immunoprecipitation (IP). The blue arrow indicates full-length mTrop2 (FLTrop2). Full-length Trop2 appears between 35 and 50 kD. One out of three independent experiments is shown. Schematic representation of the generation of 15-kD ICP upon treatment with DAPT is shown on the *right*. (*B*) TRAMP-C2 expressing mTrop2 with a C-terminal Myc tag to follow the ICD were treated with DMSO (vehicle), DAPT, or TAPI-2. Twenty-four hours post-treatment, cells were fixed and stained with anti-Myc tag or anti-ECD antibody and DAPI and subjected to confocal microscopy. Bar, 10 μm. One out of two independent experiments is shown. The graph represents the percentage of cells with nuclear ICD. (*C*) PEB expressing Trop2-Myc tag cells were transfected with nontargeting (Cont), PS-1, PS-2, or both PS-1 and PS-2 siRNA, followed by Western blot with the indicated antibodies. Similar to DAPT treatment, knockdown of presenilins caused ICP appearance, as indicated by the red arrow. The blue arrow shows full-length Trop2 (FLTrop2). One out of three independent experiments is shown. (*D*) PEB cells were infected with lentivirus expressing RFP (control), mTrop2-Myc tag and RFP (mTrop2), or V286K-Myc tag (V286) mutant. Cells were lysed and subjected to Western blot with antibodies against Myc tag or the ECD of Trop2. The red arrow shows ICP appearance in V286K, demonstrating not fully processed Trop2. One out of three independent experiments is shown. (*E*) Serum-free medium from TRAMP-C2 cells transduced with RFP lentivirus (control), mTrop2-Myc tag (mTrop2), or V188K-Myc tag (V188K) was precipitated, followed by Western blot using commercial anti-ECD antibody or anti-Myc tag recognizing the ICD. Only the ECD of Trop2 was detected in the precipitated media from cells expressing wild-type Trop2, but not from cells expressing V188K. Two independent experiments were performed. (*F*) LSCT^{hi} cells were isolated by FACS, and an equal number of cells was infected with RFP (control), mTrop2, V286K, or V188K mutants expressing lentivirus and plated in triplicate. Sphere number and diameter in microns were quantified after Gen 1 and Gen 2. (*Left* graphs) Sphere number in each sample is presented as the percentage normalized to the RFP-infected spheres (control). Data are represented as mean ± SEM. Sphere size measured by sphere diameter in microns is presented in the *right* graphs. Purple bars represent RFP (control), blue bars indicate mTrop2, yellow bars represent V286K mutant, and green bars indicate V188K mutant-infected spheres. Each sample in the experiment was plated in triplicate. Three independent experiments were performed.

distinct processes in defined cell populations even though both proteins are regulated by RIP.

Trop2 is cleaved at two distinct sites

While EpCAM cleavage sites still remain unknown, Notch1 processing sites have been well characterized (Schroeter et al. 1998; Mumm et al. 2000). Based on Notch cleavage sites (Schroeter et al. 1998; Mumm et al. 2000), we predicted the likely TACE cleavage site within the ECD (between Ala187 and Val188) and γ-secretase cleavage site within the transmembrane domain (between Gly285 and Val286). Each valine was substituted to a lysine (V188K and V286K). PEB cells were transduced with the γ-secretase cleavage mutant (V286K), TACE cleavage mutant (V188K), wild-type Trop2-Myc tag (mTrop2), or RFP (control) lentivirus. V286K and V188K localize on the cell surface similarly to the wild-type Trop2, as measured by FACS (Supplemental Fig. S6A). We tested whether mutation at the γ-secretase cleavage site would result in the appearance of ICP. Similar to treatment with DAPT, accumulation of ICP was observed in the V286K mutant but not in the wild-type Trop2 (Fig. 3D). We further tested whether the V188K mutant is cleaved. Precipitated medium from prostate cells expressing TACE cleavage mutant (V188K), wild-type Trop2-Myc tag (mTrop2), or RFP (control) lentivirus was subjected to Western blot analysis with antibodies against Myc tag (ICD) and the ECD. Cleaved and shed ECD was detected in the medium from cells expressing wild-type Trop2 (mTrop2) but not from the cells expressing the V188K cleavage mutant (Fig. 3E).

Cleavage of Trop2 is required for its self-renewal and proliferative activity

To address whether Trop2 processing by RIP is necessary to carry out its self-renewal function, we tested the V286K and V188K mutants in the sphere assay (Fig. 3F; Supplemental Fig S6B). LSCT^{hi} cells were infected with lentivirus expressing RFP (control), mTrop2, V286K, or V188K cleavage mutants and plated in the in vitro sphere assay (Fig. 3F, Supplemental Fig S6B). While heightened levels of wild-type Trop2 promoted sphere formation, the cleavage mutants V286K and V188K failed to enhance self-renewal (Fig. 3F; Supplemental Fig S6B). Moreover, V286K negatively affected sphere formation (Fig. 3F; Supplemental Fig S6B). These results demonstrate that V286K may have a dominant-negative effect on endogenous Trop2, while V188K acts as a loss-of-function mutant. Pharmacological inhibition of Trop2 cleavage was also tested in the sphere assay. DAPT and TAPI-2 negatively impacted sphere formation in LSCT^{hi} cells by reducing sphere number and size (Supplemental Fig. S7A).

We asked whether Trop2 overexpression increases the percent of cycling cells in benign epithelial cells, as has been reported in cancer cells (Cubas et al. 2010). Both cleavage mutants V286K and V188K failed to increase proliferation and demonstrated cell cycle profiles similar to the control, while heightened Trop2 led to an increase in cycling cells (Supplemental Fig. S7B). Taken together, the combined genetic and small molecule inhibition results demonstrate that cleavage of Trop2 is necessary for its enhanced growth and self-renewal activity in Trop2^{hi} cells.

Trop2 is cleaved in human prostate cancer

We next asked whether cleavage of Trop2 is observed in human prostate cancer. Frozen serial sections (4-μm thickness) of tissues from 11 prostate cancer patients containing both benign and cancer regions were subjected to coimmunofluorescence with antibodies against the ICD and ECD of human Trop2 or H&E staining (Fig. 4; Supplemental Fig. S8). Stained tissues were analyzed for ICD and ECD cellular localization by confocal microscopy. Nuclear ICD was detected only in the cancer specimens but not in the benign counterparts in six out of the 11 patient samples analyzed (Fig. 4; Supplemental Fig. S8). The ECD was detected only in the cytoplasm and

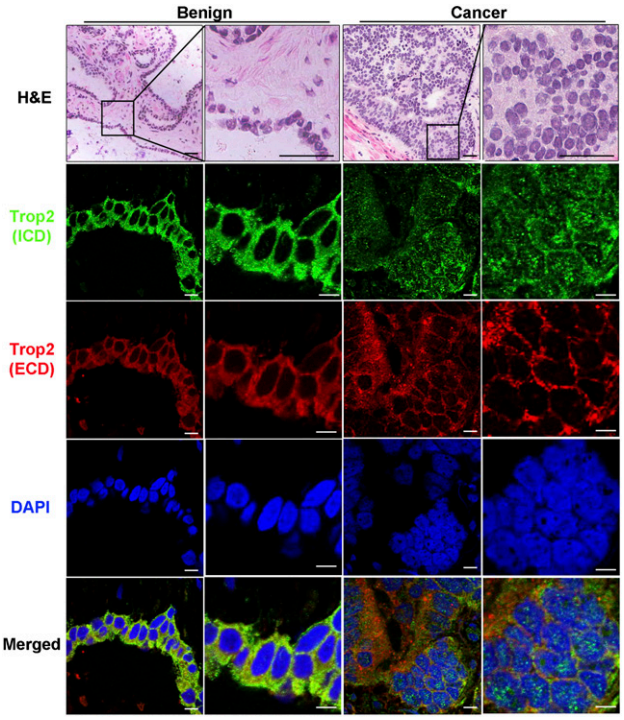

Figure 4. Nuclear localization of the ICD is found in human prostate cancer. Immunofluorescence with anti-ECD and anti-ICD antibodies and DAPI of tissues from human prostate cancer patients. One out of 11 patient samples is shown. A benign region is presented in the *left* two columns, and a cancer region is shown in the *right* two columns. Histology is shown in the *top* two panels by H&E staining. Bars, 100 μm. ICD nuclear localization can be detected only in cancer but not in the benign prostate (green). The ECD is found in the cytoplasm and on the membrane in the benign and cancer regions (red). DAPI demonstrates nuclear staining (blue). Merged images are presented in the *bottom* panels. In the immunofluorescence images to visualize ICD and ECD localization, bars represent 10 μm.

on the membrane in all patient samples in both cancer and benign regions (Fig. 4; Supplemental Fig. S8). These results indicate that cleavage and activation of Trop2 are associated with human prostate cancer.

Heightened expression of the ICD initiates PIN in vivo

To address the link between self-renewal and proliferative activity of Trop2 and its role in prostate tumorigenesis, we tested whether heightened Trop2 is sufficient to transform naive epithelium and whether activation through cleavage is required for its function (Fig. 5A). We hypothesized that the expression of ICD alone will mimic active Trop2, while a cleavage mutant will represent a loss of function in vivo. Full-length mTrop2 was compared with γ-secretase cleavage mutant V286K, RFP alone, ICD to mimic active Trop2, and a potent oncogenic signal such as activated AKT in the in vivo regeneration assay (Fig. 5B). Infection efficiency was assessed by the presence of the RFP or GFP color marker carried by each lentiviral vector. Enhanced expression of V286K, mICD, mTrop2, or AKT was confirmed by immunofluorescence or immunohistochemistry analysis in three independent grafts. Trop2 was able to drive hyperplasia, while the ICD was more potent, giving rise to lesions observed upon activation of AKT that morphologically resemble PIN, a precursor to carcinoma (Fig. 5B; Bostwick and Montironi 1995). V286K regenerated grafts resembled the RFP control and showed normal tubule regeneration, demonstrating that cleavage and activation of Trop2 is required for its transformation activity (Fig. 5B). The ECD alone was also sufficient to induce hyperplasia in the in vivo prostate regeneration assay (Supplemental Fig. S9).

Trop2 signals through β-catenin

Our findings that $LSCT^{hi}$ cells express higher levels of β-catenin when compared with $LSCT^{lo}$ (Supplemental Fig. S2) led us to investigate whether Trop2 signals through β-catenin. A polyclonal antibody against the ICD was generated in our laboratory to assess whether the ICD and β-catenin physically interact. Due to higher levels of endogenous β-catenin in TRAMP-C2 cells, TRAMP-C2 cells expressing Trop2-Myc tag were used in immunoprecipitation experiments. The ICD coimmunoprecipitates with endogenous β-catenin (Fig. 6A). We next performed immunoprecipitation with an antibody against the ECD of Trop2. β-Catenin was not detected in the ECD immunoprecipitants (Fig. 6B). We set out to investigate whether Trop2 is involved in β-catenin signaling. Overexpression of Trop2 led to up-regulation of the β-catenin downstream targets cyclin D1 and c-myc, demonstrating that Trop2 signals through β-catenin (Fig. 6C,D; Supplemental Fig. S10).

β-Catenin is required for Trop2-driven self-renewal and hyperplasia

Having demonstrated that β-catenin binds to Trop2 and is involved in Trop2 signaling, we next investigated localization of the ICD and β-catenin in human prostate tissues. Nuclear β-catenin was found in the cancer region of three out of 11 patient samples analyzed, all of which express nuclear Trop2 ICD (Fig. 7A; Supplemental Fig. 11). Importantly, β-catenin colocalized with Trop2 ICD in all three patients (Fig. 7A; Supplemental Fig. 11). Nuclear colocalization was restricted to the cancer region and was not observed in the benign region (Fig. 7A; Supplemental Fig. 11).

To determine whether the biological activity of Trop2 is dependent on β-catenin, we investigated the link between β-catenin and Trop2-driven self-renewal and hyperplasia. Trop2 was overexpressed in wild-type or β-catenin-deleted epithelium and tested for self-renewal potential. $LSCT^{hi}$ cells from β-catenin conditional knockout mice (loxP/loxP) were infected with either mTrop2- and RFP-expressing or RFP-expressing lentivirus and either Cre recombinase- and GFP-expressing (to drive excision of loxP sites, $\beta\text{-cat}^{-/-}$) or GFP-expressing ($\beta\text{-cat}^{+/+}$) lentivirus and plated in the sphere assay (Fig. 7B; Supplemental Fig. S12). Trop2 was able to drive an increase in sphere formation only in the presence of β-catenin (Fig. 7B; Supplemental Fig. S12). Loss of β-catenin abrogated the self-renewal driven by heightened Trop2 and showed baseline self-renewal activity comparable with the control.

To assess whether the activity of Trop2 is dependent on β-catenin in vivo, Trop2 was overexpressed in wild-type or β-catenin-deleted epithelium and tested for the ability to drive hyperplasia in the in vivo regeneration assay. Dissociated primary prostate cells from β-catenin conditional knockout mice were transduced with mTrop2 and RFP and either Cre recombinase-and GFP-expressing ($\beta\text{-cat}^{-/-}$) or GFP-expressing ($\beta\text{-cat}^{+/+}$) lentivirus. Transduced prostate cells were combined with UGSM cells and subjected to in vivo regeneration. Upon histological analysis of the recovered grafts, we observed that Trop2 was able to induce hyperplasia only in the presence of β-catenin (mTrop2/$\beta\text{-cat}^{+/+}$) (Fig. 7C). Loss of β-catenin blocked the hyperplasia induced by heightened Trop2 (mTrop2/$\beta\text{-cat}^{-/-}$) and showed normal prostate tubule regeneration (Fig. 7C). These findings demonstrate that Trop2 function requires the presence of β-catenin (Fig. 7B,C).

Discussion

Recent evidence suggests that many human cancers arise from transformed stem cells due to their enhanced self-renewal capacity (Visvader, 2011). Identifying the factors that regulate self-renewal will enhance our understanding of the tumorigenic process and lead to the design of novel cancer therapies. We showed here that Trop2 is a new regulator of stem/progenitor activity in the prostate. Trop2 controls self-renewal, proliferation, and tissue hyperplasia through two cleavage products (ICD and ECD) generated by RIP. We speculate that elevated expression of Trop2 is selected for in cancer due to its capacity to enhance self-renewal and proliferation.

We found that Trop2 cleavage is mediated by both PS-1 and PS-2 in the γ-secretase complex. Our observations that knockdown of PS-1 and, to lesser extent, PS-2

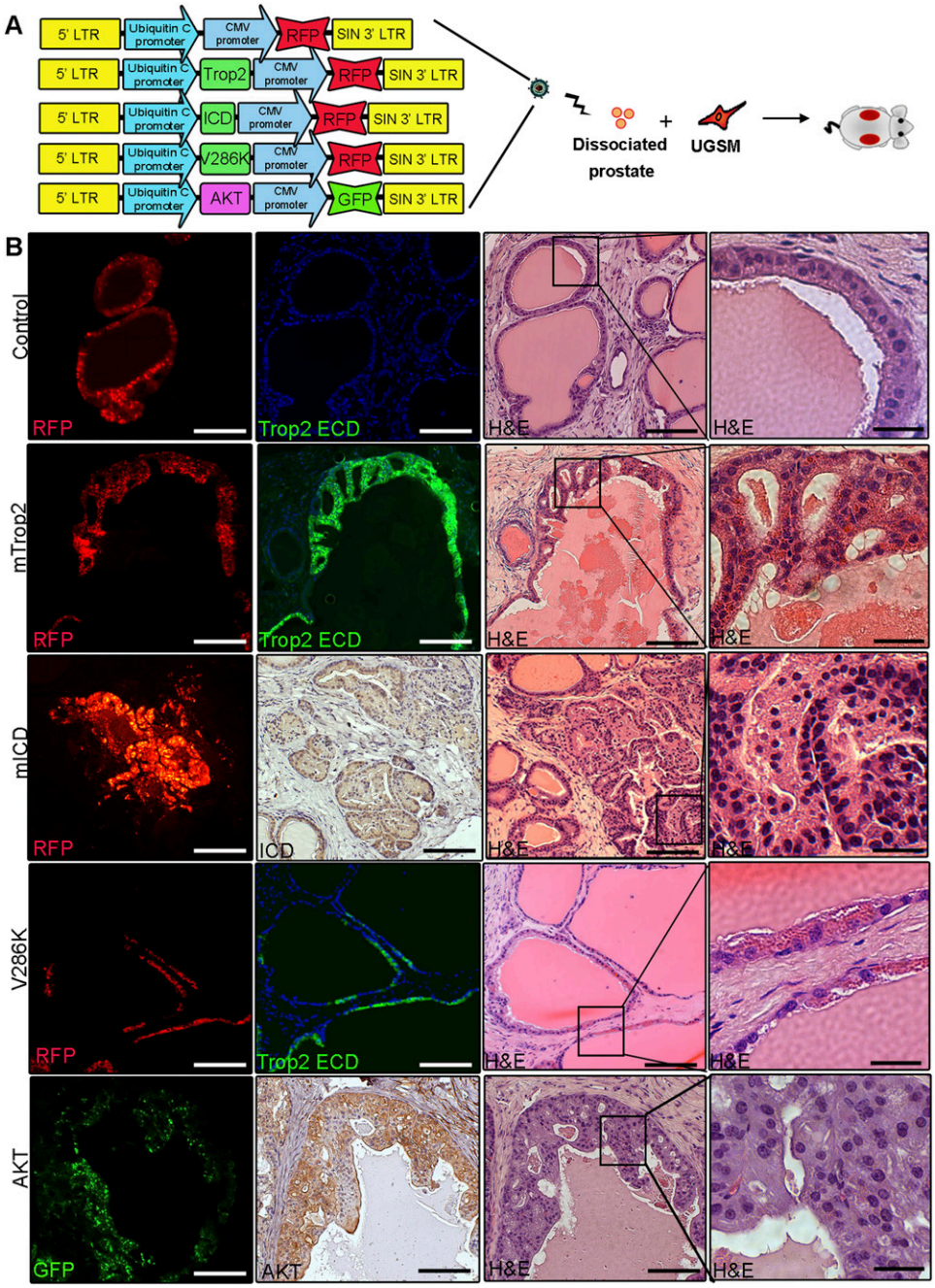

Figure 5. Trop2 and the ICD alone drive hyperplasia in vivo. (*A*) Schematic representation of the in vivo regeneration assay and lentiviral construct used. (*B*) Dissociated primary prostate cells were transduced with lentivirus expressing RFP (control), Trop2, mICD, V286K, or AKT. Infected prostate cells were combined with UGSM and subjected to the in vivo regeneration assay. Eight weeks later, grafts were recovered, fixed in formalin, and sectioned for histological analysis. The *left* panels represent immunofluorescence (IF) showing infected tubules, and the *middle* panel shows immunofluorescence with anti-Trop2 ECD or immunohistochemistry (IHC) with anti-ICD or anti-AKT, respectively. The *right* two panels show the histology of the recovered grafts. One out of three independent experiments is shown. Bars: *right* panels, 200 or 50 μm.

resulted in elevated surface Trop2 suggest that PS-1 is the predominant enzyme involved in Trop2 processing. In contrast, EpCAM cleavage by RIP is carried out strictly by PS-2 (Maetzel et al. 2009).

Analysis of Trop2 and EpCAM localization in the mouse prostate revealed that these related proteins have different expression patterns, which may have a biological consequence. While we demonstrated that Trop2 regulates self-renewal and tissue regeneration, no evidence has been provided to support a functional role for EpCAM in adult stem/progenitor cells. The Notch family of receptors provides one example of highly homologous

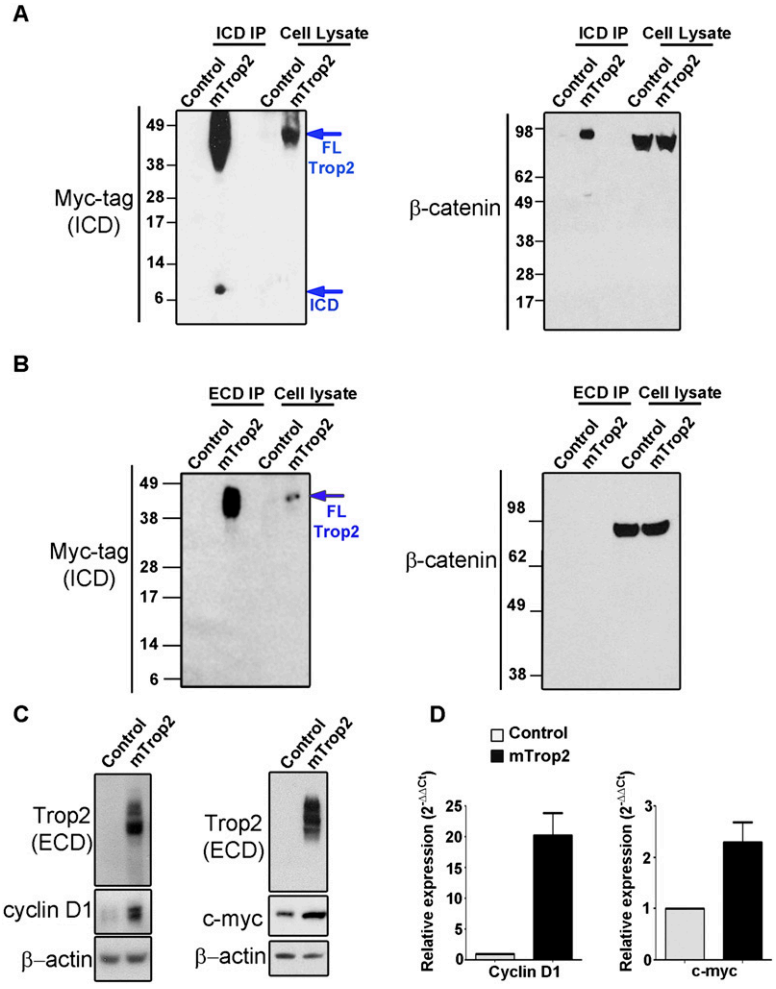

Figure 6. Trop2 signals through β-catenin. (*A*) Trop2 ICD binds β-catenin. Cell lysates from TRAMP-C2 cells expressing either RFP (control) or the mTrop2-Myc tag and RFP (mTrop2) were subjected to immunoprecipitation using antibodies against the ICD raised in our laboratory (ICD immunoprecipitation), followed by Western blot with anti-Myc tag (ICD) (on the *left*) or anti-β-catenin (on the *right*) antibodies. Trop2 is shown between 35 and 50 kD due to high glycosylation. One out of three independent experiments is shown. (*B*) Lysates from TRAMP-C2 cells transduced with a RFP-expressing lentivirus (control) or mouse Trop2 and RFP lentivirus (mTrop2) were subjected to immunoprecipitation with polyclonal antibody against the ECD of Trop2, followed by Western blot with anti-Myc tag (ICD) or anti-β-catenin antibodies. No interaction between the ECD and β-catenin was observed. One out of three independent experiments is presented. (*C*) Overexpression of Trop2 increases β-catenin target genes. Lysates from PEB expressing RFP (control) or mouse Trop2 (Trop2) were subjected to SDS-PAGE followed by Western blot with anti-Trop2 ECD, anti-cyclin D1, anti-c-myc, or anti-β-actin antibodies. One out of three independent experiments is shown. (*D*) RNA isolated from PEB expressing RFP (control) or mouse Trop2 (Trop2) was subjected to cDNA synthesis, and quantitative PCR was performed in triplicate using mouse-specific cyclin D1 and c-myc primers. One out of three independent experiments is shown. Fold change of cyclin D1 and c-myc mRNA levels is normalized to GAPDH (internal control).

proteins carrying differential functions. Notch1, Notch2, and Notch3 are expressed in distinct cell populations within the thymus, are regulated by RIP, and induce analogous signaling cascades (Felli et al. 1999). Both Notch1 and Notch2 are expressed in myeloid progenitor cells, but they are each cleaved in response to different cytokines, supporting unique downstream signaling patterns (Bigas et al. 1998).

Upon activation by RIP, we determined that Trop2 signals through β-catenin. Trop2 was not able to induce self-renewal and hyperplasia upon β-catenin loss, demonstrating that the Trop2 self-renewal and transformation function is dependent on β-catenin activity. Abnormal β-catenin localization is found in 71% of prostate cancer patients, and high levels of β-catenin are associated with metastatic prostate cancer (Yardy and Brewster 2005; Yardy et al. 2009). Elevated levels of Trop2 are found in localized and metastatic human prostate cancer compared with benign prostate tissue (T Stoyanova, AS Goldstein., J Huang, H Zhang, and ON Witte, unpubl.). We now demonstrate that nuclear β-catenin colocalizes with the ICD within the nucleus. This colocalization is restricted to cancer regions and does not occur in the benign tissues. Nuclear ICD is also observed in prostate cancer patients with low levels of nuclear β-catenin. Additional analysis will need to be performed to investigate the relationship between high nuclear β-catenin that colocalizes with the ICD and the clinical outcome of prostate cancer patients.

Due to its elevated expression in a broad range of epithelial cancers, Trop2 is a promising target for therapeutic intervention. Antibodies against Trop2 were used as carriers of radioactive elements or toxins to the tumor sites and demonstrated great anti-cancer efficacies in xenograft models of multiple cancers (Shih et al. 1995; Stein et al. 1997; Govindan et al. 2004; Cardillo et al. 2011). Trop2 antibodies can also be used as direct therapeutic effectors. Nonconjugated Trop2 antibodies exhibit potent anti-cancer activity in cancer xenografts of many epithelial cancers (Young et al. 2008; Alberti 2012). These studies suggest that the antibodies interfere with Trop2 signaling, most likely by compromising cancer self-renewal and proliferation. Thorough interrogation of the functional role of Trop2 in stem/progenitor self-renewal and transformation and of the molecular mechanisms of Trop2 function defined in our study will be applicable in developing novel targeted therapies. Activation and signaling driven by Trop2 require RIP, as cleavage mutants

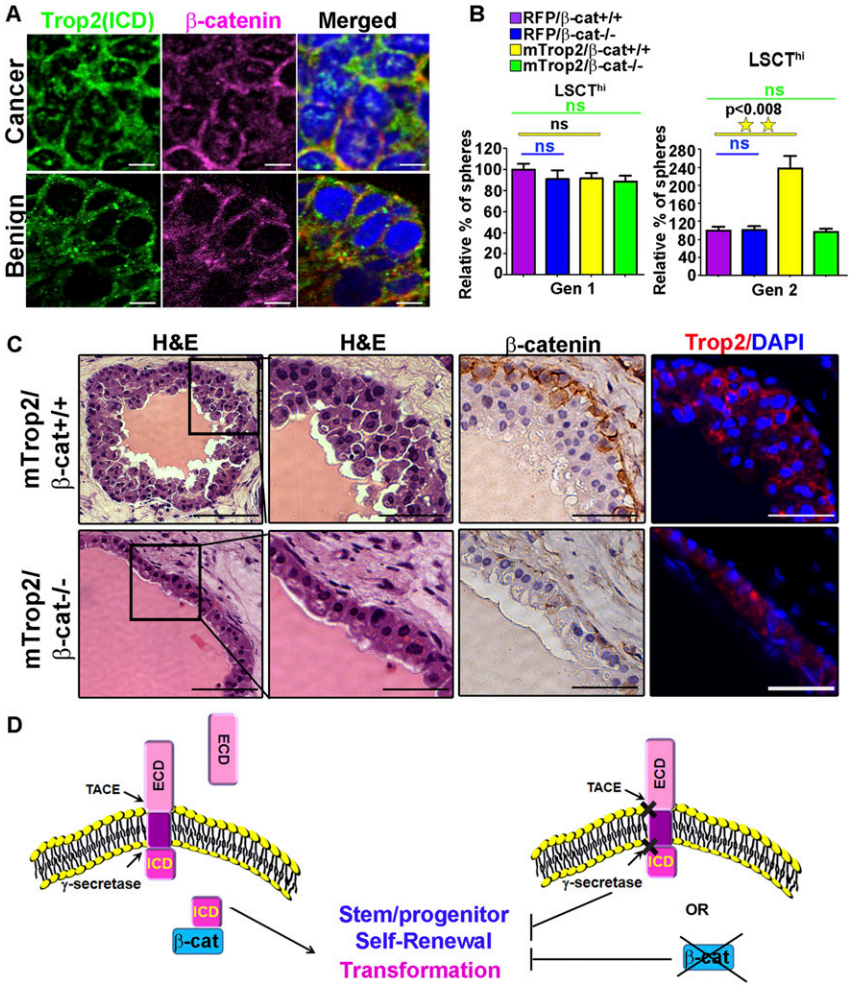

Figure 7. Trop2 regulates self-renewal and transformation though β-catenin. (*A*) Immunofluorescence of tissues from human prostate cancer patients with anti-ICD and anti-β-catenin antibodies and DAPI. One out of 11 patient samples is shown. A cancer region is presented in the *top* panels, and a benign region is shown in the *bottom* panels. The ICD (green) colocalizes with β-catenin (pink) in the nucleus only in cancer but not in the benign prostate. DAPI demonstrates nuclear staining (blue). Merged images are presented in the *bottom* panels. Bars, 10 μm. (*B*) Trop2-mediated enhanced self-renewal requires β-catenin. Isolated progenitor cells ($LSCT^{hi}$) from β-catenin conditional knockout mice (loxP/loxP) were infected with either mTrop2- and RFP-expressing lentivirus or control RFP (RFP) and either Cre recombinase- and GFP-expressing lentivirus (to drive excision of loxP sites, $\beta\text{-cat}^{-/-}$) or control GFP-expressing lentivirus ($\beta\text{-cat}^{+/+}$). Infected cells were plated in triplicate in the sphere-forming assay, and sphere numbers were quantified 7 d post-plating for Gen 1 and further passaged to Gen 2. (*Left* graphs) Sphere number in each sample is presented as the percentage normalized to the RFP control. Data are represented as mean ± SEM. One out of three independent experiments is shown. (*C*) Dissociated primary prostate cells from β-catenin conditional knockout mice were transduced with either mTrop2- and RFP-expressing lentivirus and either Cre recombinase ($mTrop2/\beta\text{-cat}^{-/-}$) or GFP ($mTrop2/\beta\text{-cat}^{+/+}$) and combined with UGSM and subjected to the in vivo regeneration assay. Eight weeks later, grafts were recovered, fixed in formalin, and sectioned for histological analysis. The *left* four panels represent histology (H&E staining). The *right* panels show immunohistochemistry (IHC) with anti-β-catenin or immunofluorescence with anti-Trop2 ECD and DAPI. Bars: *right* panels, 100 or 50 μm. (*D*) Trop2 is activated through RIP by the TACE and γ-secretase complex. RIP of Trop2 results in shedding of the ECD and release of the ICD to the nucleus. The ICD promotes self-renewal through β-catenin. The models suggest that the ICD promotes transformation through its self-renewal activity.

were deficient in self-renewal and transformation, suggesting that inhibition of regulated processing might inhibit proliferation and survival in prostate cancer cells (Fig. 7D). Small molecules able to block Trop2 proteolysis or monoclonal antibodies that interfere with Trop2 processing and activation could represent a promising strategy to target not only prostate, but other epithelial cancers exhibiting elevated levels of Trop2 (Fig. 7D).

Materials and methods

Vector production

Mouse Trop2 was PCR-amplified from pCR-BluntII-TOPO vector containing the ORF of mouse Trop2 (purchased from Open Biosystems). Trop2 was modified by adding a Myc tag at the C-terminal end, and XbaI restriction digest sites were added to both ends. The amplified Trop2 was subcloned into the XbaI site of FUCRW downstream from the ubiquitin promoter. Trop2 ICD was PCR-amplified, and XbaI and EcoR1 sites were added, followed by subcloning into FUCRW downstream from the ubiquitin promoter.

To generate V188K and V286K Trop2 mutants, mouse Trop2 was subcloned in pBSKSII vector. Stratagene's QuikChange site-directed mutagenesis kit was used to introduce a single-amino-acid change with the following oligonucleotides: V188K (CTT CCTATCCGCGAAACACTATGAGGAGCCCACC and GGTG GGCTCCTCATAGTGTTTCGCGGATAGGAAG) and V286K (TAGCGGTAGTGGCTGGTAAGGTGGTCTTGGTGGT and ACCACCAAGACCACCTTACCAGCCACTACCGCTA). V188K and V286K Trop2 mutants were subcloned into the FUCRW XbaI and EcoR1 sites downstream from the ubiquitin promoter.

The BLOCK-iT PolII miRNAi expression vector kit was used for generation of miRNA scrambled-GFP and miRNA Trop2-GFP with the following oligonucleotides: miRNA scrambled-GFP (TGCTGAAATGTACTGCGCGTGGAGACGTTTTGGCCACT GACTGACGTCTCCACGCAGTACATTTCAGG) and miRNA Trop2-GFP (TGCTGAACTCAATGAGGATGTGGTGGGTTTT GGCCACTGACTGACCCACCACACTCATTGAGTTCAGG).

Viral packaging

Third-generation lentiviral vectors FUCGW and FUCRW, derived from FUGW (Lois et al. 2002; Xin et al. 2006), were used for the construction of the mouse Trop2, ICD, ECD-Fc, V286K, and V188K cleavage mutant overexpression.

Mouse strains

C57BL/6 and CB17$^{Scid/Scid}$ mouse strains were purchased from The Jackson Laboratory. Mice were housed in the University of California at Los Angeles (UCLA) animal facilities under the regulation of the Division of Laboratory Animal Medicine.

Prostate regeneration assays

Housing, maintenance, and all surgical procedures were undertaken in compliance with the regulations of the Division of Laboratory Animal Medicine of UCLA. All experimental procedures were approved by the Division of Laboratory Animal Medicine of UCLA. The details of the regeneration process have been explained previously (Lukacs et al. 2010).

Prostate cell dissociation, cell sorting, and in vitro sphere assay

Isolation of prostate epithelial cells, antibody staining, and FACS for LSCT^{lo}, LSCT^{hi}, and luminal cells were performed as previously described (Goldstein et al. 2008; Lukacs et al. 2010). Five thousand to 50,000 sorted LSCT^{hi} or LSCT^{lo} prostate cells were used for sphere assay following the previously published protocol (Lukacs et al. 2010).

Prostate patient samples

Patient samples were obtained from the UCLA Translational Pathology Core Laboratory (TPCL), which is authorized by the UCLA Institutional Review Board (IRB) to distribute annonymized tissue to researchers. All tissues were from prostatectomy specimens that contained prostate cancer as well as benign prostate. Fresh prostates were serially sectioned into five to seven slices, depending on their sizes. Levels 2 and 4 were submitted to the TPCL. Each level was divided into four quadrants, and a rapid-frozen section diagnosis was performed. Cancer and benign areas were clearly marked on the frozen section slides, and the frozen tissue was stored in −80°C freeze. Additional sections were cut from the tissue for H&E staining and immunofluorescence studies.

Western blot and immunoprecipitation

For Western blot assay, cells were washed twice with 1× PBS and lysed in RIPA buffer contacting 50 mM Tris-HCl (pH 8.0), 150 mM NaCl, 0.1% SDS, 0.5% SD, 1% NP-40, 1 mM EDTA, cocktail protease inhibitors (Roche), and phosphatase inhibitor 1 and 2 (Sigma). Extracts (10–50 μg) were subjected to sodium dodecyl sulfate–10% polyacrylamide gel electrophoresis, followed by blotting to nitrocellulose with the indicated antibodies. For immunoprecipitation, cells were lysed by suspension in 2 vol of buffer containing 0.4 M NaCl, 20 mM Tris-HCl (pH 7.5), 0.1% NP-40, 5% (v/v) glycerol and cocktail protease inhibitors (Roche), and phosphatase inhibitor 1 and 2 (Sigma). Extracts (500 μg) were subjected to immunoprecipitation with 1 μg of anti-ICD, anti-ECD or with isotype-matched immunoglobulin (IgG) followed by Western blot.

Immunofluorescence

For cytospins and immunofluorescence, 1×10^5 cells were spun on slides and fixed in ice-cold acetone, followed by staining with the indicated antibodies. Antibodies and dilutions are provided in the Supplemental Material. Slides were counterstained with DAPI and visualized with confocal fluorescence microscopy.

Immunohistochemistry

Indicated tissues were fixed in 10% buffer formalin and paraffin-embedded. Four-micron sections were deparaffinized in xylene and rehydrated in 100%, 95%, and 70% ethanol. Antigen retrieval was performed with citrate buffer (pH 6.0) for 20 min at 95°C. Sections were further blocked using mouse-on-mouse blocking reagents (Vector Laboratories, BMK-2202). The sections were incubated with the indicated antibodies overnight. Slides were washed with 1× PBS and incubated with anti-mouse HRP or anti-rabbit HRP antibodies (DAKO) for 1 h, developed with HRP substrate (DAKO), and counterstained with hematoxylin.

Antibodies

Western blot analysis and immunoprecipitation experiments were performed using the following antibodies: anti-Trop2 ECD (R&D Systems, FAB1122A, FAB1122F, and BAF1122), anti-Myc tag (Cell Signaling, no. 2276S and no. 2278), anti Erk-2 (Santa Cruz Biotechnology, sc-154), anti-α-tubulin (Santa Cruz Biotechnology, sc-5286), anti-PS-1 (Cell Signaling, no. 5643S), anti-PS-2 (Cell Signaling, no. 2192), anti-cyclinD1 (Cell Signaling, no. 2926), anti-β-catenin (Transduction Laboratories, 610454), anti-EpCAM (Abcam, ab68892), and anti-EpCAM C terminus (Epitomics, 1144-1).

siRNA

On-Target Plus smart pool siRNA targeting mouse PS-1 and PS-2 and nontargeting siRNA control were purchased from Dharmacon as previously described (Zhao et al. 2010): PS-1 siRNA (CC AAAGGCCCACUUCGUAU, GAAGGAUAGCUCCGAGUAA, GGAGCAUUCUAACGAGUGA, and CCGGAAGGACGGUC AGCUA) and PS-2 siRNA (CCUCAAGUAUGGGGCGAAA, CUAUCAAGUCUGUGCGUUU, AAGAGGACCCGGACCGC UA, and CAGCUUGCCUGUCGGAGCA).

Inhibitors

DAPT (10 μM) (Sigma Aldrich, D5942) or 40 μM TAPI-2 (Enzo Life Sciences, BML-PI135-0001) were used.

Statistical analysis

All experiments were performed with at least three different primary cultures or animals in independent experiments. Significance was evaluated by Student's *t*-test. Data are presented as mean ± SEM.

ICD antibody generation

Anti-ICD rabbit polyclonal antibody was generated by Open Biosystems, following the Custom Polyclonal Antibody Production protocol. Briefly, KLH-conjugated mouse and human ICD peptides were used as antigens (mouse, TKRRKSGKYKK VELKELGEMRSEPSL; human, TNRRKSGKYKKVEIKELGELR KEPSL). Immunoglobulin fraction was purified from the rabbit serum through protein A/G purification. Purified immunoglobulins

were tested by ELISA, immunoprecipitation, immunofluorescence, and immunohistochemistry for reactivity with the mouse and human ICD.

Acknowledgments

We thank Donghui Cheng for FACS, Mireille Riedinger for anti-ICD antibody generation, and Hong Zhang for human tissue preparation. We thank members of the Witte laboratory and Marta Morey for helpful comments and discussion on the manuscript, and Sandra Orellana for technical help. T.S. is supported by the California Institute for Regenerative Medicine Training Grant (TG2-01169) and the Department of Defense Prostate Cancer Research Program (PC110638). A.S.G. is supported by a Career Development Award from the SPORE in prostate cancer (Principal Investigator [PI]: Robert Reiter) and the Joe and Ali Torre-Prostate Cancer Foundation Young Investigator Award. J.M.D. is supported by the Department of Defense Prostate Cancer Research Program (PC101928) and UCLA Tumor Biology Program (Ruth L. Kirschstein Institutional National Research Service Award no. T32 CA009056). J.H. is supported by UCLA SPORE in Prostate Cancer (PI: Robert Reiter), Department of Defense Prostate Cancer Research Program grants W81XWH-11-1-0227 (PI: Jiaoti Huang) and W81XWH-12-1-0206 (PI: Lily Wu), and the National Cancer Institute (1R01CA158627-01; PI: Leonard Marks). J.H., A.S.G., and O.N.W. are supported by a Prostate Cancer Foundation Challenge Award (PI: Owen Witte). A.S.G. and O.N.W. are supported by a Prostate Cancer Foundation Creativity Award (PI: Owen Witte). O.N.W. is an Investigator of the Howard Hughes Medical Institute.

References

Alberti S. 2012. *Anti-trop-2 monoclonal antibodies and uses thereof in the treatment and diagnosis of tumors*. U.S. Patent US 20120052076.

Basu A, Goldenberg DM, Stein R. 1995. The epithelial/carcinoma antigen EGP-1, recognized by monoclonal antibody RS7-3G11, is phosphorylated on serine 303. *Int J Cancer* **62:** 472–479.

Bigas A, Martin DI, Milner LA. 1998. Notch1 and Notch2 inhibit myeloid differentiation in response to different cytokines. *Mol Cell Biol* **18:** 2324–2333.

Bostwick DG, Montironi R. 1995. Prostatic intraepithelial neoplasia and the origins of prostatic carcinoma. *Pathol Res Pract* **191:** 828–832.

Brown MS, Ye J, Rawson RB, Goldstein JL. 2000. Regulated intramembrane proteolysis: A control mechanism conserved from bacteria to humans. *Cell* **100:** 391–398.

Cardillo TM, Govindan SV, Sharkey RM, Trisal P, Goldenberg DM. 2011. Humanized anti-Trop-2 IgG-SN-38 conjugate for effective treatment of diverse epithelial cancers: Preclinical studies in human cancer xenograft models and monkeys. *Clin Cancer Res* **17:** 3157–3169.

Chen G, Shukeir N, Potti A, Sircar K, Aprikian A, Goltzman D, Rabbani SA. 2004. Up-regulation of Wnt-1 and β-catenin production in patients with advanced metastatic prostate carcinoma: Potential pathogenetic and prognostic implications. *Cancer* **101:** 1345–1356.

Cubas R, Zhang S, Li M, Chen C, Yao Q. 2010. Trop2 expression contributes to tumor pathogenesis by activating the ERK MAPK pathway. *Mol Cancer* **9:** 253. doi: 10.1186/1476-4598-9-253.

Cunha GR, Lung B. 1978. The possible influence of temporal factors in androgenic responsiveness of urogenital tissue recombinants from wild-type and androgen-insensitive (Tfm) mice. *J Exp Zool* **205:** 181–193.

De Strooper B, Annaert W, Cupers P, Saftig P, Craessaerts K, Mumm JS, Schroeter EH, Schrijvers V, Wolfe MS, Ray WJ, et al. 1999. A presenilin-1-dependent γ-secretase-like protease mediates release of Notch intracellular domain. *Nature* **398:** 518–522.

Dontu G, Abdallah WM, Foley JM, Jackson KW, Clarke MF, Kawamura MJ, Wicha MS. 2003a. In vitro propagation and transcriptional profiling of human mammary stem/progenitor cells. *Genes & Dev* **17:** 1253–1270.

Dontu G, Al-Hajj M, Abdallah WM, Clarke MF, Wicha MS. 2003b. Stem cells in normal breast development and breast cancer. *Cell Prolif* **36:** 59–72.

Dontu G, Jackson KW, McNicholas E, Kawamura MJ, Abdallah WM, Wicha MS. 2004. Role of Notch signaling in cell-fate determination of human mammary stem/progenitor cells. *Breast Cancer Res* **6:** R605–R615. doi: 10.1186/bcr920.

Fang YJ, Lu ZH, Wang GQ, Pan ZZ, Zhou ZW, Yun JP, Zhang MF, Wan DS. 2009. Elevated expressions of MMP7, TROP2, and survivin are associated with survival, disease recurrence, and liver metastasis of colon cancer. *Int J Colorectal Dis* **24:** 875–884.

Felli MP, Maroder M, Mitsiadis TA, Campese AF, Bellavia D, Vacca A, Mann RS, Frati L, Lendahl U, Gulino A, et al. 1999. Expression pattern of notch1, 2 and 3 and Jagged1 and 2 in lymphoid and stromal thymus components: Distinct ligand-receptor interactions in intrathymic T cell development. *Int Immunol* **11:** 1017–1025.

Fong D, Moser P, Krammel C, Gostner JM, Margreiter R, Mitterer M, Gastl G, Spizzo G. 2008a. High expression of TROP2 correlates with poor prognosis in pancreatic cancer. *Br J Cancer* **99:** 1290–1295.

Fong D, Spizzo G, Gostner JM, Gastl G, Moser P, Krammel C, Gerhard S, Rasse M, Laimer K. 2008b. TROP2: A novel prognostic marker in squamous cell carcinoma of the oral cavity. *Mod Pathol* **21:** 186–191.

Foster BA, Gingrich JR, Kwon ED, Madias C, Greenberg NM. 1997. Characterization of prostatic epithelial cell lines derived from transgenic adenocarcinoma of the mouse prostate (TRAMP) model. *Cancer Res* **57:** 3325–3330.

Goldstein AS, Lawson DA, Cheng D, Sun W, Garraway IP, Witte ON. 2008. Trop2 identifies a subpopulation of murine and human prostate basal cells with stem cell characteristics. *Proc Natl Acad Sci* **105:** 20882–20887.

Goldstein AS, Huang J, Guo C, Garraway IP, Witte ON. 2010. Identification of a cell of origin for human prostate cancer. *Science* **329:** 568–571.

Govindan SV, Stein R, Qu Z, Chen S, Andrews P, Ma H, Hansen HJ, Griffiths GL, Horak ID, Goldenberg DM. 2004. Preclinical therapy of breast cancer with a radioiodinated humanized anti-EGP-1 monoclonal antibody: Advantage of a residualizing iodine radiolabel. *Breast Cancer Res Treat* **84:** 173–182.

Govindan S, Qu Z, Hansen H, Goldenberg D. 2009. *RS7 antibodies*. U.S. Patent US 7517964 B2.

Kobel M, Kalloger SE, Boyd N, McKinney S, Mehl E, Palmer C, Leung S, Bowen NJ, Ionescu DN, Rajput A, et al. 2008. Ovarian carcinoma subtypes are different diseases: Implications for biomarker studies. *PLoS Med* **5:** e232. doi: 10.1371/journal.pmed.0050232.

Lal M, Caplan M. 2011. Regulated intramembrane proteolysis: Signaling pathways and biological functions. *Physiology* **26:** 34–44.

Lawson DA, Xin L, Lukacs RU, Cheng D, Witte ON. 2007. Isolation and functional characterization of murine prostate stem cells. *Proc Natl Acad Sci* **104:** 181–186.

Lobry C, Oh P, Aifantis I. 2011. Oncogenic and tumor suppressor functions of Notch in cancer: It's NOTCH what you think. *J Exp Med* **208:** 1931–1935.

Lois C, Hong EJ, Pease S, Brown EJ, Baltimore D. 2002. Germline transmission and tissue-specific expression of transgenes delivered by lentiviral vectors. *Science* **295:** 868–872.

Lukacs RU, Goldstein AS, Lawson DA, Cheng D, Witte ON. 2010. Isolation, cultivation and characterization of adult murine prostate stem cells. *Nat Protoc* **5:** 702–713.

Maetzel D, Denzel S, Mack B, Canis M, Went P, Benk M, Kieu C, Papior P, Baeuerle PA, Munz M, et al. 2009. Nuclear signalling by tumour-associated antigen EpCAM. *Nat Cell Biol* **11:** 162–171.

Maretzky T, Reiss K, Ludwig A, Buchholz J, Scholz F, Proksch E, de Strooper B, Hartmann D, Saftig P. 2005. ADAM10 mediates E-cadherin shedding and regulates epithelial cell–cell adhesion, migration, and β-catenin translocation. *Proc Natl Acad Sci* **102:** 9182–9187.

Memarzadeh S, Zong Y, Janzen DM, Goldstein AS, Cheng D, Kurita T, Schafenacker AM, Huang J, Witte ON. 2010. Cell-autonomous activation of the PI3-kinase pathway initiates endometrial cancer from adult uterine epithelium. *Proc Natl Acad Sci* **107:** 17298–17303.

Muhlmann G, Spizzo G, Gostner J, Zitt M, Maier H, Moser P, Gastl G, Zitt M, Muller HM, Margreiter R, et al. 2009. TROP2 expression as prognostic marker for gastric carcinoma. *J Clin Pathol* **62:** 152–158.

Mulholland DJ, Xin L, Morim A, Lawson D, Witte O, Wu H. 2009. $Lin^{-}Sca\text{-}1^{+}CD49f^{high}$ stem/progenitors are tumor-initiating cells in the Pten-null prostate cancer model. *Cancer Res* **69:** 8555–8562.

Mumm JS, Schroeter EH, Saxena MT, Griesemer A, Tian X, Pan DJ, Ray WJ, Kopan R. 2000. A ligand-induced extracellular cleavage regulates γ-secretase-like proteolytic activation of Notch1. *Mol Cell* **5:** 197–206.

Nakashima K, Shimada H, Ochiai T, Kuboshima M, Kuroiwa N, Okazumi S, Matsubara H, Nomura F, Takiguchi M, Hiwasa T. 2004. Serological identification of TROP2 by recombinant cDNA expression cloning using sera of patients with esophageal squamous cell carcinoma. *Int J Cancer* **112:** 1029–1035.

Ohmachi T, Tanaka F, Mimori K, Inoue H, Yanaga K, Mori M. 2006. Clinical significance of TROP2 expression in colorectal cancer. *Clin Cancer Res* **12:** 3057–3063.

Okabe M, Tsukahara Y, Tanaka M, Suzuki K, Saito S, Kamiya Y, Tsujimura T, Nakamura K, Miyajima A. 2009. Potential hepatic stem cells reside in $EpCAM^{+}$ cells of normal and injured mouse liver. *Development* **136:** 1951–1960.

Ralhan R, Cao J, Lim T, Macmillan C, Freeman JL, Walfish PG. 2010a. EpCAM nuclear localization identifies aggressive thyroid cancer and is a marker for poor prognosis. *BMC Cancer* **10:** 331. doi: 10.1186/1471-2407-10-331.

Ralhan R, He HC, So AK, Tripathi SC, Kumar M, Hasan MR, Kaur J, Kashat L, MacMillan C, Chauhan SS, et al. 2010b. Nuclear and cytoplasmic accumulation of Ep-ICD is frequently detected in human epithelial cancers. *PLoS ONE* **5:** e14130. doi: 10.1371/journal.pone.0014130.

Ranganathan P, Weaver KL, Capobianco AJ. 2011. Notch signalling in solid tumours: A little bit of everything but not all the time. *Nat Rev Cancer* **11:** 338–351.

Reynolds BA, Weiss S. 1996. Clonal and population analyses demonstrate that an EGF-responsive mammalian embryonic CNS precursor is a stem cell. *Dev Biol* **175:** 1–13.

Ripani E, Sacchetti A, Corda D, Alberti S. 1998. Human Trop-2 is a tumor-associated calcium signal transducer. *Int J Cancer* **76:** 671–676.

Salm SN, Koikawa Y, Ogilvie V, Tsujimura A, Coetzee S, Moscatelli D, Moore E, Lepor H, Shapiro E, Sun TT, et al. 2000. Generation of active TGF-β by prostatic cell cocultures using novel basal and luminal prostatic epithelial cell lines. *J Cell Physiol* **184:** 70–79.

Schroeter EH, Kisslinger JA, Kopan R. 1998. Notch-1 signalling requires ligand-induced proteolytic release of intracellular domain. *Nature* **393:** 382–386.

Shahi P, Seethammagari MR, Valdez JM, Xin L, Spencer DM. 2011. Wnt and Notch pathways have interrelated opposing roles on prostate progenitor cell proliferation and differentiation. *Stem Cells* **29:** 678–688.

Shih LB, Xuan H, Aninipot R, Stein R, Goldenberg DM. 1995. In vitro and in vivo reactivity of an internalizing antibody, RS7, with human breast cancer. *Cancer Res* **55:** 5857s–5863s.

Shou J, Ross S, Koeppen H, de Sauvage FJ, Gao WQ. 2001. Dynamics of notch expression during murine prostate development and tumorigenesis. *Cancer Res* **61:** 7291–7297.

Solanas G, Cortina C, Sevillano M, Batlle E. 2011. Cleavage of E-cadherin by ADAM10 mediates epithelial cell sorting downstream of EphB signalling. *Nat Cell Biol* **13:** 1100–1107.

Stein R, Chen S, Haim S, Goldenberg DM. 1997. Advantage of yttrium-90-labeled over iodine-131-labeled monoclonal antibodies in the treatment of a human lung carcinoma xenograft. *Cancer* **80:** 2636–2641.

Trerotola M, Cantanelli P, Guerra E, Tripaldi R, Aloisi AL, Bonasera V, Lattanzio R, Lange RD, Weidle UH, Piantelli M, et al. 2012a. Upregulation of Trop-2 quantitatively stimulates human cancer growth. *Oncogene* (in press). doi: 10.1038/onc.2012.36.

Trerotola M, Li J, Alberti S, Languino LR. 2012b. Trop-2 inhibits prostate cancer cell adhesion to fibronectin through the β1 integrin–RACK1 axis. *J Cell Physiol* **227:** 3670–3677.

Tsukahara Y, Tanaka M, Miyajima A. 2011. TROP2 expressed in the trunk of the ureteric duct regulates branching morphogenesis during kidney development. *PLoS ONE* **6:** e28607. doi: 10.1371/journal.pone.0028607.

van Leenders GJLH, Dukers D, Hessels D, van den Kieboom SWM, Hulsbergen CA, Witjes JA, Otte AP, Meijer CJ, Raaphorst FM. 2007. Polycomb-group oncogenes EZH2, BMI1, and RING1 are overexpressed in prostate cancer with adverse pathologic and clinical features. *Eur Urol* **52:** 455–463.

Visvader JE. 2011. Cells of origin in cancer. *Nature* **469:** 314–322.

Wang XD, Leow CC, Zha J, Tang Z, Modrusan Z, Radtke F, Aguet M, de Sauvage FJ, Gao WQ. 2006. Notch signaling is required for normal prostatic epithelial cell proliferation and differentiation. *Dev Biol* **290:** 66–80.

Wang J, Day R, Dong Y, Weintraub SJ, Michel L. 2008. Identification of Trop-2 as an oncogene and an attractive therapeutic target in colon cancers. *Mol Cancer Ther* **7:** 280–285.

Wang J, Zhang K, Grabowska D, Li A, Dong Y, Day R, Humphrey P, Lewis J, Kladney RD, Arbeit JM, et al. 2011. Loss of Trop2 promotes carcinogenesis and features of epithelial to mesenchymal transition in squamous cell carcinoma. *Mol Cancer Res* **9:** 1686–1695.

Weng AP, Ferrando AA, Lee W, Morris JP IV, Silverman LB, Sanchez-Irizarry C, Blacklow SC, Look AT, Aster JC. 2004. Activating mutations of NOTCH1 in human T cell acute lymphoblastic leukemia. *Science* **306:** 269–271.

Xin L, Ide H, Kim Y, Dubey P, Witte ON. 2003. In vivo regeneration of murine prostate from dissociated cell populations of postnatal epithelia and urogenital sinus mesenchyme. *Proc Natl Acad Sci* **100:** 11896–11903.

Xin L, Teitell MA, Lawson DA, Kwon A, Mellinghoff IK, Witte ON. 2006. Progression of prostate cancer by synergy of AKT with genotropic and nongenotropic actions of the androgen receptor. *Proc Natl Acad Sci* **103:** 7789–7794.

Xin L, Lukacs RU, Lawson DA, Cheng D, Witte ON. 2007. Self-renewal and multilineage differentiation in vitro from murine prostate stem cells. *Stem Cells* **25:** 2760–2769.

Yardy GW, Brewster SF. 2005. Wnt signalling and prostate cancer. *Prostate Cancer Prostatic Dis* **8:** 119–126.

Yardy GW, Bicknell DC, Wilding JL, Bartlett S, Liu Y, Winney B, Turner GD, Brewster SF, Bodmer WF. 2009. Mutations in the AXIN1 gene in advanced prostate cancer. *Eur Urol* **56:** 486–494.

Yoshimoto M, Cutz JC, Nuin PA, Joshua AM, Bayani J, Evans AJ, Zielenska M, Squire JA. 2006. Interphase FISH analysis of PTEN in histologic sections shows genomic deletions in 68% of primary prostate cancer and 23% of high-grade prostatic intra-epithelial neoplasias. *Cancer Genet Cytogenet* **169:** 128–137.

Young DSF, Findlay HP, Hahn SE, DaCruz LAG, Ferry AL. 2008. *Cytotoxicity mediation of cells evidencing surface expression of TROP-2*. U.S. Patent US 7420041 B2.

Zhao G, Liu Z, Ilagan MX, Kopan R. 2010. γ-Secretase composed of PS1/Pen2/Aph1a can cleave notch and amyloid precursor protein in the absence of nicastrin. *J Neurosci* **30:** 1648–1656.

Supplemental Information

Regulated Proteolysis of Trop2 Drives Epithelial Hyperplasia and Stem Cell Self-Renewal via β-catenin Signaling

Tanya Stoyanova, Andrew S. Goldstein, Houjian Cai, Justin M. Drake, Jiaoti Huang and Owen N. Witte

Inventory

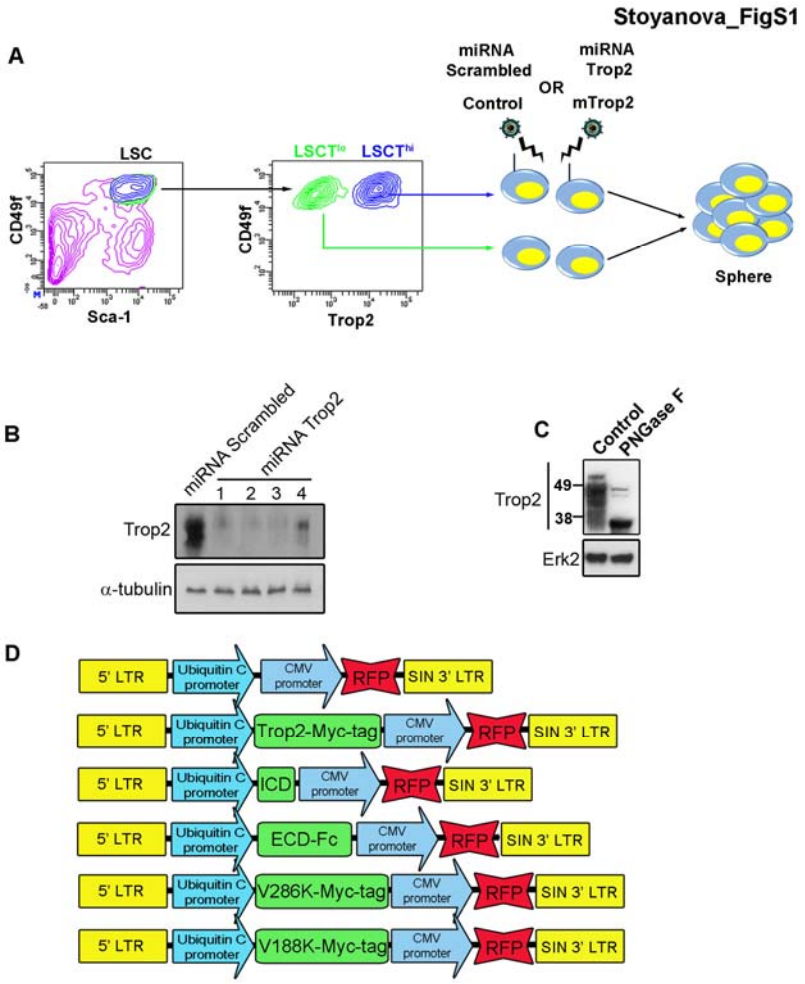

Figure S1. *Schematic representation of sphere assay and constructs used.* (*A*) Schematic of the *in vitro* sphere assay with a representative fluorescence-activated cell sorting (FACS) plot used for purification of LSCT^{hi} and LSCT^{lo} primary mouse prostate cells. (*B*) 293T cells were transfected with mouse Trop2 (mTrop2) and scrambled miRNA or different Trop2 miRNA expressing constructs (1-4). Trop2 miRNA #2 was chosen for further experiments. (*C*) Prostate epithelial cells transduced with mTrop2 were either treated with PNGase F or left untreated (control). Trop2 is highly glycosylated and appears as an irregular band between 35 and 50 kDa. Treatment with PNgase F removes N-linked glycans from Trop2. (*D*) Schematic representation of lentiviral constructs used for ectopic expression of Trop2, ICD, ECD and cleavage mutants V286K, V188K.

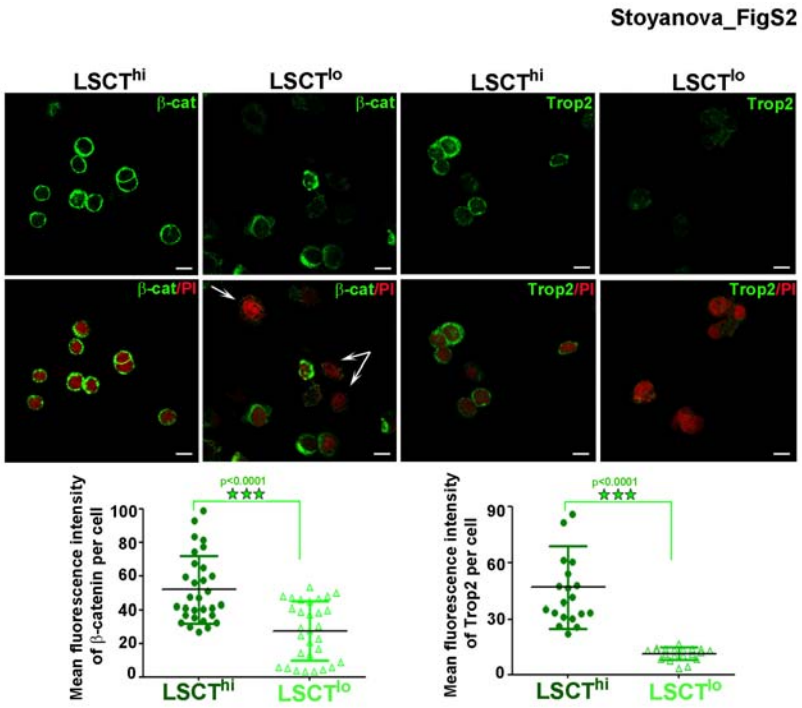

Figure S2. *LSCT^{lo} cells express lower level of β-catenin.* LSCT^{hi} and LSCT^{lo} primary mouse prostate cells were isolated by FACS. Cells were stained with anti-β-catenin or anti-Trop2 antibodies and Propidium Iodine (PI) followed by confocal microscopy. White arrows point to LSCT^{lo} cells with low expression of β-catenin. Scale bars represent 10 microns. Mean fluorescence intensity of β-catenin and Trop2 staining in LSCT^{hi} and LSCT^{lo} cells is plotted.

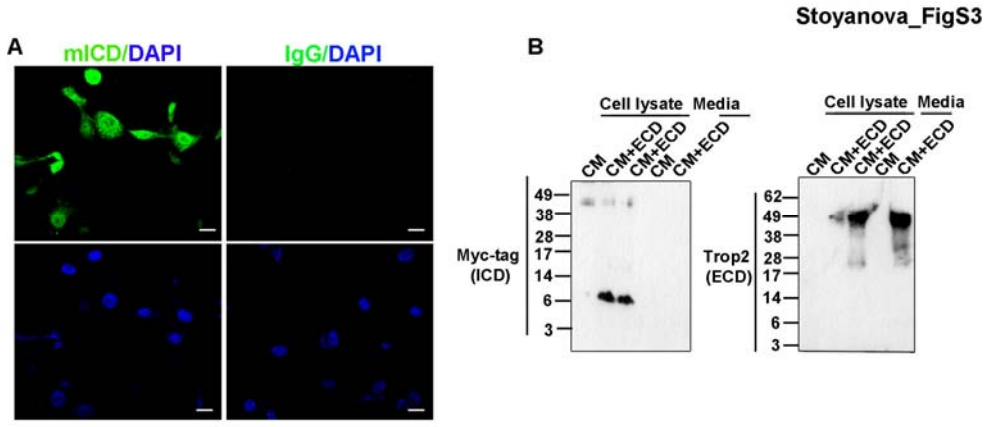

Figure S3. *Trop2 ECD induces cleavage of Trop2.* TRAMP-C2 cells were infected with lentivirus expressing mouse Trop2 ICD (mICD). Cells were fixed and subjected to immunofluorescence using anti-ICD or a control (IgG) antibody. Confocal microscopy images are presented. Scale bars represent 10 microns. (*B*) PEB-Trop2-Myc-tag cells were either treated with conditioned media from 293T infected with a control RFP lentivirus (CM) or from 293T cells stably expressing and secreting Trop2-ECD-Fc and RFP (CM+ECD) at two different concentrations. Cell lysates from PEB cells (Cell lysate) and the conditioned media from 293T infected with a control RFP lentivirus (CM) or from 293T cells stably expressing and secreting Trop2-ECD-Fc and RFP (CM+ECD) (Media) were subjected to SDS Page followed by western blot with anti-Myc-tag or anti-Trop2 ECD antibody.

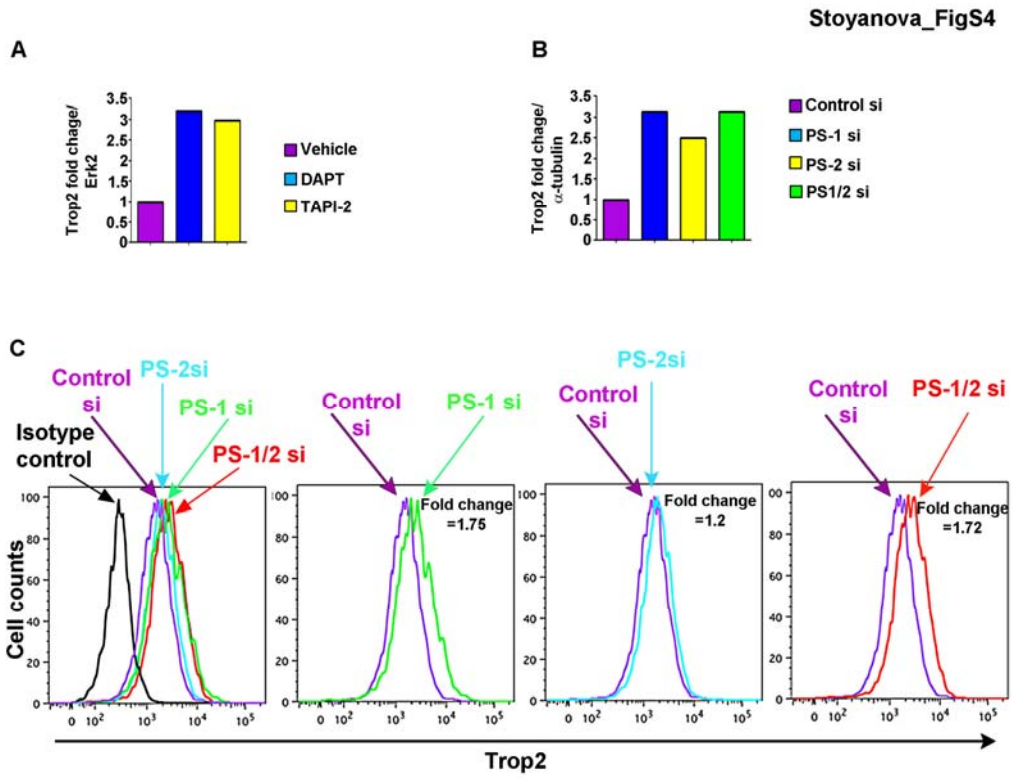

Figure S4. *Down-regulation of PS-1 leads to increased surface Trop2 expression.* (*A)* Intensity of Trop2 full length signal in Figure 3A was quantified and normalized to Erk2 using Image J software. The quantification values were normalized to the Vehicle control. (*B)* Intensity of Trop2 full length signal in Figure 3B was quantified and normalized to α-tubulin using Image J software. The quantification values were normalized to the Control si. (*C*) PEB cells transduced with mTrop2-RFP were transfected with control, PS-1, PS-2 or both PS-1 and PS-2 siRNA and stained with anti-Trop2 ECD antibody followed by FACS analysis. Fold change of mean fluorescent intensity compared to control siRNA is shown.

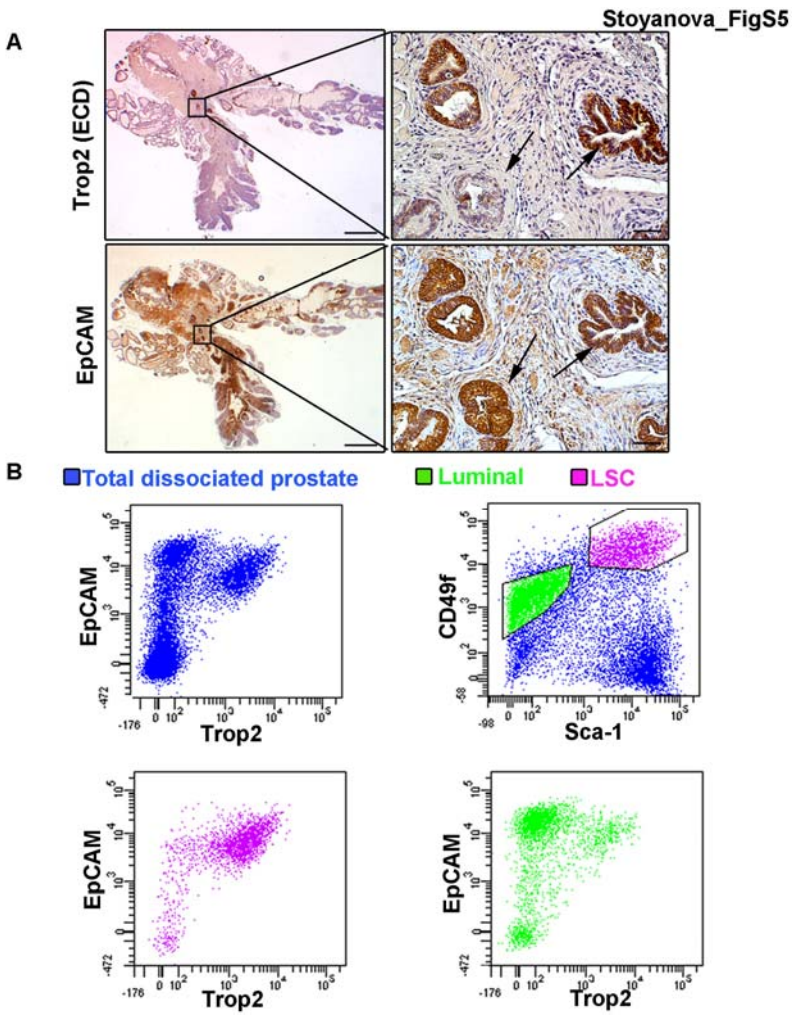

Figure S5. *Trop2 and EpCAM are differentially expressed in the mouse prostate.* (*A*) Immunohistochemistry of a representative 12 week old mouse prostate stained with antibodies against the extracellular domain of Trop2 indicated as Trop2 (ECD) or EpCAM. Arrows indicate tubules with high or low levels of Trop2 and corresponding EpCAM staining. Scale bars represent 1 mm (left panels) or 100 microns (right panels). (*B*) FACS analysis of Trop2 and EpCAM surface levels in basal and luminal primary prostate cells. Luminal cells were gated on CD49f ^{lo} and Sca-1^{-} and are marked in green. Basal cells (LSC) were gated on CD49f ^{hi} and Sca1^{+} and are marked in pink.

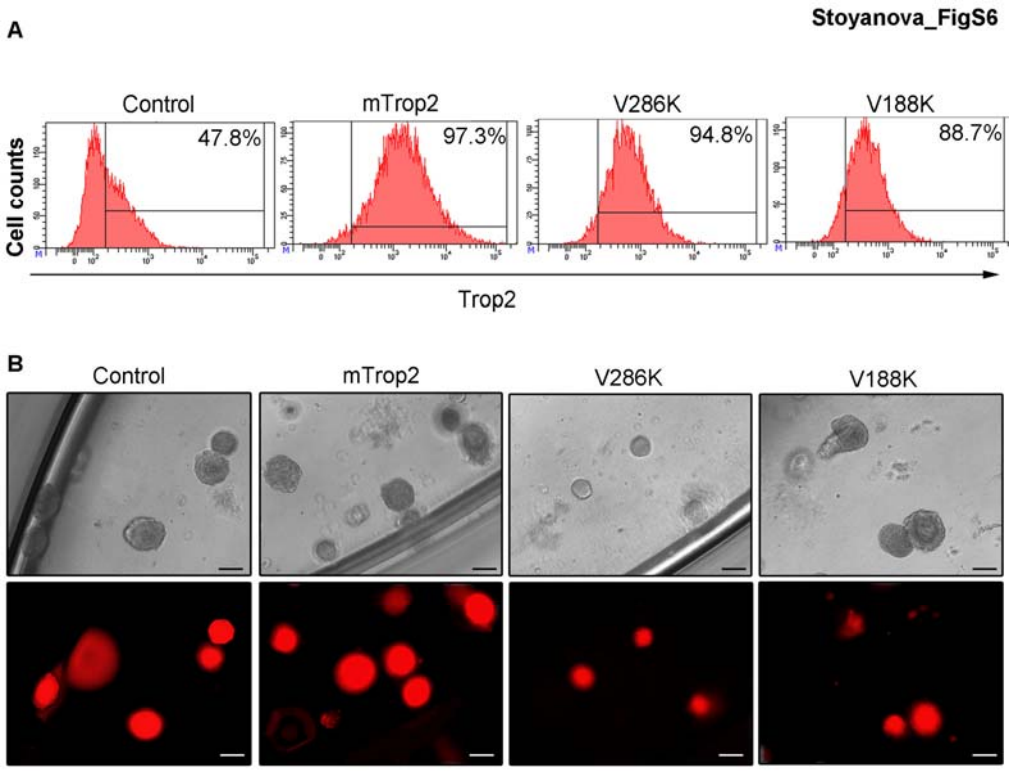

Figure S6. *Trop2 cleavage mutants localize to the cell surface but are deficient in inducing self-renewal in vitro.* (*A*) FACS analysis of PEB cells transduced with lentivirus carrying RFP (Control), mTrop2, V188K or V286K and stained with anti-Trop2 ECD antibody for analysis by FACS. mTrop2, V188K and V286K localize to the cellular membrane. (*B*) Representative pictures of spheres expressing mTrop2, V286K or V188K mutants from Figure 3F. Scale bars represent 100 microns. Bottom panels show RFP expression, indicating the infection efficiency.

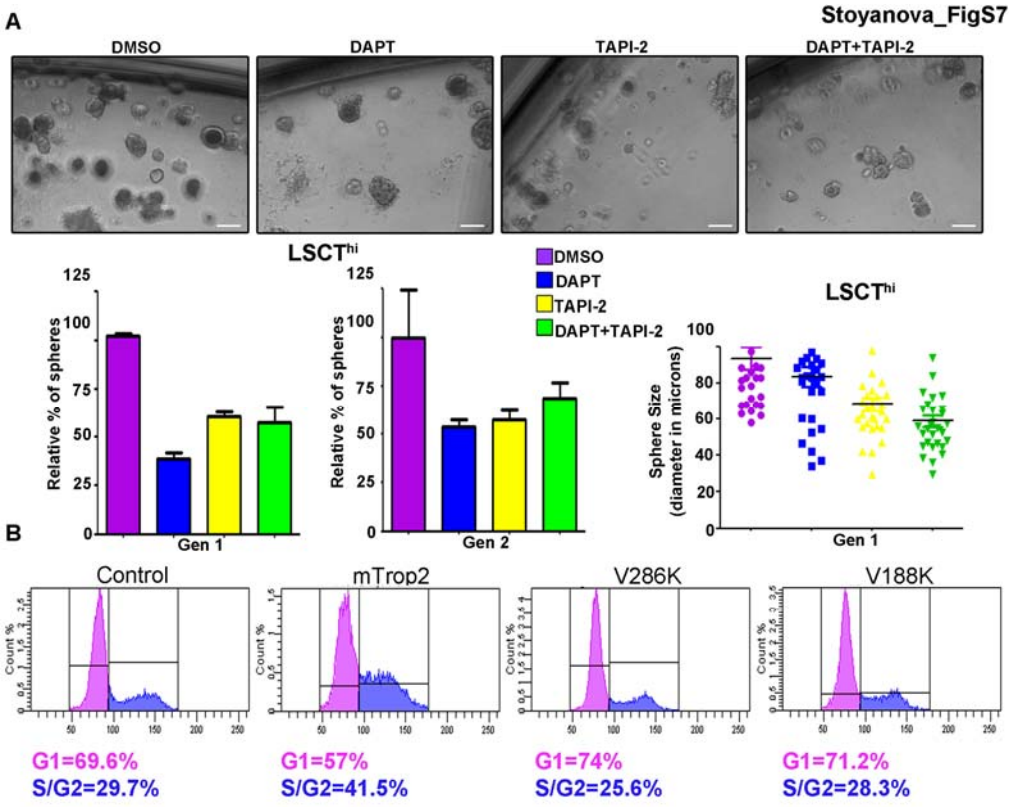

Figure S7. *Cleavage of Trop2 is necessary for its self-renewal and proliferative function.* (*A*) Equal numbers of progenitor cells (LSCT^{hi}) were plated in triplicate and treated with DMSO, DAPT, TAPI-2 or the combination of DAPT and TAPI-2 every 48h hours. Upper panels show images of spheres grown in the indicated conditions. Scale bars represent 100 microns. Sphere number and sphere size was reduced upon treatment with DAPT and TAPI-2 (bottom graphs). Sphere size was measured at Gen 1. (*B*) Cell cycle analysis of PEB cells transduced with lentivirus carrying RFP (Control), mTrop2, V188K or V286K and stained with PI. Both mutants V188K and V286K fail to increase cycling PEB cells.

Stoyanova_FigS8

Prostatic Adenocarcinoma			Nuclear ICD	
Gleason grade	Pathologic stage	Age	Benign	Cancer
9	pT3a pN0 Mx	60	No	Yes
9	pT3a pN0 Mx	60	No	Yes
8	pT3a N1 Mx	71	No	Yes
7	pT2c Nx Mx	52	No	No
7	pT2c Nx Mx	56	No	Yes
7	pT2c Nx Mx	67	No	Yes
7	pT2a N0 Mx	71	No	No
7	pT3a Nx Mx	56	No	Yes
7	pT3b N0 Mx	60	No	No
7	pT3b N0 Mx	68	No	No
6	pT2b N0 Mx	49	No	No

Figure S8. *Nuclear localization of ICD is found in human prostate cancer.* Table shows patient samples analyzed in Figure 4. Pathologic stage is based on the 7th Edition AJCC Cancer Staging Manual. The presence (Yes) or absence (No) of nuclear ICD is shown in the last two columns.

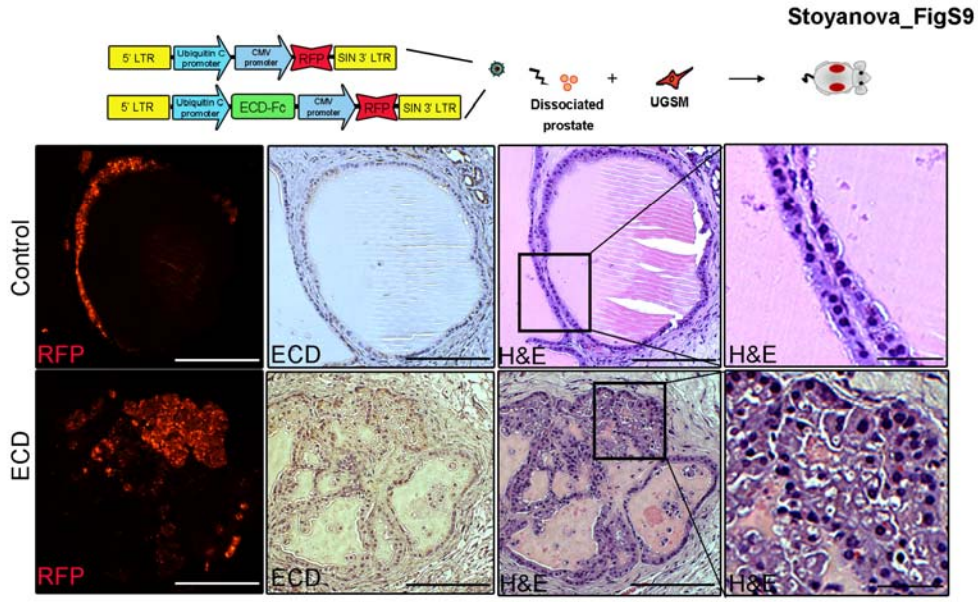

Figure S9. *ECD alone drive hyperplasia in vivo.* Schematic representation of the *in vivo* regeneration assay and lentiviral constructs used is presented. Dissociated primary prostate cells were transduced with lentivirus carrying RFP (Control) or ECD-Fc. Infected prostate cells were combined with UGSM and subjected to the *in vivo* regeneration assay. Eight weeks later, tissues were removed and gland histology was examined. Left panels represent immunofluorescence (IF) showing infected tubules, middle panels show IHC with anti-Trop2 ECD. Right two panels show the histology of the recovered grafts. One out of two independent experiments is shown. Scale bars represent 100 or 50 (right panels) microns.

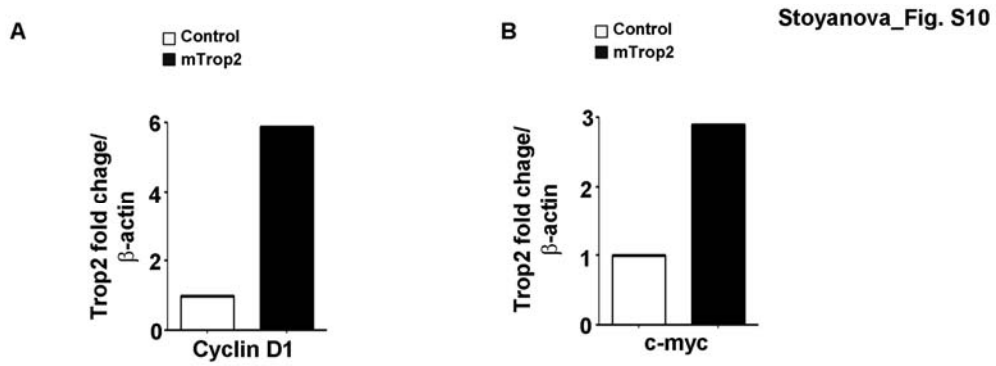

Figure S10. *Over-expression of Trop2 increases β-catenin target genes* (*A*) Intensity of cyclin D1 signal in Figure 6C was quantified and normalized to β-actin using Image J software. (*B*) Intensity of c-myc signal in Figure 6C was quantified and normalized to β-actin using Image J software. In both cases, the quantification values were normalized to the Control.

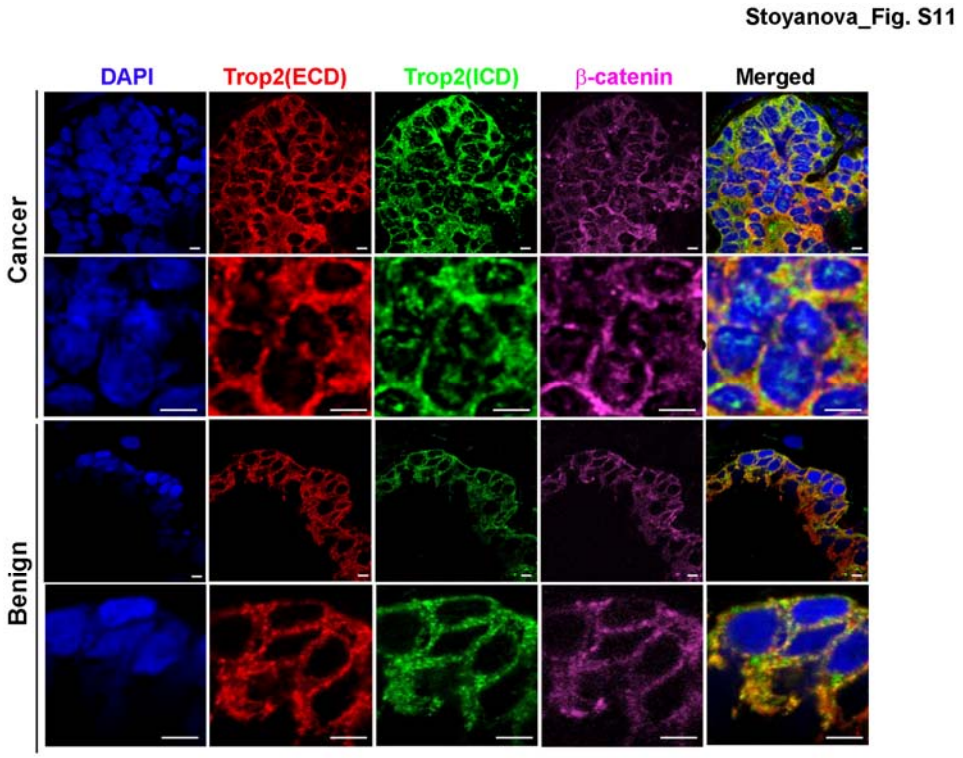

Figure S11. *Trop2 co-localizes with β-catenin in human prostate cancer.* Complete immunofluorescence panel presented in Figure 7A is shown. Human prostate cancer patient samples were stained with anti-ICD, ECD and anti-β-catenin antibodies and DAPI. ICD (green) co-localizes with -β-catenin (pink) in the nucleus only in cancer, but not in the benign prostate. DAPI demonstrates nuclear staining (blue). Merged images are presented in the bottom panels. Scale bars represent 10 microns.

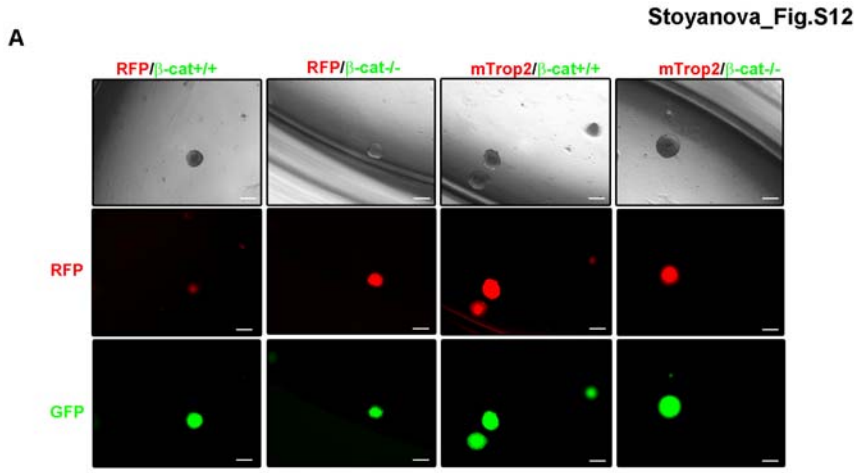

Figure S12. *Trop2 regulates self-renewal though β-catenin.* Representative pictures of spheres shown in Figure 7B. Scale bars represent 100 microns.

Prostate cancer originating in basal cells progresses to adenocarcinoma propagated by luminal-like cells

Tanya Stoyanova[a], Aaron R. Cooper[b], Justin M. Drake[a], Xian Liu[c], Andrew J. Armstrong[d], Kenneth J. Pienta[e], Hong Zhang[f], Donald B. Kohn[a,g,h], Jiaoti Huang[f,g,h], Owen N. Witte[a,c,g,h,i,1], and Andrew S. Goldstein[c,g,h,j,1]

[a]Microbiology, Immunology and Molecular Genetics, [b]Molecular Biology Interdepartmental Ph.D. Program, [c]Departments of Molecular and Medical Pharmacology, [f]Pathology and Laboratory Medicine, [g]Jonsson Comprehensive Cancer Center, David Geffen School of Medicine, [h]Eli and Edythe Broad Center of Regenerative Medicine and Stem Cell Research, [i]Howard Hughes Medical Institute, and [j]Department of Urology, University of California, Los Angeles, CA 90095; [d]Duke Cancer Institute, Duke University Medical Center, Durham, NC 27710; and [e]Brady Urological Institute, The Johns Hopkins School of Medicine, Baltimore, MD 21287

Contributed by Owen N. Witte, November 1, 2013 (sent for review October 18, 2013)

The relationship between the cells that initiate cancer and the cancer stem-like cells that propagate tumors has been poorly defined. In a human prostate tissue transformation model, basal cells expressing the oncogenes Myc and myristoylated AKT can initiate heterogeneous tumors. Tumors contain features of acinar-type adenocarcinoma with elevated eIF4E-driven protein translation and squamous cell carcinoma marked by activated beta-catenin. Lentiviral integration site analysis revealed that alternative histological phenotypes can be clonally derived from a common cell of origin. In advanced disease, adenocarcinoma can be propagated by self-renewing tumor cells with an androgen receptor-low immature luminal phenotype in the absence of basal-like cells. These data indicate that advanced prostate adenocarcinoma initiated in basal cells can be maintained by luminal-like tumor-propagating cells. Determining the cells that maintain human prostate adenocarcinoma and the signaling pathways characterizing these tumor-propagating cells is critical for developing effective therapeutic strategies against this population.

Tumors that arise from a given tissue in the body exhibit heterogeneity with respect to their molecular alterations, biological behavior, and response to therapy (1). Such variation presents a serious challenge for clinical cancer management. In many organ sites, tumors have been classified into subtypes based on their molecular and histological features (2). Subtypes of cancer can reflect distinct states of differentiation within a given tissue, leading Visvader and coworkers to propose that different epithelial tumor subtypes can arise from transformation of distinct cells of origin with different developmental potential (3). Functional studies in the mouse mammary gland and mouse lung support this model (4, 5). However, there is limited functional evidence for such a mechanism in human epithelial cancer.

Several recent studies using mouse models have revealed that the same phenotypic cell that initiates cancer can be responsible for tumor maintenance or propagation. Lgr5+ intestinal stem cells can initiate and maintain murine intestinal adenomas (6, 7). In mouse models of skin cancer, hair follicle bulge stem cells can serve as target cells for transformation (8) and CD34+ cells resembling their normal bulge stem cell counterpart are capable of propagating the disease as a cancer stem cell population (9). Mouse models of breast cancer demonstrate that tumors can arise from the transformation of luminal cells (4), and recent studies using human tumor samples indicate that breast cancer can also be propagated by luminal-like cells (10). In most human epithelial cancers it has not been determined whether the cell types that give rise to cancer are also capable of maintaining advanced disease.

The predominant histological subtype of prostate cancer is acinar-type adenocarcinoma (11), with features of luminal secretory cells, rare neuroendocrine cells, and an absence of basal cells. A number of less common histological variants are found in prostate cancer, including small cell carcinoma and squamous cell carcinoma. Both of these variants are associated with poor prognosis, aggressive disease, and resistance to hormonal therapy (androgen deprivation and/or androgen receptor blockade) (11). Small-cell carcinoma is characterized by proliferating neuroendocrine cells and loss of p53 (12). Squamous cancers have features of basal cells and can occur either in the context of adenocarcinoma or alone as squamous cell carcinoma (11, 13, 14). Based on their different phenotypes and response to hormonal therapy, different histological variants of prostate cancer are predicted to arise from distinct cells of origin (13).

The relationship between the cells that initiate and maintain human prostate adenocarcinoma is not known. Naïve human prostate basal cells can initiate acinar-type adenocarcinoma in response to oncogenic stimulation (15). Consistent with these findings, basal cells from the BPH-1 human prostate cell line can initiate human prostate cancer in response to combined estrogen and testosterone treatment (16). These collective data suggest that human prostate tumors may set aside a subset of basal cells within the tumor to ensure continuous production of malignant luminal-like cancer cells.

Human prostate cancer cells with a basal phenotype have been reported to produce luminal cancer progeny in vitro (17). Using cell lines that were originally derived from human prostate tumors, it was shown that basal cell marker CD44 enriched for tumor-propagating cells in the absence of differentiated luminal cell markers (18). A recent study demonstrates that advanced chemotherapy-resistant prostate cancer is maintained by cells lacking basal or luminal cytokeratins (19). No study has defined the role of basal or luminal-like cells isolated directly from primary human prostate cancer in tumor propagation.

In the present study, we use a tissue-regeneration model of human prostate cancer to determine whether the cells at the origin of prostate cancer are continually required to maintain the disease as tumor-propagating cells. Benign cell populations isolated from primary human prostate tissue were first tested for

Significance

This study determined that two histological phenotypes of cancer can arise from a common target cell. Whereas luminal cells are not efficient cells of origin, luminal-like tumor cells isolated from human prostate adenocarcinoma can serially propagate advanced disease.

Author contributions: T.S., A.R.C., D.B.K., J.H., O.N.W., and A.S.G. designed research; T.S., A.R.C., J.M.D., X.L., H.Z., and A.S.G. performed research; A.J.A. and K.J.P. contributed new reagents/analytic tools; T.S., A.R.C., J.H., O.N.W., and A.S.G. analyzed data; and T.S., A.R.C., O.N.W., and A.S.G. wrote the paper.

The authors declare no conflict of interest.

Freely available online through the PNAS open access option.

[1]To whom correspondence may be addressed. E-mail: owenwitte@mednet.ucla.edu or agoldstein@mednet.ucla.edu.

This article contains supporting information online at www.pnas.org/lookup/suppl/doi:10.1073/pnas.1320565110/-/DCSupplemental.

their susceptibility to transformation by defined oncogenes. In the resulting tumors, cancer cell populations were further transplanted to define the cells capable of propagating the disease. Tumors driven by expression of oncogenes Myc and myristoylated/activated AKT (myrAKT) initiating in basal cells exhibit features of both adenocarcinoma and squamous cell carcinoma with different signaling pathways characteristic of each histological pattern. eIF4E-driven protein translation pathway is elevated in adenocarcinoma, whereas activation of beta-catenin is associated with squamous differentiation in experimental and clinical human prostate cancer. Using lentiviral integration site analysis, we determined that alternative histological phenotypes of prostate cancer can arise from a clonal cell of origin. Adenocarcinoma can be serially propagated by cells with a luminal phenotype. Our results indicate that cancer initiated in basal cells can evolve to adenocarcinoma maintained by luminal-like cells.

Results

Basal Cells Initiate Heterogeneous Human Prostate Cancer. Two of the most common alterations identified in human prostate tumors are increased expression of Myc (20) and activation of AKT, typically via loss of PTEN (21). Coexpression of Myc and phosphorylated AKT are rarely observed in primary localized prostate cancer, but are commonly found in advanced metastatic prostate tumors (Fig. 1*A*). The oncogenes Myc, myrAKT, or both Myc and myrAKT were introduced via lentivirus into highly enriched populations of human prostate basal ($CD45^{-}Trop2^{+}CD49f^{hi}CD26^{-}$) and luminal ($CD45^{-}Trop2^{+}CD49f^{lo}CD26^{+}$) cells isolated by FACS. Basal and luminal epithelial cells were purified from preparations of dissociated, freshly isolated prostate tissue from six patients undergoing radical prostatectomy. Transduced human prostate epithelial cells were combined with inductive murine urogenital sinus mesenchyme (UGSM) with Matrigel and implanted s.c. into immune-deficient NOD-SCID-IL2Rγ^{null} mice (Fig. S1*A*). Consistent with previous findings (15), infection of human prostate luminal-enriched cells did not result in any detectable epithelial structures after 12 wk in vivo, regardless of whether cells were transduced with a single oncogene or the combination of Myc and myrAKT. Even implantation of 100,000 luminal cells was insufficient to generate primary tumors (Fig. S1*B*).

When expressed in naïve human prostate basal-enriched cells, Myc or myrAKT alone gave rise to benign glands or low-grade prostatic intraepithelial neoplasia lesions with distinct p63+ basal and androgen receptor-positive (AR+) luminal layers (Fig. 1 *B* and *C*). The two oncogenes dramatically synergized in human prostate basal cells to consistently generate large tumors in as little as 6 wk (Fig. 1*B*). Transduced basal cells were implanted in limiting numbers (10^5, 5×10^4, 10^4, and 10^3) in vivo to determine the number of target cells required to respond to oncogenic stimulation. As few as 10,000 basal cells were sufficient to initiate tumors in 12 wk (Fig. S1*B*). Metastasis was not observed in tumor-bearing mice, indicating that further genetic alterations or a longer time period may be required to observe metastatic lesions.

Regenerated tumors contained both acinar-type adenocarcinoma and squamous features (Fig. 2*A*). Adenocarcinoma regions were defined by high levels of expression of the luminal markers Keratin 8 (K8) and CD26, heterogeneous expression of AR, scattered chromogranin A+ neuroendocrine-like (NE) cells and an absence of basal markers Keratin 14 (K14), p63, and Keratin 5 (K5) (Fig. 2*B*). Conversely, squamous regions expressed basal cell markers K14, p63, and K5 and lacked cells expressing K8, CD26, AR, or chromogranin A. All tumors were confirmed to express oncogenes Myc and myrAKT and have a human origin based on staining with a pan-HLA antibody (Fig. 2*B* and Fig. S2). This heterogeneous tumor provides a model to investigate the relationship between different histological phenotypes within an individual cancer. In clinical prostate cancer, the squamous phenotype is rare in primary tumors. Squamous differentiation is predominantly observed in aggressive metastatic tumors that are resistant to androgen-deprivation therapy (22).

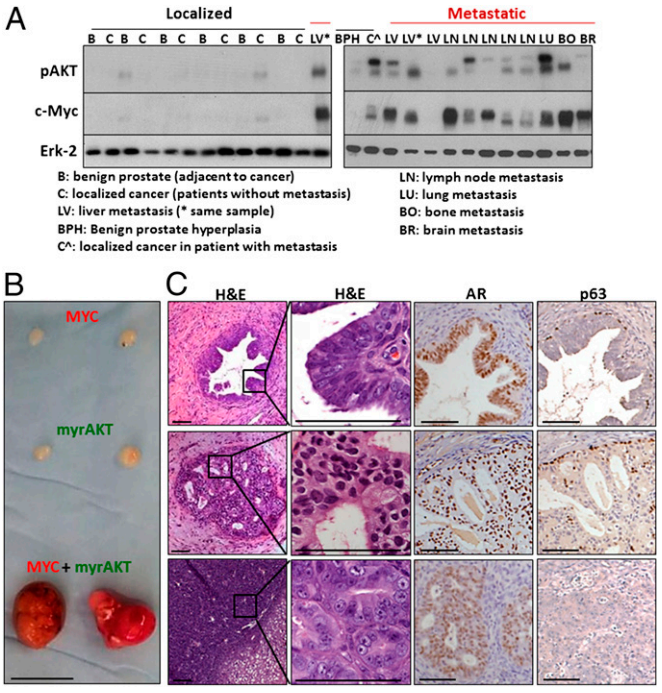

Fig. 1. Myc and myrAKT are coexpressed in advanced prostate cancer and synergize to initiate human prostate cancer. (*A*) Localized (black line) and metastatic (red line) human prostate cancer specimens were subjected to Western blot analysis with antibodies against phosphorylated AKT (pAKT), Myc, and Erk as a loading control. (*B*) Naïve benign basal or luminal cells were transduced with Myc, myrAKT, or both Myc and myrAKT at varying cell doses. Representative tumors initiated from basal cells expressing Myc, myrAKT, or both after 8 wk of regeneration. (Scale bar, 1 cm.) (*C*) Histology of representative lesions initiated from basal cells expressing Myc, myrAKT, or both stained for H&E, AR, and p63. (Scale bars, 100 μm.)

Distinct Histological Phenotypes Share a Clonal Origin. Human prostate cancer often presents as a multifocal disease where distinct cancerous lesions are present within an individual patient's tissue. Multiple tumor foci can regularly be identified within regenerated tumors using the in vivo tissue-regeneration assay (15). We identified certain regions containing cells with adjacent squamous (K14/p63/K5) and luminal (K8/CD26) phenotypes in close proximity without defined borders (Fig. 3 *A* and *B*). These mixed regions made up an average of six foci per tumor, covering ~18% of the total tumor area (Fig. S3). These regions containing both histological phenotypes originate either from the merging of two neighboring glands of distinct histological phenotypes or from a single gland capable of multilineage differentiation. The most definitive method to distinguish these possible outcomes is lentiviral integration site analysis (23).

Tumors were initiated from naïve human prostate basal cells transduced with lentivirus, resulting in the integration of viral DNA into the genome of the target cell and all of its progeny. If both adenocarcinoma and squamous phenotypes within an individual region arise from the same transformed basal cell, they should share a set of common lentiviral integration sites. However, if distinct histological phenotypes in an individual region arise from distinct cells of origin, they should not share any common integration sites.

Laser capture microdissection was performed on neighboring adenocarcinoma and squamous phenotypes within an individual lesion (region X) and DNA was isolated separately from

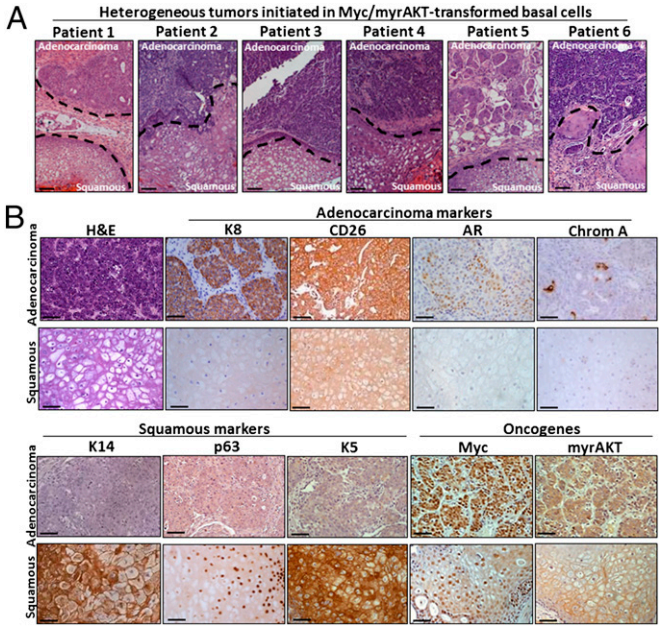

Fig. 2. Heterogeneous human prostate tumors containing squamous and acinar-type adenocarcinoma phenotypes. (*A*) H&E stains demonstrate heterogeneous tumors generated from the transformation of naïve benign basal cells from six distinct individuals. Dotted lines represent the borders of adenocarcinoma and squamous phenotypes. (Scale bars, 100 μm.) (*B*) Representative adenocarcinoma and squamous regions are identified based on staining for H&E and antibodies against luminal markers K8, CD26, and AR, the neuroendocrine marker chromogranin A, and basal/squamous markers K14, p63, and K5, and oncogenes Myc and myrAKT/pAKT. (Scale bars, 100 μm.)

adenocarcinoma and squamous cells for lentiviral integration site analysis (Fig. 3*B*). DNA was also isolated from an individual lesion containing only the adenocarcinoma phenotype (region Y). In a distinct tumor, DNA was collected from neighboring adenocarcinoma and squamous phenotypes in close proximity (region Z). PCR primers specific for the viral DNA were used to extend into the genomic DNA (Fig. 3*C*). Illumina sequencing was performed and reads were aligned to the genome to map integration sites (Fig. 3*C*). Neighboring adenocarcinoma and squamous cells (region X) shared common integration sites (Fig. 3 *D* and *E*), showing that they are derived from a clonal origin. In contrast, tissue taken from a distinct adenocarcinoma lesion (region Y) had entirely unique integration sites (Fig. 3 *D* and *E*). Common integration sites were also shared between neighboring adenocarcinoma and squamous phenotypes taken from a separate tumor (Region Z, Fig. 3 *D* and *E*). No overlapping integration sites were observed between different regions, as would be expected.

Beta-catenin signaling has been implicated in squamous differentiation and tumorigenesis in the prostate, mammary gland, and skin (9, 24, 25). In human regenerated prostate tumors, the expression of total and activated forms of beta-catenin was evaluated in both adenocarcinoma and squamous tissues. In contrast to total beta-catenin, which is expressed in both histological variants, active beta-catenin is highly expressed in squamous areas (Fig. S4). Elevated Wnt signaling in the prostate microenvironment can transform adjacent naïve benign epithelium (26). Wnt ligands are elevated in prostate cancer stromal cells following treatment, leading to beta-catenin activation in the adjacent tumor cells (27). This is consistent with the presence of squamous differentiation in prostate cancer, which is rare in primary tumors but more commonly observed in late-stage prostate cancer following treatment (14, 22). High levels of activated beta-catenin could also be detected in clinical metastatic castration-resistant prostate cancer with squamous differentiation (Fig. S4).

Luminal-Like Cancer Cells Serially Propagate Adenocarcinoma in the Absence of Basal-Like Cells. Previous studies have established optimal conditions for tumorigenicity of dissociated human tumor cell preparations (28). Regenerated primary human prostate tumor cells initiated from the transformation of five distinct benign patient samples were dissociated to single cells. Human tumor cells were identified by FACS based on staining of a pan-HLA antibody (Fig. 4*A*). Luminal-like tumor cells were then isolated on the basis of low expression of CD49f and transplanted into secondary NSG mice.

Upon transplantation, isolated CD49f^{lo} tumor cells were capable of generating secondary tumors in recipient mice. Immunohistochemical staining on tumor-derived tissue sections identified a phenotype consistent with luminal/acinar-type adenocarcinoma (29) with a predominance of K8+ CD26+ luminal-like cells and an absence of K14+ p63+ basal-like cells (Fig. 4*B*). CD49f^{lo} tumor cells failed to regenerate the squamous phenotype. Secondary tumors derived from CD49f^{lo} cancer cells were almost entirely composed of a CD49f^{lo} Keratin 18+ luminal-like phenotype as analyzed by flow cytometry (Fig. 5*A*) and expressed oncogenes Myc and myrAKT (Fig. S5). As few as 100 CD49f^{lo} cells taken from secondary tumors could generate tertiary tumors with a strictly adenocarcinoma phenotype (Fig. 5*B*). These data suggest that CD49f^{lo} tumor cells can self-renew in a unipotent manner in vivo.

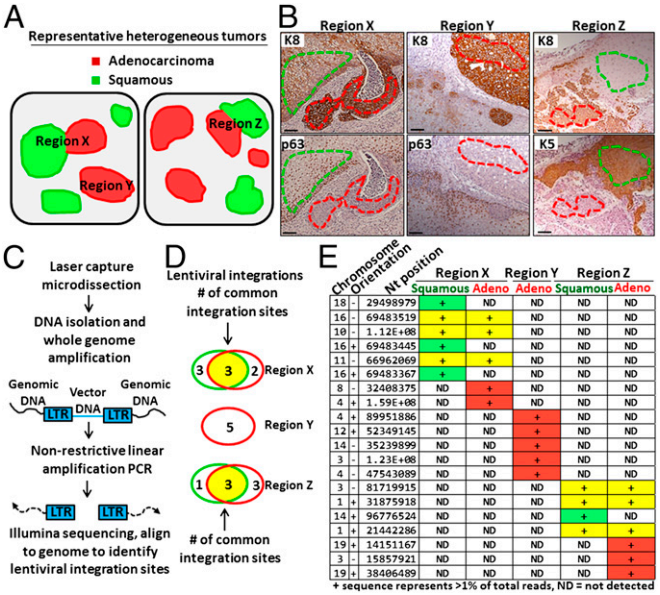

Fig. 3. Distinct histological variants in heterogeneous tumors can share a clonal origin. (*A*) Schematic of two different heterogeneous tumors containing adenocarcinoma, squamous, or both phenotypes. Regions X, Y, and Z. (*B*) Representative regions X, Y, and Z are shown with serial tissue sections stained with K8 to highlight adenocarcinoma and either p63 or K5 to highlight squamous regions. Dotted lines indicate region excised using laser capture microdissection. (Scale bars, 100 μm.) (*C*) Schematic of lentiviral integration site analysis. LTR, long terminal repeat (viral DNA). (*D*) Venn diagrams depict shared lentiviral integration sites in DNA isolated and amplified from neighboring adenocarcinoma (red) and squamous (green) phenotypes (region X), distinct adenocarcinoma gland (region Y), and additional neighboring adenocarcinoma and squamous phenotypes (region Z). (*E*) Table lists all unique integration sites (IS) with genomic location identifiers (chromosome, orientation, and nucleotide position) representing at least 1% of total reads (indicated by +) in each sample. Rows in yellow represent shared IS between distinct histological phenotypes in the same region, rows in red indicate IS unique to adenocarcinoma, and green represent IS unique to squamous.

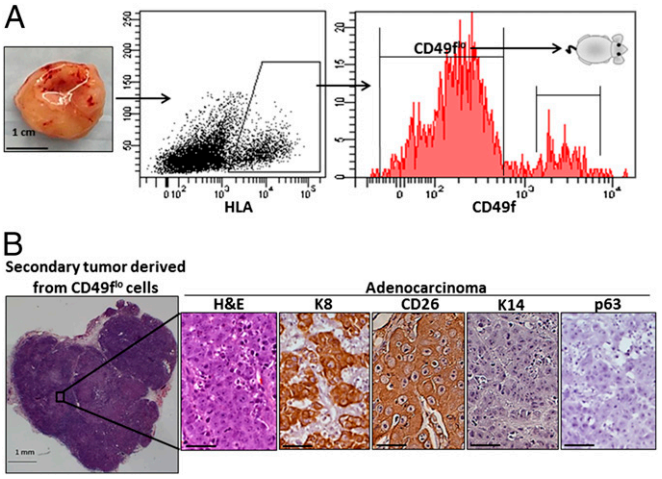

Fig. 4. Luminal-like cells isolated from primary tumors propagate adenocarcinoma. (*A*) Tumors initiated from CD49f^{hi} cells expressing Myc and myrAKT are dissociated to single cells and gated based on HLA+ and CD49f. Isolated HLA+ CD49f^{lo} cells are transplanted back into recipient mice and harvested 6–12 wk later. (Scale bar, 1 cm.) (*B*) H&E-stained overview of a representative secondary tumor generated from 10,000 isolated CD49f^{lo} tumor cells. Only the adenocarcinoma phenotype is observed as evidenced by stains for H&E, K8, CD26, K14, and p63. (Scale bars, 50 μm.)

CD49f^{hi} tumor cells were also tested in transplantation assays. We found that CD49f^{hi} tumor cells could regenerate secondary lesions exhibiting a mixture of squamous (K14+ p63+) and adenocarcinoma (K8+ CD26+) areas (Fig. S6) that both expressed Myc and myrAKT (Fig. S7). These data suggest the presence of multipotent cells in the CD49f^{hi} fraction capable of propagating both squamous and adenocarcinoma phenotypes.

In numerous tissues, high expression of Myc is associated with a block in differentiation and reprogramming to pluripotency (30). In prostate epithelium, Myc overexpression has been shown to reduce levels of AR (31) and its target prostate-specific antigen (PSA) (32). We hypothesized that high levels of Myc in Myc/myrAKT-driven tumors might cause a block in differentiation, resulting in reduced levels of AR and PSA. In primary regenerated tumors, we found low and heterogeneous expression of AR with only rare PSA+ glands (Fig. 1*C* and Fig. S8). Levels of AR and PSA were low in secondary and tertiary tumors upon serial transplantation (Fig. 5*C* and Fig. S8). These results are consistent with recent studies demonstrating that low or negative levels of AR and PSA are associated with tumor-propagating cells in prostate cancer xenografts (18, 19, 33, 34). Low levels of AR and PSA are also characteristic of DU145 (35) and PC3 (36) aggressive metastatic prostate cancer cells. In fact, expression of PSA, characteristic of clinical acinar-type adenocarcinoma, is inversely correlated with patient survival (18).

Luminal-Like Cancer Cells Exhibit Elevated eIF4E-Driven Protein Translation. Our findings demonstrate that whereas naïve benign luminal cells are not efficient cells of origin for prostate cancer, CD49f^{lo} tumor cells with a luminal phenotype can self-renew and maintain human prostate adenocarcinoma in the absence of CD49f^{hi} or K14+ p63+ basal-like cells. Signaling pathways that are absent in benign luminal cells may become expressed in malignant luminal cells and contribute to their capacity to self-renew and initiate tumorigenesis. Two pathways implicated in prostate tumorigenesis are the MAPK pathway (37) and the JAK/STAT pathway (38). Myc and myrAKT-driven tumor cells exhibited low levels of phosphorylated Erk1/2, downstream of the MAPK pathway, and weak staining for phosphorylated STAT3, a readout of the JAK/STAT pathway (Fig. S9).

The protein translation factor eIF4E is downstream of the PI3K pathway and has been shown to cooperate with Myc in promoting cell growth and tumorigenesis (39). eIF4E is unable to promote translation when bound by 4EBP1. mTOR-mediated phosphorylation of 4EBP1 (p4EBP1) relieves this interaction and allows eIF4E-driven translation initiation. High levels of eIF4E and p4EBP1 are associated with poor prognosis in prostate cancer (40) and have been shown to drive tumor invasion (41).

Elevated levels of eIF4E, 4EBP1 and p4EBP1 were found in luminal-like tumor cells isolated from Myc and myrAKT-driven tumors but not in benign luminal cells or in neighboring squamous cells (Fig. 6 *A* and *B* and Fig. S10). Luminal-like tumor cells also express MTA1 and Sox2 (Fig. 6 *A* and *B*), two targets of eIF4E translation associated with prostate cancer progression. The self-renewal regulator Sox2 has been previously demonstrated to promote the proliferation of prostate cancer cells (42). eIF4E, p4EBP1, MTA1, and Sox2 were identified in subsets of benign basal cells but not benign luminal cells (Fig. 6*A*). These findings suggest that luminal-like tumor cells may acquire a limited set of self-renewal and cell-survival factors normally associated with stem-like basal cells to promote tumor propagation.

Luminal-like cancer cells were grown in vitro and treated with pharmacological inhibitors previously demonstrated to interfere with eIF4E-driven protein translation. mTOR-mediated phosphorylation of 4EBP1 can be prevented by treatment with Rapamycin, allowing nonphosphorylated 4EBP1 to bind and inhibit eIF4E. PP242 inhibits both mTORC1 and mTORC2 and has been previously demonstrated to deplete eIF4E-driven protein translation (43). Dasatinib is a Src family kinase inhibitor that does not alter 4EBP1 phosphorylation. We tested the effect of eIF4E-driven protein translation inhibition on luminal-like cancer cells isolated from Myc and myrAKT-driven tumors. Treatment with rapamycin and PP242, but not with Dasatinib, caused a reduction in MTA1 and Sox2 protein levels and depleted sphere number and size in vitro (Fig. 6 *C*–*E*).

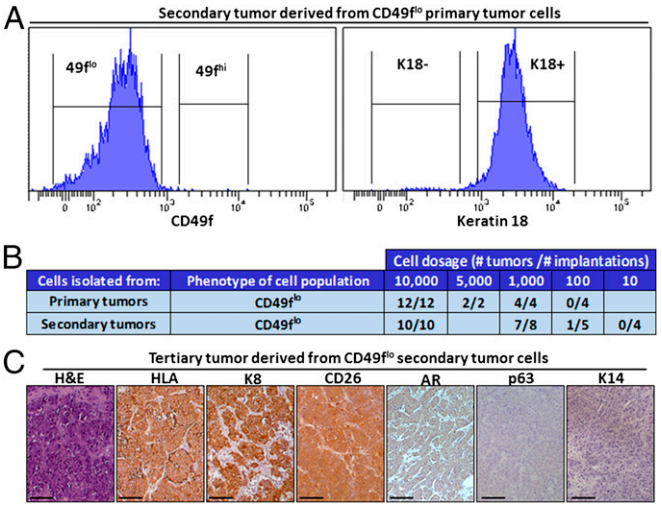

Cells isolated from:	Phenotype of cell population	Cell dosage (# tumors /# implantations) 10,000	5,000	1,000	100	10
Primary tumors	CD49f^{lo}	12/12	2/2	4/4	0/4	
Secondary tumors	CD49f^{lo}	10/10		7/8	1/5	0/4

Fig. 5. Luminal-like tumor-propagating cells maintain human prostate adenocarcinoma in the absence of basal-like cells. (*A*) Flow cytometry characterization of secondary tumors derived from CD49f^{lo} tumor cells. Secondary tumors derived from CD49f^{lo} tumor cells were dissociated to single cells and stained for surface levels of CD49f or subjected to intracellular flow cytometry and stained for K18. (*B*) Table indicates number of tumors formed per transplantation of CD49f^{lo} cells (taken from either primary or secondary tumors) at varying cell doses. (*C*) CD49f^{lo} secondary tumor cells can generate tertiary tumors upon transplantation. Representative tertiary tumor sections are shown, stained for H&E, the pan-human HLA-A/B/C antibody, and markers of luminal adenocarcinoma (K8 and CD26) and basal cells (K14 and p63). (Scale bars, 100 μm.)

Discussion

Epithelial cancers often exhibit significant heterogeneity at the histological level (1). By engineering expression of oncogenes or loss of tumor suppressors in specific lineages via cre-lox technology, it has been reported that different histological variants of mouse breast and lung cancer can arise from distinct cells of origin (4, 5). We have used a tissue-regeneration model to determine the origins of prostate cancer heterogeneity. Based on their distinct phenotypes and biological behaviors, histological variants of prostate cancer have been proposed to arise from different cells of origin (13). Myc- and myrAKT-initiated tumors exhibit features of both acinar-type adenocarcinoma and squamous cell carcinoma. Using lentiviral integration site analysis, we demonstrate that alternative human epithelial cancer phenotypes can arise from a common clonal target cell. Activated beta-catenin is elevated in areas with squamous differentiation both in experimental and clinical prostate cancer, suggesting a role for the beta-catenin pathway either in promoting or maintaining the squamous phenotype.

Our findings that basal cells are efficient cells of origin for human prostate cancer are consistent with previous findings by our group and others (15, 16). These studies on the human disease have all used a tissue-regeneration approach to model development concomitant with tumorigenesis. Several different groups have investigated the origins of murine prostate cancer using genetically engineered mouse models in which the tumor suppressor Pten is deleted in a subset of basal or luminal cells from a young age. Depending on the genetic background of the mouse and the frequency of Pten deletion by the promoters used, there is considerable disagreement on whether basal or luminal cells generate a more proliferative, aggressive tumor that can model lethal human prostate cancer (44–46). Regardless of the assay system, studies using both mouse and human tissue confirm that transformed basal cells can generate malignant luminal progeny in vivo.

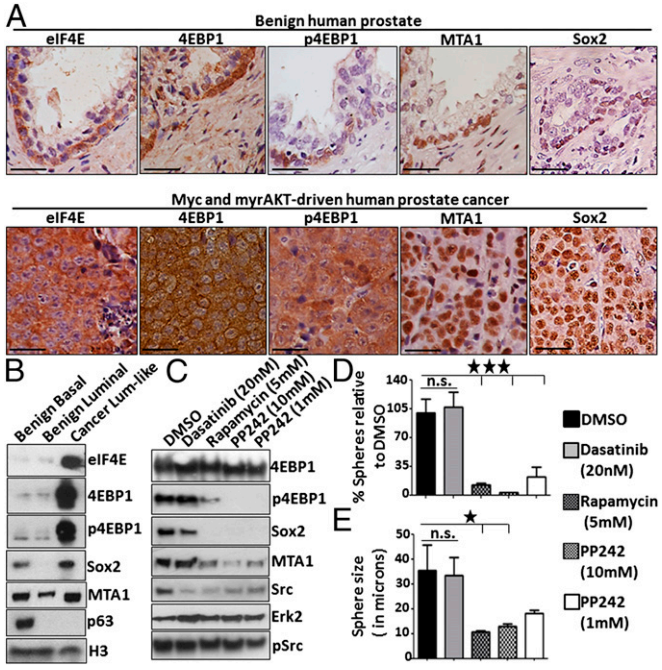

Fig. 6. Luminal-like tumor-propagating cells exhibit elevated eIF4E-driven protein translation. (*A*) Immunohistochemical analysis of benign human prostate and primary tumors initiated by Myc and myrAKT stained for antibodies against eIF4E, 4EBP1, phosphorylated 4EBP1 (Thr37/46), and the eIF4E target MTA1. (Scale bars, 50 μm.) (*B*) Western blots of FACS-purified benign basal and luminal cells compared with luminal-like tumor cells stained with antibodies aginst eIF4E, phosphorylated 4EBP1 (Thr37/46), 4EBP1, MTA1, Sox2, the basal marker p63, and loading control Histone H3. (*C*) Luminal-like cells isolated from Myc and myrAKT-driven tumors were treated with DMSO, Dasatinib, Rapamycin, and PP242 for 18 h followed by an additional treatment 1 h before harvesting. Lysates were subjected to Western blot for phosphorylated 4EBP1 (Thr37/46), Sox2, MTA1, total and phosphorylated Src (Y416), and Erk2 as a loading control. (*D*) Luminal-like cells isolated from Myc- and myrAKT-driven tumors were plated into Matrigel and grown in a sphere assay. Cells were treated with DMSO, Dasatinib, Rapamycin, and PP242 every 48 h and sphere number and size was quantified after 10 d in vitro. Sphere number is presented as a percentage normalized to the DMSO control. (*E*) Sphere size is presented as the diameter in microns. Error bars represent SEM. Statistical analysis was performed using ANOVA and Newman–Keuls multiple comparison test. $*P < 0.05$, $***P < 0.0005$. n.s., not statistically significant.

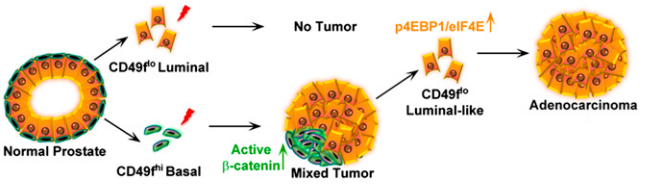

Fig. 7. Model of human prostate cancer initiation and propagation by distinct phenotypic cell populations.

In the present study, we find that human prostate adenocarcinoma initiated by transformed basal cells can be propagated by phenotypically luminal cancer cells (Fig. 7). Such a model resembles chronic myelogenous leukemia (CML). CML is initiated in transformed hematopoietic stem cells (47, 48). Advanced disease can be maintained by granulocyte-macrophage progenitor-like cells that have gained self-renewal (49–51).

Several regulators of growth and self-renewal normally restricted to the stem-like basal cell compartment are likely to be expressed in malignant luminal cells in human prostate cancer and cooperate to promote their tumorigenic activity. In Myc- and myrAKT-driven human prostate tumors, luminal-like cancer cells exhibit elevated levels of p4EBP1 and eIF4E. Luminal-like tumor cells express MTA1 and Sox2, two targets of eIF4E-driven protein translation that are normally expressed in self-renewing basal cells but not benign luminal cells. These findings suggest that eIF4E-driven protein translation may contribute to luminal-like tumor-propagating cell survival and self-renewal. In fact, activation of eIF4E downstream of Pten deletion in murine models of prostate cancer may play an important role in luminal cell transformation (44, 46).

Methods

Full methods, including antibodies, lentiviral vectors, laser capture microdissection, DNA isolation, and nonrestrictive linear amplification-mediated (nrLAM) PCR are found in *SI Methods*.

Human Tissue. Acquisition and processing of human tissue, dissociation and isolation of distinct epithelial subsets, lentiviral transduction, and in vivo implantation have all been described in detail (52). Patient tissue is provided in a de-identified manner and is exempt from institutional review board approval. Immunohistochemistry, Western blotting, and intracellular flow cytometry were performed as previously described (15).

Sequential Tumor Transplantation. Primary tumors were minced into small pieces, dissociated in 1 mg/mL type I collagenase (Invitrogen), 1mg/mL Dispase (Invitrogen) and 50 μg/mL DNase I (Roche) at 37 °C on an Adams Nutator Mixed (BD Biosciences) for 2–4 h and further digested with 0.05% trypsin/EDTA (Invitrogen) for 5 min at 37 °C if necessary before sequential passing through 100-, 70-, and 40-μm cell strainers (BD Biosciences). Cells were stained with antibodies at 4 °C for 15–30 min and tumor cell populations were sorted on a BD FACS ARIA II into media with 50% (vol/vol) FBS (Omega Scientific). Isolated cells were counted by hemacytometer using trypan blue stain (Invitrogen), resuspended in 30 μL Matrigel (BD Biosciences), and implanted s.c. into NOD-SCID-IL2Rγ^{null} (NSG) mice with or without UGSM cells.

CELL BIOLOGY

Animal Work. All primary, secondary, and tertiary tumors were transplanted s.c. into NOD-SCID-IL2Rγ^{null} (NSG) mice. NSG mice were originally purchased from the Jackson Laboratories and were housed and bred under the care of the Division of Laboratory Animal Medicine at the University of California, Los Angeles (UCLA). Surgical castration (orchiectomy) of tumor-bearing mice was performed according to protocols approved by UCLA's Animal Research Committee.

ACKNOWLEDGMENTS. We thank D. Cheng for cell sorting and the Tissue Procurement Core Laboratories for tissue preparation. Laser capture microdissection was performed at the California NanoSystems Institute Advanced Light Microscopy/Spectroscopy Shared Resource Facility at University of California, Los Angeles (UCLA), supported with funding from the Biosciences Core Facilities program at UCLA. T.S., J.M.D., and J.H. are supported by the Department of Defense Prostate Cancer Research Program. A.R.C. is supported by Ruth L. Kirschstein National Research Service Award GM007185. J.H. is supported by the UCLA Specialized Program of Research Excellence (SPORE) in prostate cancer (Prinicipal Investigator R. Reiter), a creativity award from the Prostate Cancer Foundation (PCF) (Principal Investigator M. Rettig) and National Institutes of Health Grant 1R01CA158627 (Principal Investigator L. Marks). A.S.G. is supported by the SPORE in Prostate Cancer (Principal Investigator R. Reiter) and a PCF Young Investigator Award. O.N.W. is an Investigator of the Howard Hughes Medical Institute and is supported by the Eli and Edythe Broad Center of Regenerative Medicine and Stem Cell Research. A.S.G and O.N.W. are supported by a PCF Creativity Award (Principal Investigator O.N.W.). A.S.G, J.H., and O.N.W. are supported by a PCF Challenge Award (Principal Investigator O.N.W.).

1. Visvader JE (2011) Cells of origin in cancer. *Nature* 469(7330):314–322.
2. Perou CM, et al. (2000) Molecular portraits of human breast tumours. *Nature* 406(6797):747–752.
3. Lim E, et al.; kConFab (2009) Aberrant luminal progenitors as the candidate target population for basal tumor development in BRCA1 mutation carriers. *Nat Med* 15(8): 907–913.
4. Molyneux G, et al. (2010) BRCA1 basal-like breast cancers originate from luminal epithelial progenitors and not from basal stem cells. *Cell Stem Cell* 7(3):403–417.
5. Sutherland KD, et al. (2011) Cell of origin of small cell lung cancer: Inactivation of Trp53 and Rb1 in distinct cell types of adult mouse lung. *Cancer Cell* 19(6):754–764.
6. Barker N, et al. (2009) Crypt stem cells as the cells-of-origin of intestinal cancer. *Nature* 457(7229):608–611.
7. Schepers AG, et al. (2012) Lineage tracing reveals Lgr5+ stem cell activity in mouse intestinal adenomas. *Science* 337(6095):730–735.
8. Lapouge G, et al. (2011) Identifying the cellular origin of squamous skin tumors. *Proc Natl Acad Sci USA* 108(18):7431–7436.
9. Malanchi I, et al. (2008) Cutaneous cancer stem cell maintenance is dependent on beta-catenin signalling. *Nature* 452(7187):650–653.
10. Kim J, et al. (2012) Tumor initiating but differentiated luminal-like breast cancer cells are highly invasive in the absence of basal-like activity. *Proc Natl Acad Sci USA* 109(16):6124–6129.
11. Humphrey PA (2012) Histological variants of prostatic carcinoma and their significance. *Histopathology* 60(1):59–74.
12. Chen H, et al. (2012) Pathogenesis of prostatic small cell carcinoma involves the inactivation of the P53 pathway. *Endocr Relat Cancer* 19(3):321–331.
13. Mott LJ (1979) Squamous cell carcinoma of the prostate: Report of 2 cases and review of the literature. *J Urol* 121(6):833–835.
14. Parwani AV, et al. (2004) Prostate carcinoma with squamous differentiation: an analysis of 33 cases. *Am J Surg Pathol* 28(5):651–657.
15. Goldstein AS, Huang J, Guo C, Garraway IP, Witte ON (2010) Identification of a cell of origin for human prostate cancer. *Science* 329(5991):568–571.
16. Taylor RA, et al.; Australian Prostate Cancer Bioresource (2012) Human epithelial basal cells are cells of origin of prostate cancer, independent of CD133 status. *Stem Cells* 30(6):1087–1096.
17. Collins AT, Berry PA, Hyde C, Stower MJ, Maitland NJ (2005) Prospective identification of tumorigenic prostate cancer stem cells. *Cancer Res* 65(23):10946–10951.
18. Qin J, et al. (2012) The PSA(-/lo) prostate cancer cell population harbors self-renewing long-term tumor-propagating cells that resist castration. *Cell Stem Cell* 10(5):556–569.
19. Domingo-Domenech J, et al. (2012) Suppression of acquired docetaxel resistance in prostate cancer through depletion of notch- and hedgehog-dependent tumor-initiating cells. *Cancer Cell* 22(3):373–388.
20. Gurel B, et al. (2008) Nuclear MYC protein overexpression is an early alteration in human prostate carcinogenesis. *Mod Pathol* 21(9):1156–1167.
21. Wang S, et al. (2003) Prostate-specific deletion of the murine Pten tumor suppressor gene leads to metastatic prostate cancer. *Cancer Cell* 4(3):209–221.
22. Rubin MA, et al. (2005) Effects of long-term finasteride treatment on prostate cancer morphology and clinical outcome. *Urology* 66(5):930–934.
23. Paruzynski A, et al. (2010) Genome-wide high-throughput integrome analyses by nrLAM-PCR and next-generation sequencing. *Nat Protoc* 5(8):1379–1395.
24. Bierie B, et al. (2003) Activation of beta-catenin in prostate epithelium induces hyperplasias and squamous transdifferentiation. *Oncogene* 22(25):3875–3887.
25. Miyoshi K, et al. (2002) Activation of beta -catenin signaling in differentiated mammary secretory cells induces transdifferentiation into epidermis and squamous metaplasias. *Proc Natl Acad Sci USA* 99(1):219–224.
26. Zong Y, et al. (2012) Stromal epigenetic dysregulation is sufficient to initiate mouse prostate cancer via paracrine Wnt signaling. *Proc Natl Acad Sci USA* 109(50): E3395–E3404.
27. Sun Y, et al. (2012) Treatment-induced damage to the tumor microenvironment promotes prostate cancer therapy resistance through WNT16B. *Nat Med* 18(9): 1359–1368.
28. Quintana E, et al. (2008) Efficient tumour formation by single human melanoma cells. *Nature* 456(7222):593–598.
29. van Leenders GJ, Aalders TW, Hulsbergen-van de Kaa CA, Ruiter DJ, Schalken JA (2001) Expression of basal cell keratins in human prostate cancer metastases and cell lines. *J Pathol* 195(5):563–570.
30. Leon J, Ferrandiz N, Acosta JC, Delgado MD (2009) Inhibition of cell differentiation: A critical mechanism for MYC-mediated carcinogenesis? *Cell Cycle* 8(8):1148–1157.
31. Ju X, et al. (2012) Novel oncogene induced metastatic prostate cancer cell lines define human prostate cancer progression signatures. *Cancer Res* 73(2):978–989.
32. Bernard D, Pourtier-Manzanedo A, Gil J, Beach DH (2003) Myc confers androgen-independent prostate cancer cell growth. *J Clin Invest* 112(11):1724–1731.
33. Maitland NJ, Frame FM, Polson ES, Lewis JL, Collins AT (2011) Prostate cancer stem cells: Do they have a basal or luminal phenotype? *Horm Cancer* 2(1):47–61.
34. Rajasekhar VK, Studer L, Gerald W, Socci ND, Scher HI (2011) Tumour-initiating stem-like cells in human prostate cancer exhibit increased NF-kappaB signalling. *Nat Commun* 2:162.
35. Chlenski A, Nakashiro K, Ketels KV, Korovaitseva GI, Oyasu R (2001) Androgen receptor expression in androgen-independent prostate cancer cell lines. *Prostate* 47(1): 66–75.
36. Kaighn ME, Narayan KS, Ohnuki Y, Lechner JF, Jones LW (1979) Establishment and characterization of a human prostatic carcinoma cell line (PC-3). *Invest Urol* 17(1): 16–23.
37. Mulholland DJ, et al. (2012) Pten loss and RAS/MAPK activation cooperate to promote EMT and metastasis initiated from prostate cancer stem/progenitor cells. *Cancer Res* 72(7):1878–1889.
38. Tam L, et al. (2007) Expression levels of the JAK/STAT pathway in the transition from hormone-sensitive to hormone-refractory prostate cancer. *Br J Cancer* 97(3):378–383.
39. Ruggero D, et al. (2004) The translation factor eIF-4E promotes tumor formation and cooperates with c-Myc in lymphomagenesis. *Nat Med* 10(5):484–486.
40. Graff JR, et al. (2009) eIF4E activation is commonly elevated in advanced human prostate cancers and significantly related to reduced patient survival. *Cancer Res* 69(9):3866–3873.
41. Hsieh AC, et al. (2012) The translational landscape of mTOR signalling steers cancer initiation and metastasis. *Nature* 485(7396):55–61.
42. Lin F, et al. (2012) Sox2 targets cyclinE, p27 and survivin to regulate androgen-independent human prostate cancer cell proliferation and apoptosis. *Cell Prolif* 45(3): 207–216.
43. Feldman ME, et al. (2009) Active-site inhibitors of mTOR target rapamycin-resistant outputs of mTORC1 and mTORC2. *PLoS Biol* 7(2):e38.
44. Lu TL, et al. (2013) Conditionally ablated Pten in prostate basal cells promotes basal-to-luminal differentiation and causes invasive prostate cancer in mice. *Am J Pathol* 182(3):975–991.
45. Wang ZA, et al. (2013) Lineage analysis of basal epithelial cells reveals their unexpected plasticity and supports a cell-of-origin model for prostate cancer heterogeneity. *Nat Cell Biol* 15(3):274–283.
46. Choi N, Zhang B, Zhang L, Ittmann M, Xin L (2012) Adult murine prostate basal and luminal cells are self-sustained lineages that can both serve as targets for prostate cancer initiation. *Cancer Cell* 21(2):253–265.
47. Huntly BJ, et al. (2004) MOZ-TIF2, but not BCR-ABL, confers properties of leukemic stem cells to committed murine hematopoietic progenitors. *Cancer Cell* 6(6):587–596.
48. Passegué E, Wagner EF, Weissman IL (2004) JunB deficiency leads to a myeloproliferative disorder arising from hematopoietic stem cells. *Cell* 119(3):431–443.
49. Krivtsov AV, et al. (2006) Transformation from committed progenitor to leukaemia stem cell initiated by MLL-AF9. *Nature* 442(7104):818–822.
50. Jamieson CH, Weissman IL, Passegué E (2004) Chronic versus acute myelogenous leukemia: A question of self-renewal. *Cancer Cell* 6(6):531–533.
51. Jamieson CH, et al. (2004) Granulocyte-macrophage progenitors as candidate leukemic stem cells in blast-crisis CML. *N Engl J Med* 351(7):657–667.
52. Goldstein AS, et al. (2011) Purification and direct transformation of epithelial progenitor cells from primary human prostate. *Nat Protoc* 6(5):656–667.

Supporting Information

Stoyanova et al. 10.1073/pnas.1320565110

SI Methods

Antibodies. Antibodies used for flow cytometry included CD49f-PE, CD45-APCeFluor 780, HLA-A/B/C-biotin, Streptavidin-APC, and Streptavidin-APC-eFluor 780 (eBiosciences); CD49f-Alexa Fluor 647 and CD26-FITC (BioLegend); and Trop2-APC (R&D Systems). Antibodies used for immunohistochemistry and Western blot included Keratin 8 and Keratin 5 (Covance); Keratin 14 and HLA-A/B/C (Abcam); p63, Erk1/2, and androgen receptor (AR) (Santa Cruz); CD26/DPP4 (LifeSpan Biosciences); chromogranin A (Dako); Myc, eIF4E, and 4EBP1 (Epitomics); Histone H3, AKT, and p4EBP1 (Thr37/46); pErk1/2 (T202/Y204), pSTAT3 (Y705), Sox2, MTA1, Src, and pSrc (Y416) (Cell Signaling); beta-catenin (BD Biosciences); and active beta-catenin (Millipore).

Lentiviral Vectors. The myristoylated AKT vector was previously described (1). For cloning of the Myc vector, the pMX-human-cMYC plasmid was purchased from Addgene (17966), cut with NotI, and blunted using Pfu polymerase. EcoRI linkers (Gene Link) were added to the 3′ end (former NotI site) by overnight blunt-end ligation using T4 DNA ligase (New England Biolabs). EcoRI was used to cut and release the MYC insert. The insert was gel-purified and cloned into the EcoRI sites of FU-CRW lentiviral backbone (2). Insert orientation was checked by ClaI digest and sequenced for confirmation. The resulting plasmid is now described as FU-Myc-CRW with the construct design presented in Fig. S1.

Laser Capture Microdissection, DNA Isolation, and Nonrestrictive Linear Amplification-Mediated PCR. Paraffin-embedded tissues were prepared on PEN membrane slides (Leica) and stained for H&E without a coverslip. Tissue corresponding to squamous and adenocarcinoma regions were isolated using the LMD7000 (Leica). Tissue was collected into a 100-μL nuclease-free PCR tube (Ambion). DNA was isolated and whole genome amplification was performed using the REPLI-g FFPE kit (Qiagen). Amplified human genomic DNA was quantitated against an absolute plasmid standard via probe-based real-time PCR using primers uc483-F (GCATGCTTCATTAACAGTGACC) and uc483-R (TTTAAAATCTGAATGCATGATAAGAATGG) and probe FAM-uc483 (FAM-AGATCCCCAGCTCATCCGTGATTG-Iowa Black) (3). An estimated 100–5,000 genomic equivalents of amplified DNA was used to perform nonrestrictive linear amplification PCR (4). Briefly, 100 cycles of linear amplification were performed with primer HIV3-linear (Biotin-AGTAGTGTGTGCCCGTCTGT). Linear reactions were purified using 1.5 volumes of AMPure XP beads (Beckman Genomics) and captured onto M-280 Streptavidin Dynabeads (Invitrogen Dynal). Captured ssDNA was ligated to read 2 linker (Phos-AGATCGGAAGAGCACACGTCTGAACTCCAGTCAC-3C Spacer) using CircLigase II (Epicentre) in a 10 μL reaction at 65° for 2 h. PCR was performed on these beads using primer HIV3right (AATGATACGGCGACCACCGAGATCTACACTG-ATCCCTCAGACCCTTTTAGTC) and an appropriate indexed reverse primer (CAAGCAGAAGACGGCATACGAGAT-index-GTGACTGGAGTTCAGACGTGT). PCR products were mixed and quantified by probe-based quantitative PCR and appropriate amounts were used to load Illumina v3 flow cells. Paired-end 50bp sequencing was performed on an IlluminaHiSEq. 2000 instrument using a custom read 1 primer (CCCTCAGACCCTTTTAGTCA-GTGTGGAAAATCTCTAGCA). Reads were aligned to the hg19 build of the human genome with Bowtie (5) and alignments were condensed and annotated using custom Perl and Python scripts to locate vector integrations. Integration sites were considered present and significant in a sample if they represented at least 1% of total sequence read alignments.

Inhibitors. HLA+ CD49f^{lo} luminal-like cells were isolated from Myc and myrAKT-driven human prostate tumors by FACS. For drug treatment, Dasatinib (20 nM), Rapamycin (20 μM), and PP242 (10 μM or 1 μM) (all from Selleck Chemicals) or DMSO control (Sigma) were used.

1. Xin L, Lawson DA, Witte ON (2005) The Sca-1 cell surface marker enriches for a prostate-regenerating cell subpopulation that can initiate prostate tumorigenesis. *Proc Natl Acad Sci USA* 102(19):6942–6947.
2. Memarzadeh S, et al. (2007) Enhanced paracrine FGF10 expression promotes formation of multifocal prostate adenocarcinoma and an increase in epithelial androgen receptor. *Cancer Cell* 12(6):572–585.
3. Cooper AR, et al. (2011) Highly efficient large-scale lentiviral vector concentration by tandem tangential flow filtration. *J Virol Methods* 177(1):1–9.
4. Paruzynski A, et al. (2010) Genome-wide high-throughput integrome analyses by nrLAM-PCR and next-generation sequencing. *Nat Protoc* 5(8):1379–1395.
5. Langmead B, Trapnell C, Pop M, Salzberg SL (2009) Ultrafast and memory-efficient alignment of short DNA sequences to the human genome. *Genome Biol* 10(3):R25.

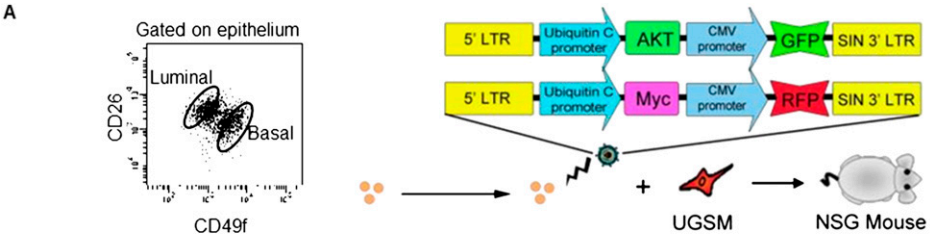

B

Naïve benign cells transduced with	Phenotype of cell population	Cell dosage (# tumors /# implantations) 100,000	50,000	10,000	1,000
Myc	Basal (CD45- Trop2+ CD49f^{hi}CD26^{-})	5/5			
	Luminal (CD45- Trop2+ CD49f^{lo}CD26^{+})	0/5			
myrAKT	Basal (CD45- Trop2+ CD49f^{hi}CD26^{-})	5/5			
	Luminal (CD45- Trop2+ CD49f^{lo}CD26^{+})	0/5			
Myc + myrAKT	Basal (CD45- Trop2+ CD49f^{hi}CD26^{-})	6/6	5/5	2/4	0/4
	Luminal (CD45- Trop2+ CD49f^{lo}CD26^{+})	0/6	0/5		

*Pooled data representing experiments using benign cells from 6 different individuals

Fig. S1. Schematic of naïve human prostate in vivo transformation. (*A*) CD45-Trop2+ epithelial cells were sorted based on CD49f and CD26 into CD49f^{hi}CD26^{-} basal-enriched and CD49f^{lo}CD26^{+} luminal-enriched subsets, transduced with lentivirus carrying Myc, myristoylated/activated AKT (myrAKT), or both, combined with urogenital sinus mesenchyme cells and transplanted into NSG mice. (*B*) The number of grafts recovered that contain epithelial lesions per number of grafts implanted in recipient mice is indicated. At doses of 100,000 or 50,000 transformed cells, a single graft was implanted from each patient sample representing five or six individuals. At lower cell doses, duplicate grafts were implanted from two individuals.

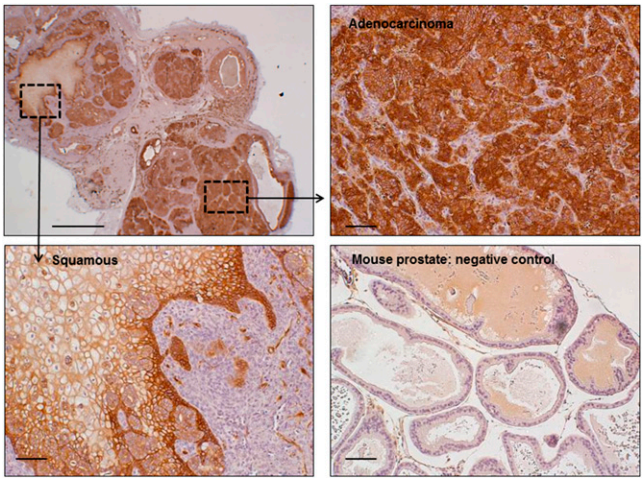

Fig. S2. Species-specific staining for HLA-A/B/C antibody. Tissue sections of human regenerated Myc/AKT tumors and mouse prostate tissue (negative control) were stained with a human-specific pan-HLA antibody to confirm species specificity. (Scale bars, 100 μm; top left overview, 1 mm.)

Tumor replicate	# glands Adeno	# glands Squamous	# glands Mixed	% area Adeno	% area Squamous	% area Mixed
1	1	3	0	65.4	34.6	0.0
2	13	8	0	95.8	9.4	0.0
3	5	12	13	4.0	44.4	51.6
4	15	1	3	74.7	12.3	13.0
5	1	11	5	5.8	84.4	9.9
6	11	11	15	23.4	41.2	35.4
Average	**7.67**	**7.67**	**6**	**44.8**	**37.7**	**18.3**

Fig. S3. Quantification of stand-alone adenocarcinoma, stand-alone squamous, or mixed glands within regenerated tumors. Tissue sections representing Myc- and myrAKT-initiated tumors were subjected to quantification of the number of glands and percentage of total tumor area harboring stand-alone adenocarcinoma, stand-alone squamous, or mixed glands.

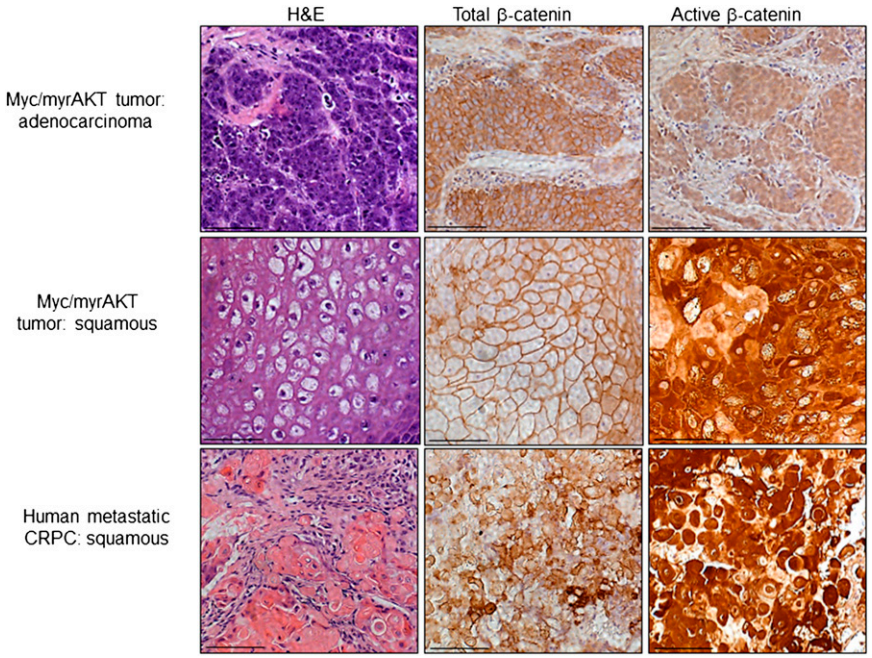

Fig. S4. Elevated expression of active beta-catenin in squamous cells. Representative adenocarcinoma and squamous regions from primary tumors driven by Myc and myrAKT, and a clinical metastatic castration-resistant prostate cancer (CRPC) sample with squamous differentiation were stained for H&E and antibodies against total and activated beta-catenin. (Scale bars, 50 μm.)

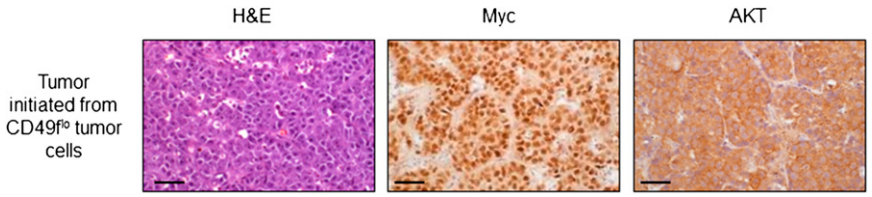

Fig. S5. Characterization of oncogene expression in histological variants present in secondary tumors initiated by CD49f^{lo} tumor cells. Secondary tumors were stained for H&E, Myc, and myrAKT and representative regions are shown. (Scale bars, 50 μm.)

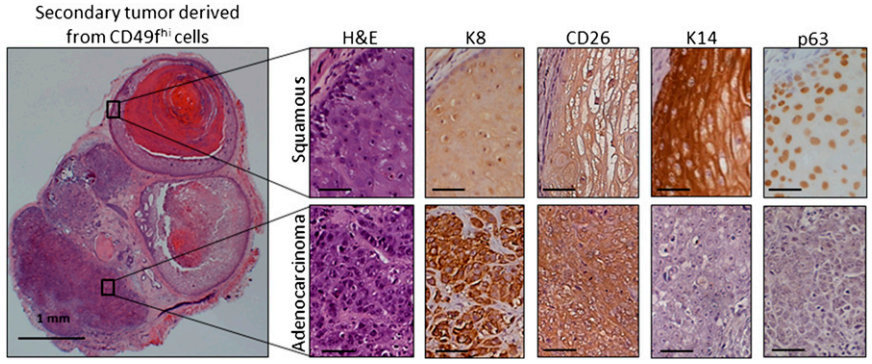

Fig. S6. Tumors initiated from CD49f^{hi} cells expressing Myc and myrAKT were dissociated to single cells, gated based on HLA+, and CD49fhi tumor cells were transplanted back into recipient mice. H&E-stained overview of a representative secondary tumor from 10,000 isolated CD49f^{hi} tumor cells after 6–12 wk in vivo. Both squamous and adenocarcinoma phenotypes are represented in secondary tumors as distinguished by stains for H&E, K8, CD26, K14, and p63. (Scale bars, 50 μm.)

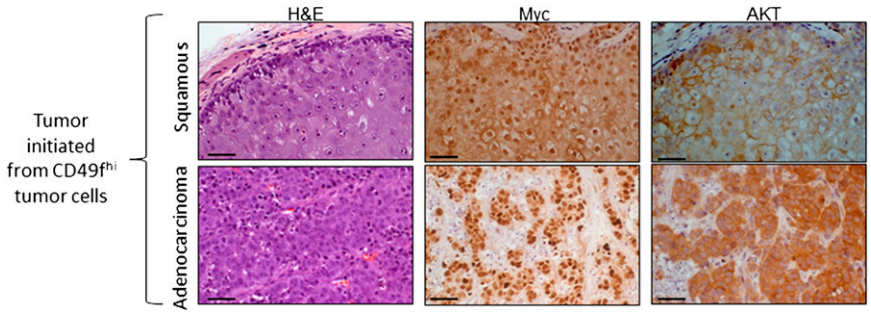

Fig. S7. Characterization of oncogene expression in histological variants present in secondary tumors initiated by CD49f^{hi} tumor cells. Primary tumors initiated in naïve benign CD49f^{hi} cells expressing Myc and myrAKT were dissociated to single cells. Isolated CD49f^{hi} tumor cells were transplanted into recipient mice to establish secondary tumors. Secondary tumors were stained for H&E, Myc, and myrAKT and representative regions are shown. Regardless of the phenotype of secondary tumors, expression of oncogenes Myc and myrAKT was maintained. (Scale bars, 50 μm.)

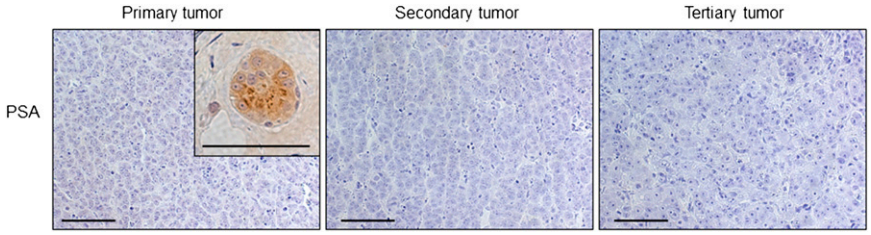

Fig. S8. Low or absent expression of prostate-specific antigen (PSA) in primary, secondary, and tertiary regenerated tumors. Immunohistochemical staining for AR and PSA, a downstream target of AR signaling, in adenocarcinoma regions of regenerated tumors. Primary regenerated tumors, initiated in naïve benign CD49f^{hi} cells, show low or negative expression of PSA except for rare PSA+ glands (*Inset*). PSA expression is absent from secondary/tertiary tumors maintained by CD49f^{lo} tumor cells. (Scale bars, 100 μm.)

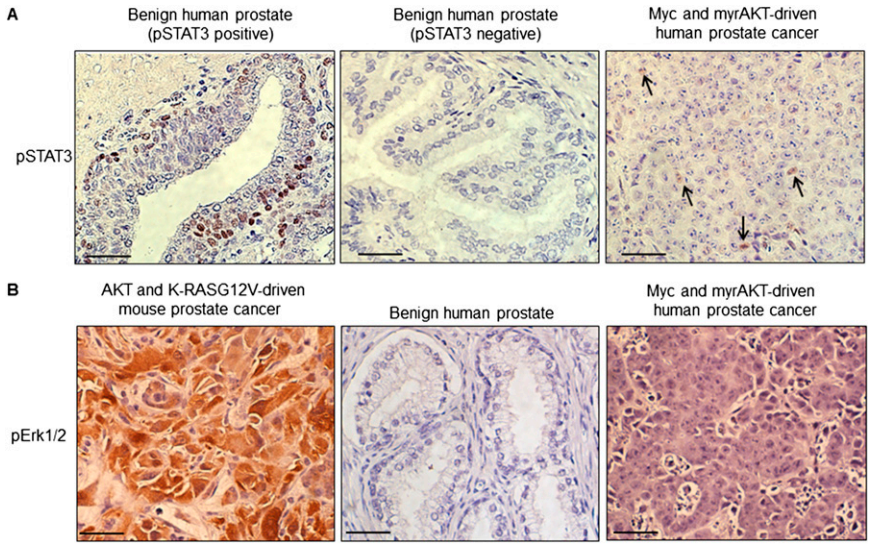

Fig. S9. Myc- and myrAKT-driven human prostate cancer exhibits low or absent expression pSTAT3 and pErk1/2 (*A*) Immunohistochemical staining for pSTAT3^{Y705} in benign human prostate and adenocarcinoma regions of regenerated Myc and myrAKT-driven tumors (arrows denote positive nuclei). (*B*) Immunohistochemical staining for pErk1/2$^{T202/Y204}$ in AKT- and K-RAS^{G12V}-driven mouse prostate cancer (positive control), benign human prostate and adenocarcinoma regions of regenerated Myc and myrAKT-driven tumors. (Scale bars, 50 μm.)

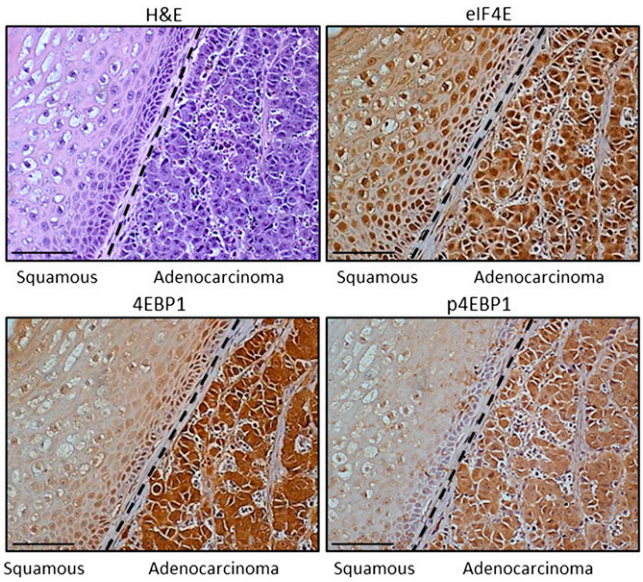

Fig. S10. Expression of EIF4E/4EBP1 pathway components in adenocarcinoma and squamous cells. Immunohistochemical staining for H&E, eIF4E, total 4EBP1, and phosphorylated 4EBP1 (p4EBP1) in Myc/myrAKT-driven primary tumors indicates elevated pathway activation in adenocarcinoma cells compared with neighboring squamous cells. (Scale bars, 100 μm.)